# THE OXIDATION STATE OF FISSION FRAGMENT IODINE IN ALKALI SULPHATES

by

JAMSHID KAMALI, B.Sc., M.Sc.

A thesis submitted for the degree of
Doctor of Philosophy of the University of London

Department of Chemical Engineering
and Chemical Technology,
Nuclear Technology Laboratories,
Imperial College of Science and Technology,
London S.W.7.

July, 1980

ABSTRACT

The oxidation states of isotopes of iodine, when they recoil as fission fragments from a thin film of irradiated uranium oxide into ionic solids, have been investigated. After irradiation the ionic solids were dissolved in excess of iodate and iodide carrier and the radioactivity of the two carriers analysed. It was found that a high fraction of the iodine in potassium sulphate exchanged with the iodate form. The fraction varied for different isotopes and also with the time and temperature of annealing of the potassium sulphate after irradiation. It also varied when the sulphates were doped with other ions such as $H^+$ (acidity), $Mg^{2+}$, $Fe^{2+}$, $Cu^{2+}$ and $Al^{3+}$. From the results on doped potassium sulphate it was shown that the increased charge of the impurity ion decreased the fractional activity of iodate. Ionic sulphates of Li, Cs, Na, Cu, Mg, Fe and Al have also been studied. For the sulphates of different cations hydration lowered the fractional activity of iodate in all cases. In alkali metal sulphates lithium showed the highest iodate and caesium the lowest, for unhydrated salts.

The electron spin resonance spectra of alkali sulphates irradiated by gamma rays from a cobalt source, by electrons in a Van de Graaff machine, and by fission fragments in the reactor, have been studied. The ESR spectra are attributed mainly to the formation of the $SO_3^-$ and associated radicals. It has been found that the thermal annealing behaviour of the ESR spectra correspond closely with annealing behaviour of the fission fragment iodine. The annealing behaviour is interpreted quantitatively as reactions between the fission fragment iodine and the radicals formed in the sulphate during the irradiation. Estimations are made for the reaction rates and activation energies involved in the annealing processes.

ACKNOWLEDGEMENTS

The author is indebted to Professor G.N. Walton, for his valuable assistance during the period of this work. Sincere thanks are due to Mr. B. Bennett for his help during the practical work and especially during the writing and correcting of this work.

Thanks are expressed to Dr. P.G. Clay for his assistance during the irradiation of the samples in the Van de Graaff Machine. The author is also grateful to Dr. J.F. Gibson and P. Beardwood, for their help throughout the ESR experiments. Thanks are also due to all the staff of the University of London Reactor Centre for the irradiation of samples.

Finally, I would like to thank my parents, my wife and my brother for the many sacrifices they made during my studies.

T O  M Y  W I F E

# CONTENTS

CHAPTER 4

CHAPTER 5

Page

CHAPTER 6

Influence of cationic dopants on the valancy states of fission fragment iodine in $K_2SO_4$



CHAPTER 7

Effects of pH and water of crystallization on the valancy states of fission fragment iodine

Page

# APPENDICES

LIST OF FIGURES

Page

Chapter 4



Chapter 5

Page

LIST OF TABLES

Page

Chapter 6



Chapter 7

INTRODUCTION

In reactor fuel uranium atoms undergo fission into two products of lower mass, which repel each other with high energy. In this process the atoms become partly stripped of electrons and can react with the surroundings and create changes in the fuel material. Little is known about the electronic conditions of the fission products, when they are first formed as isolated atoms in reactor fuels. In this thesis an attempt is made to study the chemical behaviour of fission fragment iodine in different sulphates particularly $K_2SO_4$. The results obtained in this work could be helpful for a better understanding of the behaviour of the fission products in reactors. Iodine isotopes were chosen for several reasons. Iodine is one of the major products produced by fission of uranium and uranium oxide. Since iodine is the most electronegative of all the longer lived fission products, any compound formation between the different fission products could be expected to involve iodine. Study of the fission product iodine might suggest the general conditions existing inside an irradiated fuel pin. Iodine forms a complex with $CCl_4$ and can be extracted with almost one hundred per cent efficiency.

The behaviour of fission fragment iodine in KCl formed the subject of a previous thesis (6). The radiolytic behaviour of the chloride ion was found to be a major factor in controlling the condition of the iodine fission fragments. In this study $K_2SO_4$ and assorted compounds have been used. The sulphate ionic lattice is known to have high radiolytic stability (77); it is neutral with respect to its acid and basic character and has no reducing or oxidising properties. It might be expected to act as a control medium for the investigation of iodine fission fragments stopping within the crystal lattice. As found in KCl, damage of the lattice is also a major factor in controlling fission fragments states. It was accordingly decided to investigate by electron spin resonance the damage occurring in the sulphate lattice as a result of the various types of irradiation.

# CHAPTER 1

## The fission processes and the principles of electron spin resonance

### 1.1 INTRODUCTION

In this chapter relevant aspects of the fission process are described. The range of fission fragments entering the medium is discussed. The initial charges of $^{131}I$ and $^{133}I$ when produced from fission source ($U_3O_8$) are calculated. The creation of different types of defects by fission fragments are also explained.

Electron spin resonance (ESR) of irradiated $K_2SO_4$ is discussed in Chapter Four. The radicals observed in this investigation were identified by their g-values (g-value may be taken as a parameter which governs the position of the resonance absorption) and also shape of their ESR signals. In part (2) of this chapter the basic principles of ESR are described and the type of the signals which have been observed in irradiated $K_2SO_4$ are shown and explained.

### 1.2 Fission process and fission fragments damage in the medium

#### 1.2.1 The fission process and liquid drop model

In 1939 Meitner and Frish suggested that, in a similar fashion to a mechanically vibrating liquid drop, a nucleus excited into vibration by an absorbed neutron might develop a thin waist in the middle, and then coulomb repulsion of the two halves would overcome the surface tension of the nucleus, leading to the separation of two roughly similar fragments. Bohr, Wheeler and Frankel in 1939 gave detailed description of the fission of a uranium nucleus by fast and slow neutron, and predicted successfully the spontaneous fission of heavier nuclei (1).

#### 1.2.2 The kinetic energy release in fission

The total energy of fission is mainly taken up by the fragments. Table 1.1 shows how the energy is distributed.

Table 1.1 Distribution of fission energy for $^{235}U$ (2)

| Fragments and particles | Energy (MeV) |
|---|---|
| Kinetic energy for fission fragments | 165 |
| β-decay energy of fission fragments | 9 |
| γ-decay energy of fission fragments | 7.2 |
| Neutreno energy | 16 |
| Energy of fission neutrons (promt) | 4.9 |
| Energy of the γ-ray (promt) | 7.9 |
| Total | 210 |

The following equation shows the overall energy balance:

$$M_Z^A = M_{Z1}^{A1} + M_{Z2}^{A2} + \nu n + E_n + E_M + E_\gamma \qquad (1.1)$$

where $Z_1 + Z_2 = Z$ and $A_1 + A_2 + \nu = A$

$M_Z^A$ is the mass of original nucleus

$M_{Z_1}^{A1}$ and $M_{Z_2}^{A2}$ are the masses of the products.

$\nu$ is the number of neutrons of rest mass emitted.

$E_M$ is the kinetic energy of the fragments.

$E_\gamma$ is the energy of the promt γ-ray emitted

$E_n$ is the kinetic energy of the neutron

The most important term in equation(1.1)is $E_M$ the kinetic energy of the fission fragments. This energy is produced from coulomb repulsion of the fragments at formation. An energy spectrum of $^{235}U$ fission fragments after thermal neutrons bombardment reveals an asymmetric distribution with the maximum energy for the heavier fragment at 61.4MeV and that for the lighter fragment at 93.1MeV (1).

The relative frequency of accuracy of the fission modes for different energies and mass splittings is shown by contour diagram in (3). From this figure, it is possible to estimate the kinetic energy of iodine fission fragment released in fission. The data are shown in table 1.2.

Table 1.2 Frequency of occurrance of $^{133}I$ from fission with different energy (3)

| Relative occurrence of mass 133 | | Energy |
|---|---|---|
| 0.1 | 60.0 | 77.5 |
| 0.2 | 63.0 | 76.0 |
| 0.3 | 66.0 | 73.0 |
| 0.4 | 69.0 | 72.0 |

An average energy of 69.6 MeV was found for $^{133}I$ and similarly ~72 MeV for $^{131}I$.

### 1.2.3 Distribution in nuclear charge on fragments

There is a range of possible values of the nuclear charge on each fragment. This range in most cases is very difficult to determine because the nuclei start to undergo transmutation by β-decay in a very short time after their formation. But in some cases it has been measured and it has been found that the charge for any given mass appears to be normally distributed about a most probable charge Zp. The formula for calculating $Z_p$ is given by:

$$Z_p = 46 - \frac{Z_{A2} - Z_{A1}}{2} \qquad A_1 + A_2 = A - \nu \quad (1.2),(1.3)$$

where $Z_{A1}$ is the most stable charge for the mass in question, i.e. the mean charge of the stable isobars.

The most probable charge can be predicted on the basis of the equal charge displacement postulate (4). This assumes that the difference between the most probable charge Zp and the charge of the most stable isobar of that mass chain, $Z_A$, will be equal for the light and heavy fragments.

### 1.2.4 Fission fragments decay

The fission fragments often have lower charge to mass ratios than those observed in the stable isotopes of the same element. They reach stability through β and γ-decay in radioactive decay chains. On average

each fragment undergoes three β-decays before it reaches stability. Other radioactive decay processes such as positron emission, α-particle emission and electron capture are characteristic of proton rich nuclei and have very small probability of occurrence in fission product decay. Several prompt neutrons are emitted within $10^{-2}$S, later delayed neutrons are emitted (0.0173 neutron per fission of $^{235}U$). Although the number of delayed neutrons is small they play a very important role in reactor control.

1.2.5 Initial electronic charge on the fission fragments

Bohr (5) has shown the relationship between the effective atomic charge and the velocity of the fragment.

The velocity v of an electron in an atom of effective atomic charge $Z_{eff}$ and in an orbit of effective quantum number n is given approximately by

$$v = Z_{eff}\, v_o/n \qquad (1.4)$$

where $v_o$ is the velocity of an electron in the First Bohr orbit of the hydrogen atom, with energy 13.6 ev.

The effective quantum number of outer electrons is given by $n = Z^{1/3}$ (3)

substitution of the value of n into the above equation gives

$$Z_{eff} = Z^{1/3} v/v_o \qquad (1.5)$$

using the above equations, the effective atomic charge $Z_{eff}$ for $^{133}I$ with energy 69.6 MeV (see section 1.2.2) can be calculated. It is known that electrons with orbital velocities less than the velocity of the fragment will be left behind.

Using the kinetic energy relationship $E = \frac{1}{2}mv^2$, the velocity of the fragment was found to be $1.005 \times 10^6$ m $s^{-1}$.

From the same relationship the velocity of an electron in the first Bohr orbit of the hydrogen atom is $2.186 \times 10^5$ $ms^{-1}$

Therefore when Z = 53 for $^{133}I$

$$v_o = 2.186 \times 10^5 \text{ ms}^{-1}$$

$$v = 1.005 \times 10^6 \text{ ms}^{-1}$$

The above values are replaced in equation (1.5) to give $Z_{eff}$ = 17.25 ($^{133}I$)
For $^{131}I$ with energy 72MeV and velocity 1.0298 x $10^6$m/s, $Z_{eff}$= 17.7 ($^{131}I$)

This neglects the effect of the medium as the fragment slows down, and only describes the initial relationship.

1.2.6 Fission damage in the medium. (The energy loss processes)

A heavy charged particle moving through a medium composed of atomic nuclei and electrons can lose energy by three main processes:
(A) - Interaction of charged fission fragment (energy $\sim 10^7$ ev) with the atomic electrons by Coulomb excitation or ionization.
(B) - Fragments may also lose energy by direct collisions with nuclei of the medium - but this predominates when the fragments are near the end of their path.
(C) - Energy loss due to emission of 'bremsstrahlung' and Cerenkov radiation. This energy is small compared to either of the first two processes. Therefore, the total rate of energy loss (the absolute stopping power) is a combination of the rate of energy loss due to each of the three processes, and can be written as:

$$\left(-\frac{dE}{dx}\right)_{total} = \left(-\frac{dE}{dx}\right)_{electronic} + \left(-\frac{dE}{dx}\right)_{nuclear} + \left(-\frac{dE}{dx}\right)_{radiation} \quad (1.6)$$

A fission fragment at first will be travelling too fast.
Because of its high effective charge, the fragment loses energy, mainly by Coulomb interaction with the electrons. This type of interaction causes ionization and electronic excitation of the medium, and it loses about 80-85% of its energy in this way. At a lower velocity it starts to capture electrons along its path and therefore its charge is reduced.

This situation can be considered, in the frame of reference of the fission fragment as a cloud of electrons moving towards it with its own velocity (3). The fragment will lose its electrons to the cloud when their binding energy is less than the kinetic energy of the cloud electrons with respect to the fragment.

It will start collecting electrons when their kinetic energy is less than the binding energy of the electrons on the fragment.

1.2.7 Range of fission fragments in the medium

The range of the fission fragment through the medium is related to the stopping power or rate of the energy loss.

$$R(E_o) = \int_o^{E_o} dE/(-dE/dx) \qquad (1.7)$$

The stopping power has contributions due to electronic, nuclear and radioactive processes. For heavy fission fragments, radiative losses are almost negligible.

Bohr (5) has shown that fission fragment range can be compared with the range of the $\alpha$-particles which have the same initial velocity $\underline{v}$ as the fission fragment in the material in question.

$$\frac{R_{electronic}}{R_{\simeq}} = 7.5 M_1 Z_1^{-2/3} (v_o/v)^2 \qquad (1.8)$$

where $v_o$ is the velocity of an electron in the first Bohr orbit of the hydrogen atom. $M_1$ and $Z_1$ are the mass and nuclear charge on the fragment. Since the atomic stopping power is approximately proportional to the square root of the atomic number of the material, it is possible to predict the maximum range for fission fragment in the medium using the following formula

$$X_1 \sqrt{Z_1} = X_2 \sqrt{Z_2} \qquad (1.9)$$

The range of fission products in $K_2SO_4$ is calculated in Appendix 1. The above formula gives the linear range, but due to atomic scattering, the penetration of the fragment will often be less than this value. Fig. 1.1 shows several types of ranges that can be considered (6). $R_L$ is the total path length, measured along the path of the incident particle. $R_v$ is the vector distance between start and finish. $R_p$ is the projection of the vector range onto the initial direction of motion; this gives the penetration. R is the lateral spread of the particles.

Fig 1.1 DIAGRAMATIC REPRESENTATION OF VARIOUS RANGE MEASUREMENTS

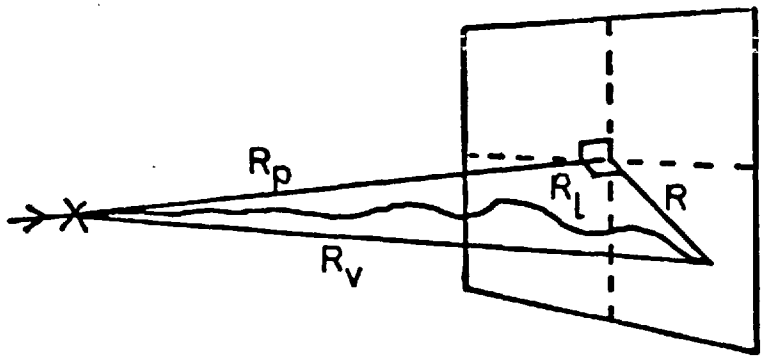


1.2.8 Creation of defects by fission fragments

Energetic fission fragments entering $K_2SO_4$ cause electronic excitation and when the fission fragment has lost most of its energy due to electronic collission, it starts to interact with the atoms in the lattice. This atomic interaction creates atomic displacement. This process leads to creation of several types of defects which would play an important role in the thermal annealing processes. There is a high probability that an atom as a complete entity will receive kinetic energy in that region of high thermal and electronic excitation which lies in the wake of a fission fragment. Therefore a number of atoms will be displaced by secondary processes arising from the electronic part of the energy loss of the fragment. Such an atom will undergo elastic and, if the energy is sufficient, inelastic collisions with its neighbours, producing more secondary and higher displacements. A cascade of displaced atoms will build up until the maximum energy of any atom falls below the displacement threshold $E_d$. In fact the value of $E_d$ depends on the characteristics of the crystal lattice and is normally about 25eV (1).

I. Displacement energy ($E_d$)

$E_d$ is a crystalographic property of the material. Displacement energy is temperature dependant and is introduced by vibration of the atoms on their lattice sites. A directional dependence for $E_d$ can be illustrated

if one considers that the displaced atom has to pass through a barrier of atoms in the crystal.

II. Replacement energy ($E_r$)

$E_r$ is minimum replacement energy, where (7)

$$2\,E_r = E_d$$

its value is taken to be 13.6 ev (the Rydburg energy). Replacement occurs after a head-on collision between two neighbouring atoms where most of the energy is transferred to the second atom. The primary knock-on is left with insufficient energy to escape the potential field of the vacancy it has created. This is a case of the interchange of the dynamic interstitial. Through a series of exchanges with atoms in normal sites, an interstitial can drift through the crystal.

III. Type of defects

Fission fragments entering $K_2SO_4$ create several types of defects apart from decomposition of the salt (decomposition of $K_2SO_4$ due to fission fragments and radiation is very small). The defects produced by fission fragments are, point, dislocation, and bulk defects. The most important of all is the point defect which could play an important role in the impurity effects on the $K_2SO_4$ containing fission fragments. Vacancy is the simplest defect, which is a site in the crystal lattice where there is a missing atom or ion. The complementary defect to a vacancy is an interstitial; it is an extra atom or ion inserted at a site where there is not normally an atom or ion of the regular crystal structure. Impurities in solids may also be considered as defects in the crystal structure. Isolated impurity atoms may occupy substitutional or interstitial sites as is shown in fig. 1.2.

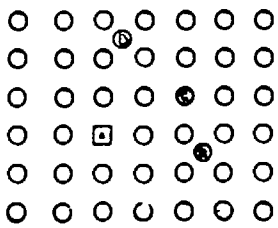

Fig. 1.2 Simple point defects. A : vacancy; B ; interstitial; C : substitutional impurity atom; D interstitial impurity atoms.

### 1.2.9 Fission spikes

The fission fragments damage in the crystal lattice affects the atoms as groups. This type of damage concentrated around the fission fragment path, is called a fission spike. Thermal and displacement spike create hot zones and atomic displacement in lattice. The defects created by fission spikes could have some effect on the valency states of fission fragments in the crystal during thermal annealing. The damage effects of fission fragments in sulphates has not been studied yet.

#### (A) - Thermal spikes

Let us suppose that a fission fragment in the interaction with an atom of the medium releases energy less than $E_d$, then the atom starts to vibrate in its potential well, and one can easily picture the vibration spreading to its neighbours, developing a localized excitation which is effectively the same as if that small region of the solid were raised to a high temperature. The vibrations will decrease rapidly in amplitude as the excitation spreads from its source until thermal equilibrium is regained. Such localized excitations are termed thermal spikes. Although the temperature concept does not rigorously apply, since equilibrium never exists within the spike, it is possible to obtain useful information regarding the dimensions and excitation profile of the spike by application of the macroscopic laws of heat condition (1).

Dienes and Vineyard (8) calculated that a spherical thermal spike of 300 eV initial energy in copper will raise the temperature of a region of diameter $30A^{o}$ to the melting point ($1086^{o}C$) in a time of $5x10^{-12}$sec and that cooling period will be of the order of $10^{-11}$ sec. Because of the short duration, the spike region does not attain a true liquid state, and may be more accurately described as a superheated solid.

(B) - Displacement spikes

The displacement spike was first suggested and explained by Brinkman (9,10). An energetic fission fragment passing through a crystal will certainly produce a great deal of thermal spike activity along its path, both by direct interaction and indirectly through the primary and secondary knock-ons which it generates. In the case of a fission fragment this situation is complicated by the large number of atomic displacements and displacement cascades, which in turn produce more thermal excitation.

Brinkman obtained an expression for the relationship between the mean free path $\lambda$ of a fragment, its energy E and the minimum energy transferred in a collision T. A typical curve for fission fragments in uranium is shown in fig. 1.4. From this it can be seen that, if T = 25eV (the displacement threshold) an atom with energy $10^3$ eV will transfer energy greater than T with a mean free path less than one interatomic distance, thus producing a multiple displacement. Brinkman hypothesized that a multiple vacancy would therefore be created at the end of the path of an incident fission fragment or an energetic primary knock-on, the configuration immediately following each event being a shell of interstitial atoms surrounding a vacancy core (see fig. 1.3). Seeger (11) has suggested that focussed

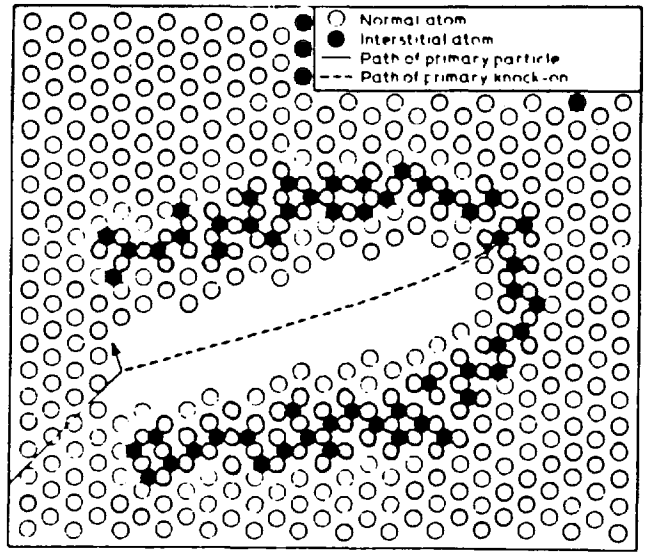


Fig.1.3 Representation of interstitial atoms around a multiple vacancy during production of Brinkman displacement spike(1)

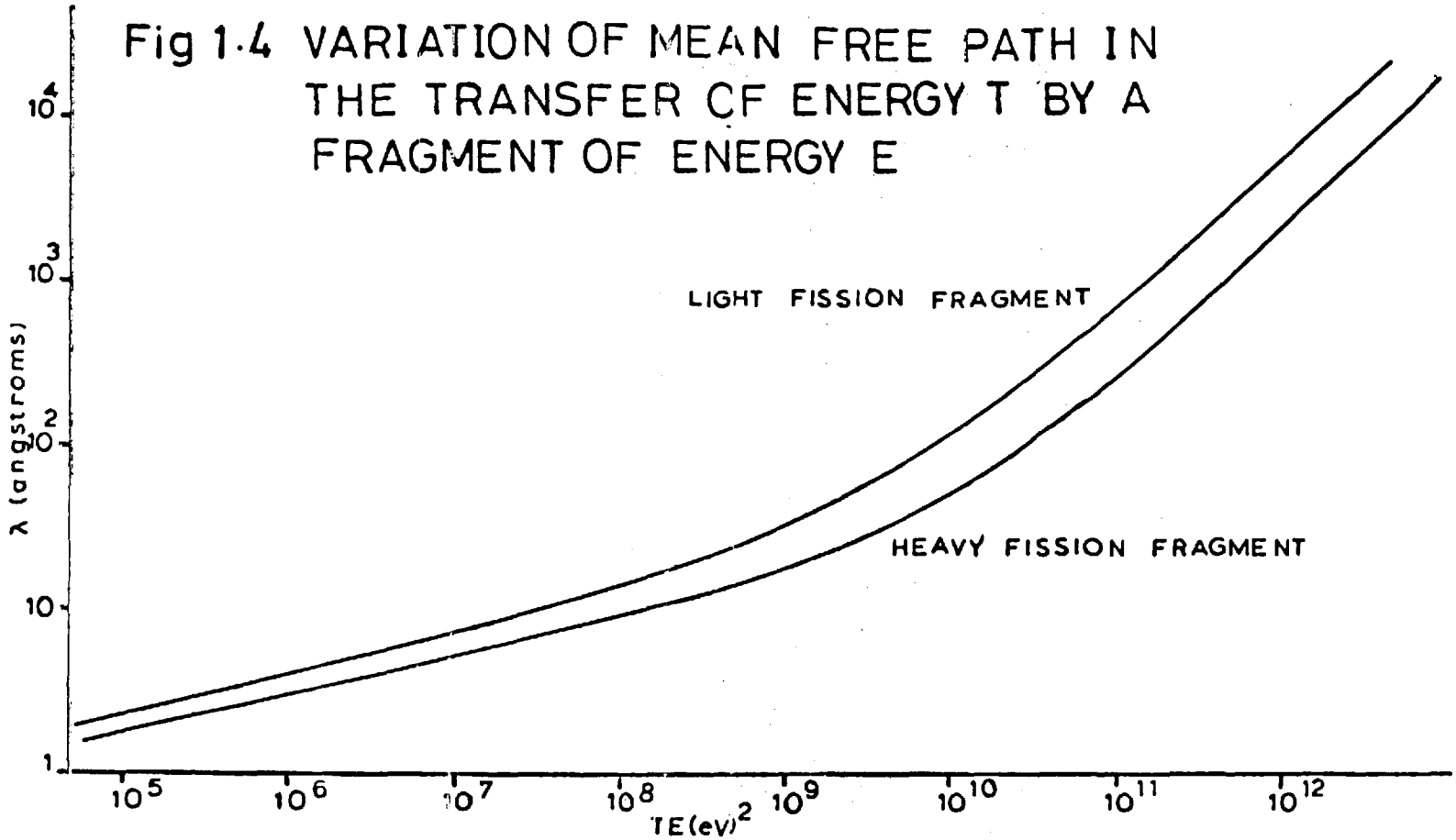
Fig 1.4 VARIATION OF MEAN FREE PATH IN THE TRANSFER OF ENERGY T BY A FRAGMENT OF ENERGY E
LIGHT FISSION FRAGMENT
HEAVY FISSION FRAGMENT
λ (angstroms)
10^4
10^3
10^2
10
1
10^5
10^6
10^7
10^8
10^9
10^10
10^11
10^12
TE(eV)^2

collision sequences could also separate the interstitials from the multiple vacancy region. This would result in a depleted zone, which would be composed of a high local density of vacancies around the stationary knock-on, with a few nearby interstitials (see fig. 1.5). A schematic representation of the fission spike is shown in fig. 1.6. (1).

Since the effective charge decreases as the fragment energy falls, this radius will also decrease, and to an approximation one can represent the thermal spike as a right circular cone with its apex on the final resting place of the fragment. (fig. 1.6a).

As the fission fragment slows down collisions with atoms become more frequent, therefore the frequency of the displacement cascade production will increase as more primary knock-ons come to rest and each producing spikes according to fig. 1.6b.

Fig. 1.6c shows the increased frequency of displacement spike formation as the fragments slow down and there is a gradual transition from "Rutherford" to "hard sphere" collisions.

## 1.3 An introduction to electron spin resonance (Basic principles)

Both theory and experiment have shown that an electron possesses intrinsic angular momentum which is known as its 'spin'. Because the electron is electrically charged and since there is a magnetic field associated with any moving charge, there is a magnetic field associated with the spinning electron. In other words an electron, by virtue of its intrinsic angular momentum, behaves as a tiny bar magnet.

In free space these magnets are aligned quite randomly, but in the presence of an externally applied magnetic field there will be a preferred direction. Quantum mechanics tells us that an electron has a spin quantum number of $\frac{1}{2}$ and that it can have only two orientations with respect to a given axis. Crudely, the electron can either spin clockwise at a particular rate or it can spin anti-clockwise at the same rate. In terms of the

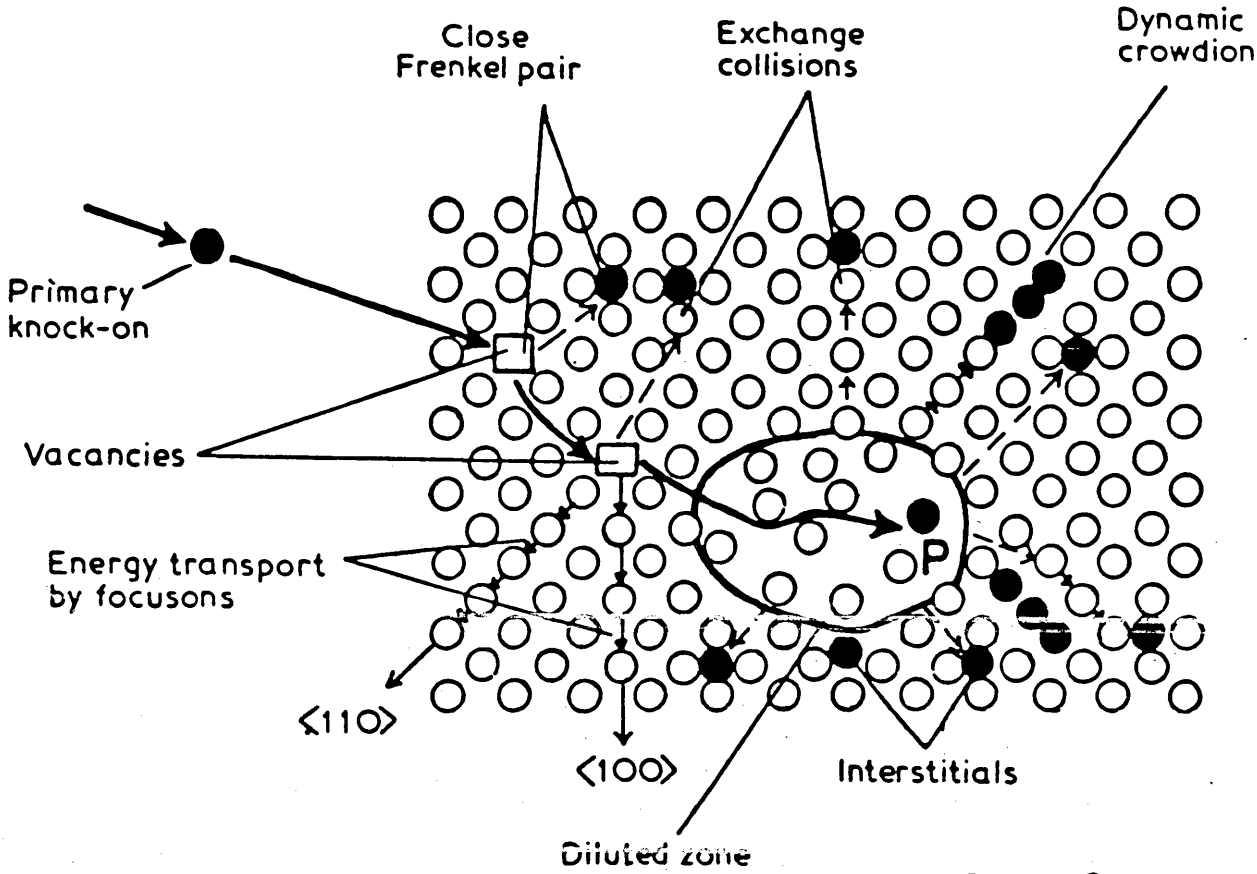


Fig 1.5 DAMAGE CREATED BY PRIMARY KNOCK ON IMPINGING FROM THE LEFT AND COMING TO REST AT P

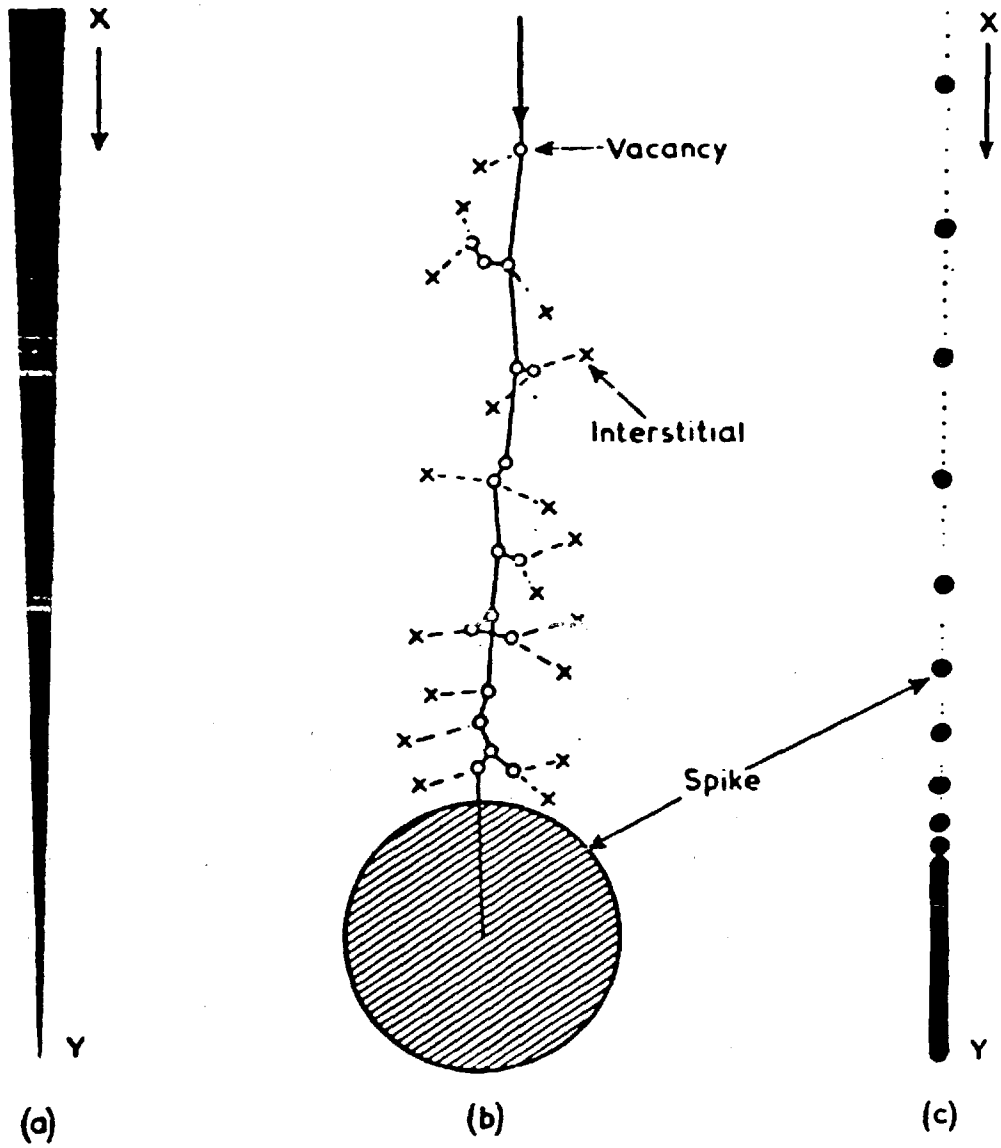


Fig 1.6 SCHEMATIC REPRESENTATION OF THE FISSION SPIKE

magnetic properties of an electron in an external field it can behave as a small bar magnet aligned effectively with the direction of the external field or against it. A diagram, such as fig. 1.7 can be used to illustrate the fact that the difference in energy between the two directions of spin (or orientation of the magnetic moment of the electron) depends on the strength of the external field. Basically, that is all that an electron spin resonance spectrum measures, namely the energy required to reverse the spin of an electron in an externally applied magnetic field. It is only

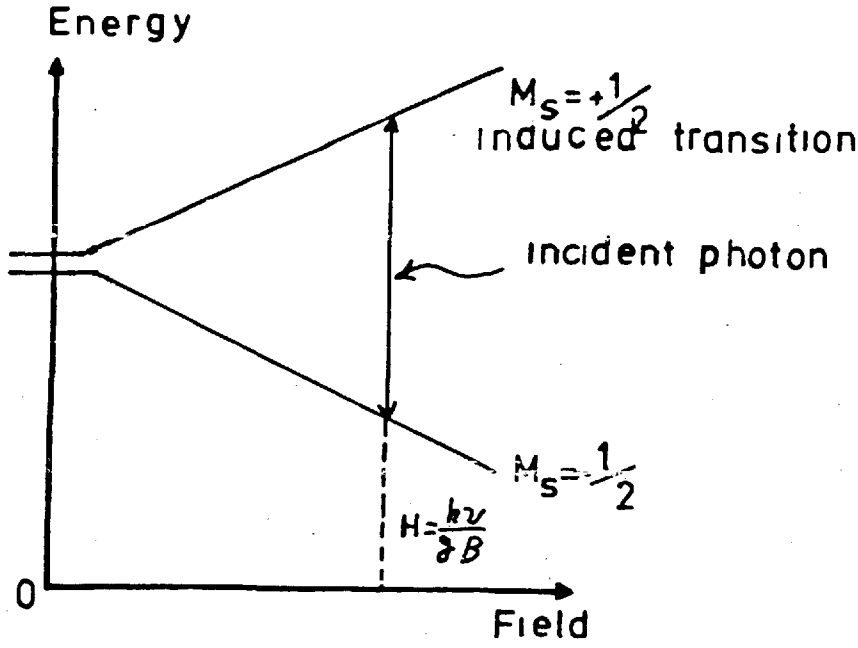


Fig.1.7 The effect of an external magnetic field upon the energy of an electron and the transition induced by an electromagnetic field (12)

necessary to bathe the electron in a reservoir of energy. If this source of energy is a beam of radio waves having a single frequency $\nu$ (and therefore, by Planck's relation, having a single energy $h\nu$), There will be an exchange of energy between the electron spin and the radio frequency field such that the energy between the two spin direction is equal to the energy of the radio frequency field.

Looking at the spectra it is clear that there are three features which differ from spectrum to spectrum. The first is that resonances for a given microwave frequency do not always occur at the same magnetic field strength. Writing the resonance conditions as: $h\nu = gBH$ (1.10)

where $\nu$ = microwave frequency

H = the magnetic field strength

B = Bohr magneton,

and finally the g value may be taken as a parameter which governs the position of the resonance absorption (12).

### 1.3.1 g-values

An important effect of radiation is the production of molecules containing an unpaired electron. These molecules, called free radicals, are paramagnetic by virtue of their unpaired electrons. The detection of free radicals by ESR spectroscopy provides information about the effective magnetic moment of the electron. This information is obtained from a measurement of the g-values associated with the paramagnetic absorption. Throughout the study of radiation effects by ESR spectroscopy, the g value will be an important characteristic for the identification of radicals. Although the expected g-value for an electron with no angular momentum except that due to its spin is 2, the actual "free-spin" value is 2.0023. This is because a relativistic correction applies.

The field at which resonance can be reached depends upon the orientation of the radical to the applied field and that different radicals can have different g-values, each one of which may be either greater or smaller than the free spin value of 2.0023.

### 1.3.2 Analysis of electron-spin resonance signal

The spectrum of a polycrystalline or amorphous sample is a super position of the spectra corresponding to radicals in various orientation and much information can be usefully gained from the examination of signals produced from such samples. In this work powder of irradiated $K_2SO_4$ ($K_2SO_4$ has been irradiated in various ways, See Chapter 4 for more details) was studied. $K_2SO_4$ has no unpaired electron unless damaged. Potassium ion also has no free spin.

(A) Isotropic signal

An isotropic g-value yields a single narrow line with insignificant broadening in the wings. This is one of the most simple cases and usually identification of the radical ions with isotropic signals is very easy compared to the other types of signal. Fig. 1.8 shows a typical isotropic signal.

(B) Anisotropic signal

(I) Signal with axial symmetry

The line shape of an arbitrarily oriented species exhibiting axial symmetry with respect to g-value variation, is characterized by a shoulder on the side of the main absorption peak. The derivative has five points of inflection and values of g perpendicular ($g_\perp = g_1 = g_2$) and g parallel ($g_{11} = g_3$) corresponds to maxima (see fig. 1.9).

(II) Paramagnetic species with three different g-values

These species are distinguished by a derivative possessing seven points of inflection. The values of $g_1$ and $g_3$ are maxima and $g_2$ corresponds to the zero point of the derivative (see fig. 1.10).

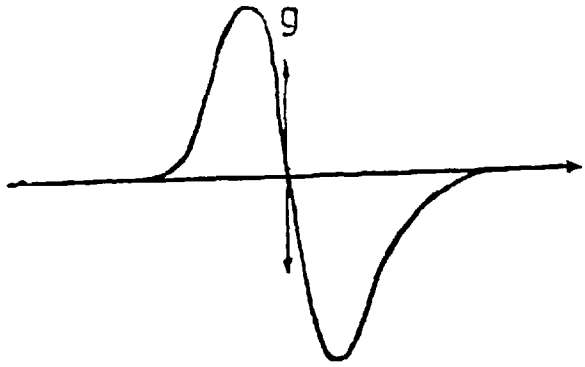


Fig. 1.8 Isotropic ($g_1 = g_2 = g_3$) signal

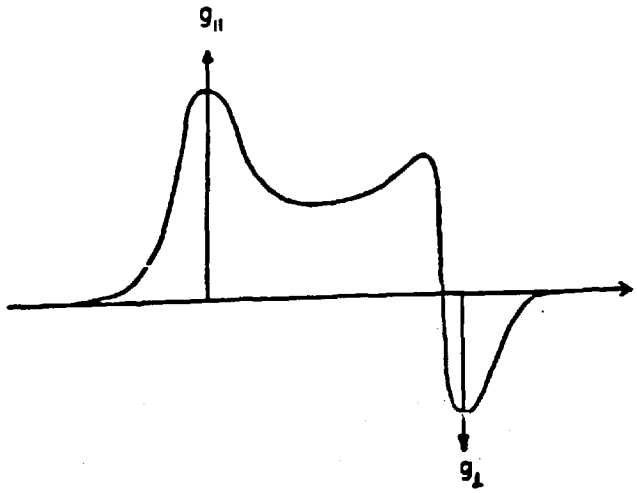


Fig. 1.9 Axial symmetry ($g_{\perp} < g_{\parallel}$) signal

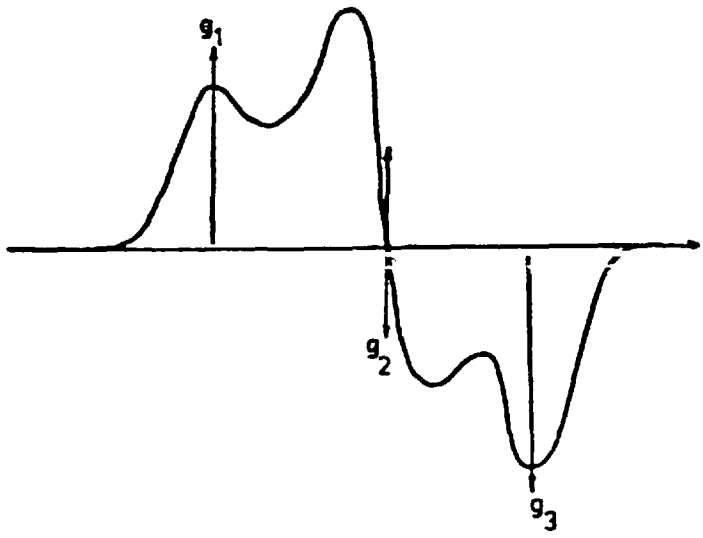


Fig. 1.10 Anisotropic ($g_1 > g_2 > g_3$) signal

# CHAPTER TWO

## Literature Survey

### 2.1 INTRODUCTION

In this chapter previous work which has been done on fission fragment iodine and related subjects, the cation effect, the ESR of irradiated $K_2SO_4$ and the water effect are reviewed.

2.2 Behaviour of the fission product iodine in different media. It appears that no work has been done on the oxidation and reduction states of fission product iodine in $K_2SO_4$ polycrystalline. The work has been done on the behaviour of fission product iodine in some other media are reviewed in this section.

The behaviour of fission product iodine has been studied by Walton and his co-workers on different media. Walton and Croall (13) have measured the $^{131}I$ arising after fission recoil from uranium oxide particles into a surrounding medium of solid potassium iodate. An increase in the fraction of the recoils stopping in the iodate form have been observed with increasing the relative amount of the iodate to uranium oxide, The chemical decomposition of the iodate phase was proportional to the number of the fission recoils stopping in the iodate phase. They observed that about 90% of the iodate was retained in the oxidized form. Walton et al (14) have worked on the chemical state of fission products in irradiated uranium metal before dissolution in acid. No evidence was found for combination of the radioactive iodine and alkali metals. Iodine appeared to be present in some form, other than iodide, which showed preferential extraction into hexane. They suggested that the iodine fragment released in fission was present as an isolated positively charged atom, in the matrix of the uranium metal. Thermodynamic considerations showed that it can extract electrons from the metal surface to become a neutral atom. It would not be expected to exert a strong Coulombic force with electrons or uranium ions in the

metal. They pointed out that the iodine would be expected to behave like a rare gas atom in the lattice.

Hall and Walton (15) have studied the valence states of fission product iodine formed in uranyliodate. Iodate ions were partly decomposed to the reduced form of iodine. The percentage in the oxidised form were 86% ($^{131}I$), 82% ($^{133}I$), 63% ($^{132}I$) and 33% ($^{135}I$). The results were explained in terms of the independent yields of the isobars and electron affinities of the outer electrons. These conditions explained the decreasing order in oxidation with increasing atomic mass, observed for all the isotopes except $^{132}I$. They pointed out that the high percentage of reduced form in $^{135}I$ could be taken as evidence that the initial electron stripping process of the fission fragment had no major effect on the final state adopted. They suggested that the $^{132}I$ lies in a region of closed nuclear shells, and this would influence the independent yield. Finally they pointed out that the independent yields predicted show that closed-shell effects increase the relative proportions of tin and antimony as precursors of $^{132}I$. As these are elements with low electron binding-energy it might be expected that $^{132}I$ would arise in a more oxidized condition, whereas it was observed to be less oxidized than $^{131}I$ and $^{133}I$. (Accordingly in the present work special attention is given to the comparison of $^{132}I$, $^{131}I$ and $^{133}I$ isotopes). The most recent work on the behaviour of fission fragment iodine has recently been reported by Waller and Walton (16); they have investigated the oxidation state of fission fragment iodine in KCl. They observed that the percentage of iodine as iodate after the end of irradiation and 25 hours after irradiation were 28.9 and 17.7% respectively. In the isothermal annealing after irradiation the oxidised form of the fission fragment iodine (iodate) decreased initially, and then started to increase relative to the reduced form (iodide), depending on the temperature of the annealing. They pointed out that the chlorine ion $Cl_2^-$ behaves as a reducing agent and could be responsible for the reduction process. They also suggested that the

chlorine could be responsible for the oxidising process to give iodine centres which became iodate ions on dissolution in water. Finally they concluded that the fission fragment iodine , which originates stripped of some electrons come to rest during the irradiation partly in an oxidised condition. It might then react with the defect centres produced by the irradiation damage in the surrounding lattice and accept the reduced condition and when the defects in the crystal were annealed the fission fragment tended to return to its initial oxidised state.

The behaviour of fission product iodine in uranyl nitrate and uranyl chloride has been studied by Spiridou and Calusaru. In the case of uranyl nitrate (17), a similar isotopic sequence to the results reported on uranyl iodate (15) was observed with a percentage of the reduced forms being increased considerably by lowering the irradiation temperature. The results obtained for oxidised form of iodine were 65%($^{131}$I), 58% ($^{133}$I) and 29.4% ($^{135}$I). In uranyl chloride (18) irradiated at room temperature and liquid nitrogen, the percentage of the reduced forms were 68.2% ($^{131}$I), 67.7% ($^{133}$I), and 76.4% ($^{135}$I), at room temperature and 73.3, 69.9 and 77.4% in liquid nitrogen.

They obtained the percentage of the reduced forms in the order of $^{131}I > ^{133}I > ^{135}I$ which was in good agreement with results reported in uranyl iodate (15) and uranyl nitrate (17). They concluded that with the stabilization of the fission products a stronger effect of the matrix could be expected for the thermal annealing process. They observed that in the thermal annealing for all three isotopes in the first hours a reduction process occurs, increasing visibly the ratio between the reduced and oxidised forms. This behaviour explained by reduction of the damaged matrix. The oxidation process had been observed after longer periods of thermal annealing. They pointed out that the chlorine atoms could be responsible for oxidising the iodine isotopes.

## 2.3 Cation effect

In this section the ESR of irradiated $K_2SO_4$ (doped with impurity), the effect of impurity on retention of $K_2CrO_4$, $KBrO_3$, $K_2SeO_4$, tellurium compound and iodate are reviewed. The structure of $K_2SO_4$ doped with $Mn^{2+}$ has been investigated using the ESR method by Chowdari and Venkateswarlu (19). Over a large temperature range $Mn^{2+}$ found to substitute for $K^+$ and leave a $K^+$ vacancy. The structure of $K_2SO_4$ doped with $Cu^{2+}$ have been studied by Abdulsabirov et al (20). From ESR of $Cu^{2+}$ in $K_2SO_4$ they found that the $Cu^{2+}$ was substituted for a potassium atom. They pointed out that the excess charge of $Cu^{2+}$ replacing $K_2^+$ was balanced by vacancies and adjacent $K_1^+$ positions.

It must be pointed out that the crystal of $K_2SO_4$ is orthorhombic and $K^+$ ions differ in oxygen environment, so they were denoted by $K_1$ and $K_2$. Krutikov et al (21) have investigated the ESR of x-ray irradiated $K_2SO_4$ doped with $Cd^+$. Two paramagnetic species have been observed to exist, $Cd_I$ and $Cd_{II}$. The spectrum due to $Cd_I$ was isotropic and that due to $Cd_{II}$ was anisotropic. They finally suggested that in crystal growth processes cadmium ions replaced $K^+$ ions in both positions, $Cd_I$ replaced $K^+$ in the $K_2$ site and $Cd_{II}$ in the $K_1$ site.

Andersen and Olesen (22) have investigated the chemical effect following thermal neutron capture in potassium chromate. They found out that Na, Rb and Cs impurities did not change the initial retention, whereas small amounts (approximately $10^{-4}$ mole fraction) of Ta, Ca, Sr, Ba, or La ions decreased the initial retention.

The incorporation of calcium ions caused an increase in the number of recoil fragments able to undergo annealing in the 110-140$^0$C region. They suggested that $Ca^{2+}$ ions acted as trapping centres for a fraction of the recoil atoms. They pointed out that after irradiation, there would be a high vacancy concentration in the region of the impurity atoms and both

electrons and recoil atoms would have a higher probability of being trapped near impurity atoms than in the rest of the crystal. The relative high concentration of calcium ions necessary to obtain a measurable effect on the retention and the fact that the percentage of reduced chromium fragments was proportional to $\log(Ca^{2+})$ suggested that diffusion of the recoil atoms towards the $Ca^{2+}$ ion might have occurred. The effect of impurities in potassium chromate at thermal and radiation annealing have been investigated by Andersen and Maddock (23). They pointed out that introducing Ca, La and Tl in the lattice of potassium chromate produced vacancies and these vacancies could be responsible for the changes in the initial retention. In the thermal annealing of the calcium-doped material they observed that the increase in the retention was proportional to the concentration of the calcium ions. They found out that Tl impurity decreases the initial retention while Ca and La increases it, although the increase in the Lanthanium-doped material was much higher than that of calcium.

Saito et al (24) studied the effect of neutron irradiation on the retention of bromates. They found out that the bromate with lower basicity showed higher retention and the order was as follows:

$$Al(BrO_3)_3 \cdot 9H_2O > Cu(BrO_3)_2 \cdot 6H_2O > Mg(BrO_3)_2 \cdot 6H_2O > KBrO_3, NaBrO_3$$

They suggested that this difference in the retention could be because of the participation of the cations in the recoil reaction. The chemical state of radioactive bromine atoms after the $^{79}Br(n,\gamma)^{80m}Br$ and $^{81}Br(n,\gamma)^{82}Br$ reactions were investigated by Saito et al (25). A correlation was found between the retention and ionization potential of the $M^{(n-1)+}$ ion to $M^{n+}$ where $M^{+}$ was the cation of the bromate as well as the crystal free space of the bromates. Bromates of metals other than alkali metals had generally higher retention values than alkali bromates. They suggested that, since the ionization potential of $M^{(n-1)+}$ ion to $M^{+}$ is a measure of the affinity of $M^{n+}$ ion for an electron, this correlation showed the participation of the

cation in the redox reaction of recoil atoms. Finally they pointed out that cations with higher affinity for electrons gave rise to higher retention by trapping the electrons near them and hence facilitating the recombination of metastable bromine species with oxygen atoms or ions. But in the bromates studied the thallous bromate gave the lowest percentage of retention, and they suggested that this was due to the reducing power of the thallous ions.

Dejesusf et al (26) have investigated the influence of the dopant cations $Al^{3+}$, $In^{3+}$ and $Ca^{2+}$ on both thermal and gamma-annealing in neutron irradiated $K_2SeO_4$. They assumed that the introduction of the dopant cations, $M^{n+}$, in the lattice led to the creation of both $M^{n+}$ sites and $K^+$-vacancies. The effect of the impurity on the initial retention was explained in terms of the overall efficiencies of these species for hole-capture, at a given temperature. They suggested that holes released from $\boxplus K^+$ on heating after irradiation should be accounted for the changes brought about by the dopants in the experimental isochronal annealing curves. They found out that the retention decreased by about 8% for all dopants, with efficiencies in the sequence $Al^{3+} > In^{3+} > Ca^{2+}$. They suggested that during the $\gamma$-irradiation of $K_2SeO_4$ in the reactor, radiation created doner/acceptor species such as

$$SeO_4^{=} \xrightarrow{\text{Radiation}} SeO_3^{-} + O^{-}$$

$$SeO_3^{-} + h \longrightarrow SeO_3$$

$$O^{-} \longrightarrow O^{=} + h \text{ (hole)}$$

Kobayashi et al (27) studied the ESR spectra of $K_2SeO_4$ doped with $Cu^{2+}$ and found that each $Cu^{2+}$ ions took substitutionally a position of potassium ions, accompanied by a vacancy of a neighbouring potassium ion. It must be pointed out that $K_2SeO_4$ is the isomorphe of $K_2SO_4$.

Radiation and thermal annealing studies have been done by Kronrad (28) on the tellurium compounds. It was found that the major part of the activity

of $^{131}I$ after neutron irradiation of tellurium compounds was present in the lower valance state ($I^-$ and $I^0$). He observed that the activity corresponding to the lower valence state in neutron irradiated $TeO_2$ and $TeO_3$ increased with increasing annealing time. He pointed out that $^{131}I$ when produced, existed in its higher valency state and it started to become reduced by further irradiation or thermal annealing. He observed that (in $TeO_2$) with increasing temperature or time of heating the reduced form increased.

The oxidation state of the radio-iodine atoms produced by the $(n,\gamma)$ and $(n,2n)$ reaction was studied (29) in various iodates and related compounds; particular attention has been paid to the effect of cations, the water of crystallization, and the type of nuclear reaction on the behaviour of the recoil iodine atoms. Heavy alkali iodates were found to give retention values higher than those of sodium and potassium iodates. In hydrates, a large cation effect was found between sodium iodate and the iodates of transition metals. For a given cation the hydrate form gives lower retention values than the anhydrous form. Rapidly frozen solutions of sodium and potassium iodates were found to show retention values very close to that of the sodium iodate monohydrates. The nature of the effect seems not to be fully understood. One possible origin of the cation effect was the differences in the affinity of cations for electrons or fragments produced in the recoil reactions. When cations were involved in the recoil reaction, the affinity of the cations for electrons, for example, might have affected the oxidation state of the recoil atoms. The differences in the crystal structure were another possible origin of the cation effect.

The mass of cations were suggested to be another factor for a parameter giving rise to the cation effect. The retention of heavy alkali iodates were found to be higher than those of sodium iodate and increased with increasing atomic number of the alkali metals. This phenomenon was not

capable of being explained on the basis of the electron affinity of cations, since the low affinity of heavy alkali metal ions for electrons would be expected to give rise to a lower retention. They have suggested that the high retention of cesium iodate could be due to the approximate equality of the mass of iodine and cesium atoms.

## 2.4 Water effect

In the last chapter the effect of moisture in $K_2SO_4$ and also the effect of water of crystallization in several sulphates are discussed. It seems that no work has been done on the effect of water on the oxidation state of fission product iodine in the sulphates. The studies which have been made of the effects of water on the recoil chemistry of solids are reviewed in this section. Properties of the species produced in the radiolysis of water are also discussed.

### (A) Properties of species produced in irradiation of water

From a very large number of experiments, the action of radiation on aqueous solutions involves reduction or oxidation. This could be explained if the radiation acts on water to form H atoms (reducing) and OH radicals (oxidizing) (30). This can be understood if in addition to decomposition of water into H atoms and OH radicals the radiation also gives some molecular hydrogen and hydrogen peroxide as primary products (31). The available evidence is now consistant with the view that the chemical effects produced on irradiation of water and dilute aqueous solutions are a consequence of the production of the radicals $e_{aq}$, OH and H and the molecular $H_2$ and $H_2O_2$

$$H_2O \longrightarrow e_{aq},\ OH,\ H,\ H_2,\ H_2O_2,\ H_3O^+$$

In x-rays, $\gamma$-rays, fast electron and low linear energy transfer (LET) radiation generally, the radical intermediates predominate, while with $\alpha$-particle and other high LET radiation the molecular products are more important.

The large yield of molecular intermediates in high LET irradiation may arise from the fact that the tracks are dense, so that various species

would often interact with each other before they had a chance to be diffused away to react with the solute. Stopping power for liquid water for different types of particles are shown in Table 2.1.

Table 2.1 Initial stopping power for liquid water (32)

| Particle | KeV/μm |
|---|---|
| 2 MeV electron | 0.18 |
| Average compton electron from $^{60}Co$ γ-ray | 0.26 |
| Typical average electron from x-ray generated at 220 kV | 0.7 |
| Uranium fission fragments | 1800 |

As the radicals diffuse away from the track there is appreciable competition between reactions with other primary products and reaction with solutes. Whereas with low LET radiation the radicals are very unlikely to react with other radicals after they have diffused even a very short distance away from their point of origin. Since molecular hydrogen, hydrogen peroxide, and hydrogen ions are relatively inert, therefore the radiation chemistry of water and dilute aqueous solutions reduces essentially to the chemistry of hydrated electrons, hydroxyl radicals and hydrogen atoms.

Hydrated electrons

The hydrated electron possesses many features in common with electrons trapped in solids. The hydrated electron may be visualized simply as an electron surrounded by oriented water molecules:

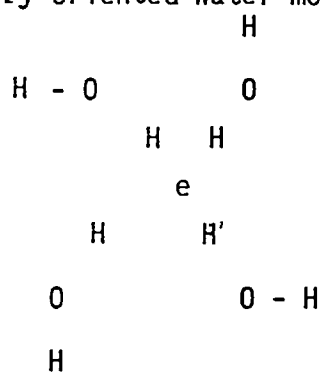

The reactivity of the hydrated electron can be understood in the light of its thermodynamic properties. It is a powerful reducing agent, and it is capable of reducing substances of low standard potential. Hydrated electrons are generally captured by substances which are known, or expected to have a positive electron affinity. Activation energies of hydrated electron reactions are invariably small, even where low reaction rates are found (33). (Finally the hydrated electron may be regarded as a reactive nucleophile.)

Hydroxyl radicals

The OH radical is a powerful oxidizing agent but in strongly alkaline solutions its reactivity appears to change markedly. This is explained by:

$$OH + OH^- \longrightarrow O^- + H_2O$$

$$O^- + H_2O \longrightarrow OH + OH^-$$

With ferrocyanide for example, $O^-$ is comparatively unreactive, but OH react rapidly according to the equation:

$$OH + Fe(CN)_6^{4-} \longrightarrow OH^- + Fe(CN)_6^{3}$$

Hydrogen atoms

Hydrogen atoms are less powerful reducing agents than are hydrated electrons. In many respects their reactions are closer to those of hydroxyl radicals, although they are distinctly less reactive.

Perhydroxyl radicals

Since perhydroxyl radicals are produced in tiny yield in the high LET radiolysis of water they may be regarded as primary intermediates. $HO_2$ and $O_2^-$ are both capable of acting as mild oxidizing agents (with the formation of $H_2O_2$) or mild reducing agents (giving $O_2$).

(B) Effect of water of crystallization on the retention

The effect of water of crystallization in different sulphates is described in Chapter 7. It appears that no work has previously been reported on the sulphates studied in this work, but other workers have

reported the effect of water of crystallization on other salts. Most of the reports show a reducing effect of the water of crystallization, but a few workers reported an oxidising effect. This section is a review of some reports on the effect of water of crystallization. McCallum and Maddock (34) have investigated the chemical effect resulting from neutron capture by manganese in different permanganates. They have observed lower retention in hydrated permanganate in comparison with the anhydrous compounds. They suggested that this could be due to the reduction properties of the water of hydration. Maddock and Muller (35) have studied the change of the retention of neutron irradiated calcium bromate both hydrated and unhydrated. They also studied the change in retention following dehydration of hydrated calcium bromate. They observed that the monohydrate of calcium bromate had the same initial retention of 18% as the anhydrous compounds. After thermal annealing of the hydrated salt for 16 hours at $160^{o}C$ and $196^{o}C$, respectively, the retention increased in both cases to values between 75 and 70%, the thermal curve showed a steeper step but in general the shape was the same as the unhydrated compound. They have pointed out that the same plateau retention was obtained at different temperatures ($160^{o}C$ and $196^{o}C$) suggesting that no further annealing after dehydration was possible.

Ackerhalt et al (36) have investigated the implanted thallium atoms in a number of targets, especially KCl and NaCl. The results suggested that traces of impurities such as water are having a marked effect on the valence finally assumed by the thallium atoms. They observed an oxidising effect of water and they suggested one possible explanation for the yield change, water molecules lying on the surface act as electron traps, thereby stabilizing the charge or valence states higher than +1 residing on the implanted Tl atoms.

Arnkar et al (37) have studied the effect of thermal annealing on the retention of $^{80m}Br$ in $(n,\gamma)$ irradiated cadmium bromate dihydrate. They

suggested that the water of crystallization retained the radiolytic oxygen during irradiation; this was made available to the ruptured bromine fragments during annealing at 150°C which was accompanied by dehydration. This results in nearly total retention while the maximum retention by this temperature was only 53% in crystals which had been dehydrated before irradiation.

Adams and Campbell (38) have studied the behaviour of $^{32}P$ recoils from $^{32}S$ (n,P)$^{32}P$ reaction in the hydrous and anhydrous salts of $Na_2SO_3$ and they found that the hydrated $Na_2SO_3$ led to a marked increase in lower valency $^{32}P$.

Peixoto and Maddock (39) have made a comparison between the products formed by the (n,$\gamma$) reaction in hydrated and anhydrous sodium hexachloro-iridate (IV), as well as in the ammonium salt. The effect of hydration and dehydration after the neutron irradiation were also described. The results showed that both water of hydration and ammonium ions led to the smaller proportion of $^{*}$Ir (IV) species. Al-Siddique and Maddock (40) investigated the effect of water of hydration in neutron irradiated $K_2SeO_4$ and $Na_2SeO_4$. Sodium selenate and hydrated sodium selenate irradiated with a neutron flux of $1.4 \times 10^{12}$ $ncm^{-2}sec^{-1}$ gave 45% and 19.8% retention respectively. But with the neutron flux of $3.6 \times 10^{13}$ the retention value increased to 75% and 46.4% for sodium selenate and hydrated sodium selenate. Potassium selenate did not show such big changes. Finally they pointed out that the hydrated salts invariably gave lower retention than the anhydrous salts for similar conditions.

Stamoul (41) has studied the distribution of $^{51}Cr$ activity among $^{51}Cr$ (IV), $^{51}Cr$ (III) - monomer and $^{51}Cr$ (III)-dimer + polymer species in hydrated and anhydrous sodium chromate and dichromate salts irradiated with neutron at room temperature and liquid nitrogen temperature. He observed that the presence of water of crystallization had a considerable

effect on the activity distribution. He found out that the sample irradiated at liquid nitrogen temperature gave lower retention in the presence of water of crystallization. The lower retention also observed in the irradiation of hydrated sodium chromate at room temperature, provided that the irradiation time was short and the samples stored immediately after irradiation in liquid nitrogen.

An investigation of the effect of lattice rearrangement accompanying loss or regain of water of crystallization on the annealing of chemical radiation damage in solid calcium bromate has been carried out by Khare and Mohanty (42). Thermal annealing of anhydrous $CaBrO_3$ showed an increase in the retention, but the increase in the retention in hydrated calcium bromate has been observed to be much more than the anhydrous salt. They observed that during thermal annealing of the hydrated salt at $100^{o}C$ the water of crystallization remained intact, but at $120^{o}C$ and above, lattice mobility occasioned by the loss of crystallization of water caused a rapid initial recovery of the damage following which there was only a small recovery even on heating for a longer period. They found out that only one annealing characteristic was obtained at various temperatures (120, 140 and $160^{o}C$) above the dehydration temperature. Finally they suggested that the lattice mobility liberates the damage oxygen and a proportion of this recombines with bromine bearing damaged fragments to reform bromate.

Walton (43), suggested that the presence of water of crystallization increased the ease with which electrons can be promoted to the conduction band in atoms excited by neutron irradiation. This allowed valency bonds to be disrupted more easily than in anhydrous compounds.

Thermal annealing of $^{51}Cr$ (III)-doped $MnSO_4$, $7H_2O$ have been studied by Ladrielle et al (44). They have observed a decrease in $^{51}Cr$ (III) yield during thermal treatment (30-$110^{o}C$). It has been attributed to the action of the disappearing radiolytic defects created by gamma radiation in the water molecules.

## 2.5 pH effect

The pH effect in $K_2SO_4$ containing fission fragments is discussed in Chapter 7. The following is a review of the effect of the pH on the retention of chromates, alkali chloride and permanganates. Gutlich et al (45) have reported that pH of the solvent was one of the factors effecting the distribution of $^{51}Cr$ activity in irradiated crystalline chromates. Kasrai and Maddock (46) studied the pH effect in relation to aerial oxidation of aqueous solutions containing dissolved irradiated alkali chlorides (neutron irradiation). Acidic solutions, with $H_2S$ as carrier exposed to air produced more oxidised species of $^{35}S$ as $SO_3^{2-}$ and $SO_4^{2-}$ than those kept and analysed in a vacuum. The absence of air and carriers led to complete oxidation, which could only have occurred by the water or by the point defects produced in the crystal during irradiation. Neutral and alkaline solutions with no carrier and in a vacuum, had appreciable proportions of reduced forms. Bracokova and Cifka (47) have studied the effect of KOH concentration in the valence distribution of $^{32}P$ and $^{35}S$ atoms in KCl (KOH added to KCl prior to irradiation) crystals irradiated at dry ice temperature in a reactor. Both distributions favoured the lowest oxidation states during thermal annealing at room temperature throughout the whole range of KOH concentration. They observed that the $^{35}S$ atoms were effected more and the percentage of reduced species of $^{35}S$ decreased in the range of 0.001 to 0.01 mole % KOH and increased in the range 0.01 to 0.1 mole %. For $^{32}P$ species the lowest oxidation states have been observed for both ranges.

They pointed out that $OH^-$ impurities also increased the sensitivity of crystals to ionising radiation. F centre formation was proportional to the $OH^-$ concentration and the decay of F centres was easier than in pure KCl crystal.

MacCallum and Maddock (34) have studied the retention of radioactive manganese in the form of the permanganate ion and its dependence upon the

pH of the solution in which the irradiated crystals were dissolved. They observed that the retention was independent of pH over a wide range, but increased slightly at low pH (pH < 2) and significantly at pH > 10. They showed that the general shape of the retention against pH curve was similar for different permanganates, but that the value of the retention in the pH independent regions depends upon the nature of the solid. They also observed that after dissolving the irradiated sample in solution (with a known pH) and then changing the pH the retention was that characteristic of the original pH.

## 2.6 Electron-spin resonance of irradiated $K_2SO_4$

The ESR of the gamma, neutron, and electron irradiated $K_2SO_4$ and also $K_2SO_4$ containing fission fragments is studied (see Chapter 4). In this section the work which has previously been reported on the ESR of irradiated $K_2SO_4$ is reviewed. Gromov and Morton (48) have studied the paramagnetic centers in x-ray irradiated single crystal of $K_2SO_4$. They have detected two types of radicals, type A ($SO_4^-$) anisotropic and type B ($SO_3^-$) isotropic. Table 2.1 shows the principle g-values.

Aiki and Kukuda (49) have investigated the single crystal of $\gamma$-irradiated $K_2SO_4$. The experiment has been done at room temperature. They have identified four types of centres in the crystal, centres A and B were due to two types of $SO_4^-$ and centre C was possibly due to $SO_3^-$. They pointed out that these centres were stable for months in the dark at room temperature. Another centres was D which was isotropic but they could not assign it (g = 2.003 $\sim$ 2.002). They observed that the two types of $SO_4^-$ disappeared at the same temperature during thermal annealing. The principle g-values for the centres are shown in Table 2.1.

Hariharan and Sobhanadri (50) have studied the paramagnetic centres in x-ray irradiated $K_2SO_4$ single crystals. They have detected several new lines in addition to $SO_4^-$ and $SO_3^-$ which have been observed by Gromov (48)

and Aiki (49). The most intense signal has been identified to be due to $SO_3^-$ radical ion with an isotropic g-value of g = 2.0025 ± 0.0005. They also observed two types of $SO_4^-$ radicals, both centres were sensitive to heat and both disappeared at the same temperature. They pointed out that there were two non-equivalent sites for the sulphate ion, and therefore two lines observed for the anisotropic spectra suggest that the centres responsible for the spectrum must be associated with the sulphate group.

Sasaki (51) has studied the ESR on thermally stimulated exoelectron emission (TSEE) from irradiated $K_2SO_4$ (Powder). $K_2SO_4$ was irradiated in dry air by $^{60}CO$ source at room temperature. The sample after irradiation was heated at 550°C at the rate of 0.62 K/s. The formation of six paramagnetic species have been observed. $SO_4^-$, $SO_3^-$, $SO_2^-$ and $O_3^-$ have been identified but the other two radicals could not be identified, although the g-value of one of them suggested another type of $SO_4^-$ radical. They observed that the ESR spectra remained almost constant up to 150°C. Heating to 203°C caused a partial decay of $SO_4^-$ and $SO_2^-$, heating to 252°C led to the complete decay of $SO_4^-$ and partial decay of $SO_2^-$. The exo-electron emission has been observed by decay of the above radicals. The exo-electrons were counted with a gas-flow type G-M detector. After heating to 442°C, the $SO_3^-$ concentration was reduced to one sixth, but the exo-electron emission initiated by the thermal decay of $SO_3^-$ was not observed. He suggested the following thermal decay for $SO_2^-$, $SO_4^-$ and $SO_3^-$.

$$SO_4^- + SO_2^- \longrightarrow SO_4^{2-} + E$$

$$SO_2^- \longrightarrow SO_2^{-*} \longrightarrow SO_2 + e^-$$

$$SO_3^- + SO_4^- \longrightarrow SO_3 + SO_4^{2-} + E$$

$$E + SO_3^- \longrightarrow SO_3 + e^-$$

where E is thought to be the radiationless energy.

It must be pointed out that in all works reviewed above the most stable and intense signal was due to $SO_3^-$ radical. Table 2.2 shows the principal g-values reported by the above workers.

Table 2.2

g-values of the radicals observed by different workers in x-ray and γ-ray irradiated $K_2SO_4$

| Type of irradiation and solid form | $SO_4^-$ Anisotropic | $SO_2^-$ | $SO_3^-$ Isotropic | Oxygen ion $O_3^-$ | Ref. |
|---|---|---|---|---|---|
| single crystal-x-ray | 2.0486, 0.0082 2.0037 | - | 2.003 | - | 48 |
| Single crystal-γ-ray | A) 2.057, 2.009 2.003 B) 2.048, 2.009 2.004 | - | - | - | 49 |
| single crystal-x-ray | A) 2.0572, 2.0246 2.009 B) 2.0512, 2.0135 2.0027 | - | 2.0025+ 0.0005 | 2.0139, 2.0127 2.0102 average 2 | 50 |
| powder γ-ray | identified (the g-value not reported) | 2.008 | 2.0023 | 2.012 | 51 |

# CHAPTER THREE

## Oxidation state of fission fragment iodine in $K_2SO_4$

### Experimental

### 3.1 Introduction

In this Chapter all the experiments which have been carried out on $K_2SO_4$ containing fission fragments are described. The results obtained from these experiments are shown in Chapter 5. Electron spin resonance of $K_2SO_4$ irradiated with fission fragments, neutron, electron and gamma rays are discussed in detail in Chapter 4. The results of ESR were used in Chapter 5 to describe the thermal annealing behaviour of iodine fission fragment in $K_2SO_4$.

### 3.2 Assembly used for neutron irradiation

Analar grade $K_2SO_4$ was ground to powder and kept in a desiccator for a few days before sending to the reactor. 0.3 grammes of $K_2SO_4$ were used in each sample. The source of fission fragments was a film of enriched $U_3O_8$ (80% $^{235}U$) prepared as described in 3.3. The uranium film was uniform and of such thickness that the self absorption of the fission product iodine was insignificant. This thickness was made less than 10mg/cm$^2$, the maximum range of fission fragment in $U_3O_8$ (3). The amount of uranium (see section 3.3) was enough to produce measurable amount of iodine isotopes of fission fragment at the end of irradiation. In order to prevent problems of the reactor operation and handling the irradiated samples, a suitable amount of $U_3O_8$ was used. A backing disc of platinum with diameter 12.72 mm and thickness 0.113mm was used. Platinum was chosen because it does not corrode in the acid used to mount the film. It has a melting point of 1760$^{o}$C and will not oxidise at this temperature.

The potassium sulphate was placed in a small polythene capsule with an internal diameter of 12.5mm and a height of 5mm. The uranium film was placed on the top of the $K_2SO_4$ powder. During the fission process material

tends to be ejected from the surface of the material in which it occurs (52). To prevent spluttered material being transferred from the $U_3O_8$ film to the $K_2SO_4$, a thin layer of aluminium foil was placed across the top of the potassium sulphate (thickness of aluminium foil = $7.62 \times 10^{-3}$mm). The thickness of aluminium foil was much less than the maximum range of the fission fragments in aluminium (3), so that an insignificant number of the fission fragments were absorbed by the aluminium. The polythene capsule containing potassium sulphate and uranium film separated by aluminium was sealed and placed in a second polythene container and sent to reactor for irradiation as described in section 3.7.

## 3.3 Preparation of triuranooctoxide film ($U_3O_8$)

The method used for coating the surface of a platinum disc with a uniform layer of $U_3O_8$ was based on references (53) and (54).

The platinum disc first placed in aqua regia and heated until the polished surface had been etched and the grain boundaries could be seen. These probably provide an anchorage for the first layers of atoms. The platinum disc was rinsed with distilled water and dried with $CHCl_3$. It was then placed in a furnace at ∿750-800°C for five minutes, in order to expel impurities from the surface, and then allowed to cool. The $U_3O_8$ film was made from a solution of uranyl sulphate (80% enriched $^{235}U$), with a concentration of 48.3542 mg/ml in 0.2M $H_2SO_4$ (see next section for determination of concentration of uranyl sulphate). This solution had been prepared in the laboratory from a mixture of enriched uranium dioxide and trioxide which was supplied by the Atomic Energy Authority at Dounreay, Scotland. The diluted solution (20λ) of uranyl sulphate with a concentration of 2.4176 μg/λ was pipetted onto the surface of the disc. The micropipette was washed with distilled water and the washings were also distributed over the disc (∿10λ). A solution of polyvinyl acetate in acetone, 0.005 g/ml, was added (10λ) and this acted as a spreading and adhesive agent. The disc was dried under a heat lamp for a

few minutes, and then transferred to a furnace at ∿750-800°C for 5 minutes. The polyvinyl acetate volatilised and the uranyl sulphate was converted to $U_3O_8$ at this temperature (55). The colour of $U_3O_8$ ranges from olive-green to black-green. $U_3O_8$ is thermally stable in the temperature range 650-900°C, and complete conversion to uranium dioxide ($UO_2$) does not occur below 2000°C (56). The disc was cooled and kept in a desiccator.

(A) Spectrophotometric determination of the concentration of uranium in uranyl sulphate solution.

A spectrophotometric method (57) was used for determination of the uranium concentration. Standard solutions of uranyl nitrate (analar grade) were made with a concentration range of 64 µg/ml - 256 µg/ml. The same amount of ammonium thiocyanate was added to the standards and unknown solution. The standards and unknown solutions were made in 0.2M $H_2SO_4$. Sulphuric acid (0.2M) was used as a blank. The optical densities of the solutions were measured in a Unicam SP500 spectrophotometer at a wave length of 365 mµ. The results are shown in Table 3.1 and a curve of the optical density against concentration is shown in fig. 3.1. After correction for dilution the concentration of uranium in uranyl sulphate was determined as (29.166 mg/mL).

| Concentration µgm/mL | O.D |
|---|---|
| 64 | 0.225 |
| 128 | 0.45 |
| 192 | 0.62 |
| 256 | 0.9 |
| Obtained from curve | unknown |
| 70 µgm/mL | 0.25 |

Table 3.1
Optical density readings of the standards and unknown solutions of uranium

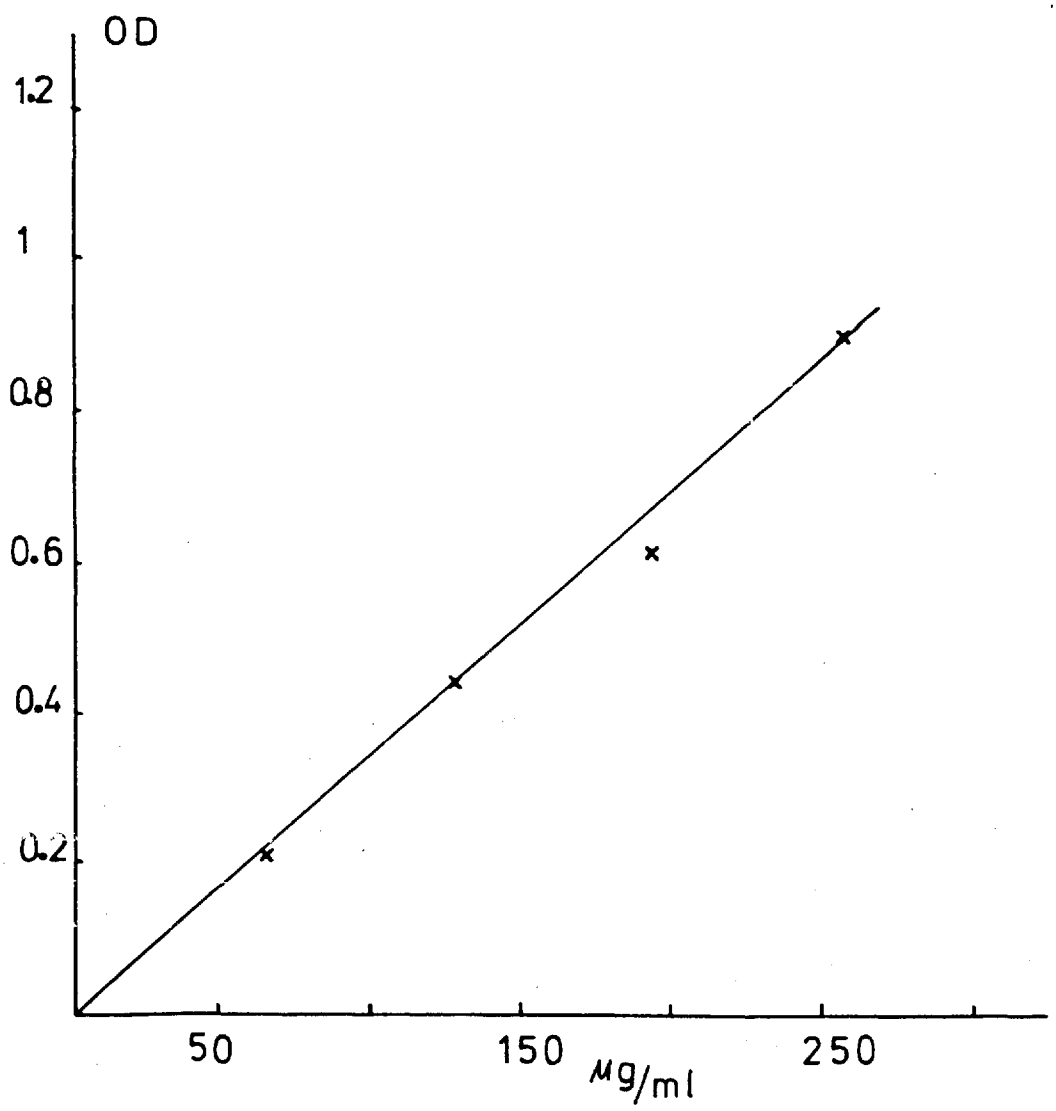


Fig. 3.1 Spectrophotometric determination of uranium in uranyl sulphate

## 3.4 Description of the University of London nuclear reactor

The University of London Reactor Centre, near Ascot, is a light water experimental reactor of 100 Kw (thermal) maximum power. The reactor has several tubes at different locations, these tubes pass down into the core and allow samples to be irradiated under different conditions. Most of the samples in this work were irradiated at core tube number 2 at position 6 with a thermal neutron flux of $0.7 \times 10^{12}$n $sec^{-1}$ $cm^{-2}$. The temperature of this position was $\sim 42^{o}C$. In some cases samples were irradiated in ICIS (In core irradiation system), the flux of the thermal neutron at this position was $\sim 2 \times 10^{12}$n $sec^{-1}$ $cm^{-2}$ at a temperature of $\sim 51^{o}C$. Reactor dose due to neutrons and $\gamma$-rays has been determined (62) by calorimetric methods and reported to be $9.32 \times 10^{6}$ rad/hr for carbon and $8.06 \times 10^{6}$ for Fe. The samples were delivered to College the day after irradiation. The samples received from the reactor were kept in the safe for three days (some time shorter), until they became safe for handling.

## 3.5 Description of the Imperial College $^{60}$Co source

The plant arrangement enables six cobalt source holders to be exposed within a shielded cell, the position of the sources in the exposed position being controlled by a variable jig assembly suspended from the ceiling. The activity of the cobalt source was 8000 curies. Samples were irradiated at the centre of the source, the dose rate at this position was 0.9 Mrad/hr with a fixed jig geometry. (Fricke dosimetry was used for measuring the dose rate).

## 3.6 Description of the Imperial College electron accelerator

The model AS-2000 Van de Graaff Accelerator, manufactured by High Voltage Engineering Corporation, Burlington, Massachusetts, was used in this work. A uniform voltage gradient, developed along the accelerator tube, accelerates the electrons to energies of up to 2MeV. The electron source was a directly heated tantalum cathode whose level of emission was controlled by the emission control unit. The machine was operated at a low pressure

of the order of $10^{-6}$ mmHg. The machine was capable of being run at different powers. The dose rate of the machine was measured using 3mm pieces of red perspex (40340), irradiated by passing them under the electron beam using a conveyor belt. The irradiation conditions were similar to those for the samples. The radiation induced blue coloration absorbing at 640mm was measured spectrophotometrically. The dose rate was found to be 4.57 and 0.49 Mrad/min for beam current of 200μA and 25μA, respectively.

## 3.7 Irradiation of $K_2SO_4$ in the reactor

The assembly described in section ( 3.2 ) was sent to the reactor for irradiation. Most of the samples were irradiated in core tube 2 at position 6 with a neutron flux of $0.7 \times 10^{12}$ n $sec^{-1}$ $cm^{-2}$ for about 7.5 hours. A few samples were irradiated in ICIS position with a neutron flux of $2 \times 10^{12}$ n $sec^{-1}$ $cm^{-2}$ for different times to study the dose effect (see Section 3.19). The active samples containing fission fragments were delivered to the College the day after irradiation. The samples were kept in the safe for about 48 hours in order to become safer for handling.

## 3.8 Carrier solution and exchange reactions

The amount of fission product iodine entering $K_2SO_4$ is so small (see Appendix 1) that no chemical analyses can be achieved. If $K_2SO_4$ containing fission fragments is added to the inactive carrier solution of potassium iodide and iodate, exchange will take place between active and inactive atoms in the same oxidation state. This leads us to an active solution which is of sufficient concentration to be analysed by chemical means.

Iodine can exist in aqueous solution as $I^-$, $I_2$, $IO_3^-$ and $IO_4^-$. Exchange has been reported between the different oxidation states (58); the results are shown in Table 3.2.

Table 3.2 Exchange reactions for iodine ions in aqueous solutions (58)

| Reactants | Temp°C | Other conditions | Separation method | $t_{\frac{1}{2}}$ exchange |
|---|---|---|---|---|
| $IO_3^- - I^{*-}$ | 50 | neutral solution | acidified $I_2$ in $C_6H_6$ | >30y |
| $I_2 - I^{*-}$ | RT | - | $I_2$ in ether | <15S |
| $IO_3^- - I_2^*$ | 25 | 0.099f $HIO_3$, $7 \times 10^{-4}$f $I_2$ | $I_2$ in $CCl_4$ or $CHCl_3$ | 280 ± 4 h |
| $IO_3^- - I_2^*$ | 25 | 0.020f $NaIO_3$, $6.7 \times 10^{-4}$f $I_2$, 1.0f $HClO_4$ | $I_2$ in $CCl_4$ | 208h |
| $IO_3^- - I_2^*$ | 25 | 0.01f $NaIO_3$, 0.001f $I_2$, 1.5f $H_2SO_4$ | $I_2$ in $CHCl_3$ | 216 ± 8hr |

From Table 3.2 it can be seen that exchange is fast between $I_2$ and $I^-$ and is very slow between $IO_3^-$ and $I^-$. The exchange between $I_2$ and $I^-$ has been confirmed by Waller and Walton (6). They did not observe any exchange between $IO_3^-$ and $I^-$. In this work any periodate present was expected to be extracted with the iodate fraction. This was suggested from the results reported in the literature and from the experimental results of this work. The aqueous residue was counted for iodine activity after the extraction procedure, with negative results. This indicated that the carrier solution of iodide and iodate was sufficient, and that no appreciable amount of fission product iodine was being lost as iodine in an unusual oxidation state in aqueous solution. From the literature, it was found that in the presence of excess iodide, periodate is reduced to iodine according to the following equation (66).

$$IO_4^- + 7I^- + 8H^+ \longrightarrow 4I_2 + 4H_2O \qquad (3.1)$$

The rate constant for the reaction is reported to be $5.7 \times 10^{-9}$ M/min. It can be seen from this value that negligible reduction would be expected.

The first step in the above reaction is the intermediate formation of iodate:

$$IO_4^- + 2I^- + H_2O \longrightarrow IO_3^- + I_2 + 2OH^-$$

It was found (58,73) that when radioactive iodide was used, the iodine produced was also active but the iodate remained completely inactive. This proved that it was produced entirely from inactive periodate. Since no activity remained in the original solution after analysis, it was assumed that any periodate present would be reduced to iodate.

## 3.9 Analysing the irradiated $K_2SO_4$ containing fission fragments

Iodine forms a unique complex with $CCl_4$, which is characterised by a strong pink colour, and is visible to concentration of 2.54 PPM (59). Repeated extractions between fresh aqueous and organic volumes allow almost 100% separation from other fission products.

Analar grade KI and $KIO_3$ were used for preparation of the carrier solution. The concentrations of the carrier solutions were enough to change the colour of $CCl_4$, but were not sufficient to saturate the organic phase. Neutral solution of KI and $KIO_3$ have been reported (59) to be very stable, but air oxidation of iodide increased rapidly with decreasing pH and is catalysed by strong sunlight. The prepared carrier solution was kept in the dark, in order to eliminate any possible reactions.

Carrier solution of KI, 0.0083 M (5ml) and $KIO_3$, 0.0051M (5ml) were pipetted into a beaker and diluted with 10ml of distilled water. The active sample was added to the solution and mixed. When the $K_2SO_4$ was completely dissolved the solution was added to Analar grade $CCl_4$ (10ml) in a separating funnel, 0.2 M $H_2SO_4$ (3ml) were added to acidify the solution, according to the following equation (67).

$$5\ I^- + IO_3^- + 6H^+ \longrightarrow 3I_2 + 3H_2O \qquad (3.2)$$

The concentration of the iodate was in excess to permit all the iodide activity to be extracted as iodine in $CCl_4$ layer. The iodine produced was separated out with two more 10ml portions of $CCl_4$, which was collected in the stoppered flask with the first $CCl_4$ extract.

The two phases obtained were: (A) - organic layer containing fission product iodine with carrier in the reduced form. The activity in phase (A) was not purely due to iodide activity, according to equation (3.2), a fraction of iodate activity will also be oxidised to iodine. (B) - the aqueous layer, containing the iodine with carrier in the oxidised form.

A solution of 0.2M $Na_2SO_3$ (15ml) was added to the organic layer in order to reduce the iodine (in the organic complex) to iodide. The organic layer free of iodine was discarded. A mixture of $NaNO_2$ and $HNO_3$ was added to oxidise the iodide to iodine, which was extracted again with three portions of (10ml) $CCl_4$. This was repeated twice in order to obtain optimum separation of $I_2$ from the other fission fragment elements. Iodine in $CCl_4$ was collected in the 30ml glass container specially prepared for counting the active solution. In a few experiments, iodine after purification was converted to iodide and then acidified slightly with nitric acid (0.1 N $HNO_3$) and a few drops of 0.1 M $AgNO_3$ were added to precipitate the iodine as AgI. The solution was heated to coagulate the precipitate and filtered through a suction filter. The precipitate was washed three times with 5 ml portions of alcohol and dried with the same amount of ether; it was mounted on a Planchette, dried under the heat lamp to constant weight, covered with cellotape and counted.

$CCl_4$ (10mL) was added to aqueous layer (B), then carrier solution of excess KI (5mL) 0.0172M was added to extract the iodate as iodine according to the above equation. The same procedure as described above was used for purifying $I_2$ from fission fragments. Since no significant difference was observed in counting iodine as $CCl_4.I_2$ and AgI, all the samples after analyses were counted as $CCl_4.I_2$. Counting iodine as $CCl_4.I_2$ had several

advantages. The time of analysis for each sample was reduced, it became possible to analyse more samples, and also the errors introduced by precipitating AgI were eliminated.

## 3.10 The isotopes used and their decay schemes

Most of the samples after irradiation were stored for at least three days. Therefore the isotope used in the experiments were required to have half lives long enough for their detection after this cooling time. The isotopes used in this work are shown in Table 3.3 with their principle $\gamma$-energies and % total disintegration (60).

The most suitable isotopes were $^{131}I$, $^{133}I$. The precursors for $^{131}I$ and $^{133}I$ should all have decayed away at the time of analysis. Therefore the correct values to use for the fission yields for these isotopes will be their cumulative yields. $^{132}I$ with a half life of 2.26h was also used in some of the experiments. $^{132}I$ mainly produced by $\beta$-decay of $^{132}Te$ ($t_{\frac{1}{2}}$ 77.7 hrs) after irradiation. To work out its activity at the end of irradiation, the half life of the $^{132}Te$ was taken into account. The corrections for calculation of the $^{132}I$ activity is discussed in detail in Appendix 2. Table 3.4 shows the decay scheme for each isotope (2).

## 3.11 Description of the Germanium detector used for counting the active samples

A Germanium detector connected to a multi-channel analyser was used for counting the samples. Resolution of the detector was $\sim$2Kev. The detector was used for detection of $\gamma$-rays with energies between 0.364 and 1.28 MeV. A typical spectrum obtained is shown in fig. 3.2. The area under the peaks was measured and the backgrounds were subtracted using Covell's method (61). The detector was each time calibrated using standard sources of $^{133}Ba$, $^{137}Cs$, $^{57}Co$, $^{60}Co$ and $^{54}Mn$. Half lives, principal photon energies, percentage total disintegration and channel number for each standard source are shown in Table 3.5. A calibration curve of energy against channel numbers is also shown in figure 3.3.

Table 3.3 The iodine isotopes used, with their principle γ-energies and % total disintegration

| Isotope | Half life | Principal photon energies (MeV) | % total disintegration |
|---|---|---|---|
| $^{131}$I | 8.05 d | Xe X-rays | |
| | | 0.08 | 2.6 |
| | | 0.284 | 5.4 |
| | | 0.364 | 82 |
| | | 0.637 | 6.8 |
| | | 0.723 | 1.6 |
| $^{132}$I | 2.26 h | 0.24 | 1.0 |
| | | 0.52 (complex) | 20.0 |
| | | 0.67 (complex) | 144.0 |
| | | 0.773 | 89 |
| | | 0.955 | 22.0 |
| | | 1.14 (doublet) | 6.0 |
| | | 1.28 | 7.0 |
| | | 1.40 (complex) | 14.0 |
| | | 1.45 | 1.0 |
| | | 1.91 | 1.3 |
| | | 1.99 | 1.3 |
| $^{133}$I | 20.3 h | 0.53 | 90.0 |
| | | (Daughter radiations from $^{133}$Xe, $^{133m}$Xe) | |
| $^{135}$I | 6.68 h | 0.42 | 7.0 |
| | | 0.86 | 11.0 |
| | | 1.04 | 9.0 |
| | | 1.14 | 37.0 |
| | | 1.28 | 34.0 |
| | | 1.46 | 12.0 |
| | | 1.72 | 19.0 |
| | | 1.80 | 11.0 |
| | | (Daughter radiations from $^{135m}$Xe, $^{135}$Xe) | |

Table 3.4 Decay schemes for isotopes

| Mass No. | Atomic No. 51 | 52 | 53 | 54 | 55 | 56 |
|---|---|---|---|---|---|---|
| 131 | 21.0 mSb (2.7) ~15% → 30 hTe 0.44 ↓ ; ~85% → 24.8 mTe 2.9 → 8.05 dI 2.9 → 1% → 12 dXe 0.03 ↓ ; 99% → Stable Xe | | | | | |
| 132 | 1.9 mSb (3.4) → 77 hTe 4.4 → 2.4 hI 4.4 → Stable Xe | | | | | |
| 133 | 4.1 mSb (3.8) ?% → 63 mTe 4.6 ↓ ; ?% → 2 mTe 6.0 → 20.8 hI 6.5 → 2.4% → 2.3 dXe 0.16 ↓ ; 97.6% → 5.27 dXe 6.5 → Stable Cs | | | | | |
| 135 | | < 2 mTe (4.2) → 6.68 hI 5.9 → 30% → 15.6 mXe 1.8 ↓ ; 70% → 9.13 hXe 6.2 → 3.0 x $10^6$ yCs 6.2 → Stable Ba | | | | |

Fig. 3.2 γ-Ray spectrum of fission product iodine

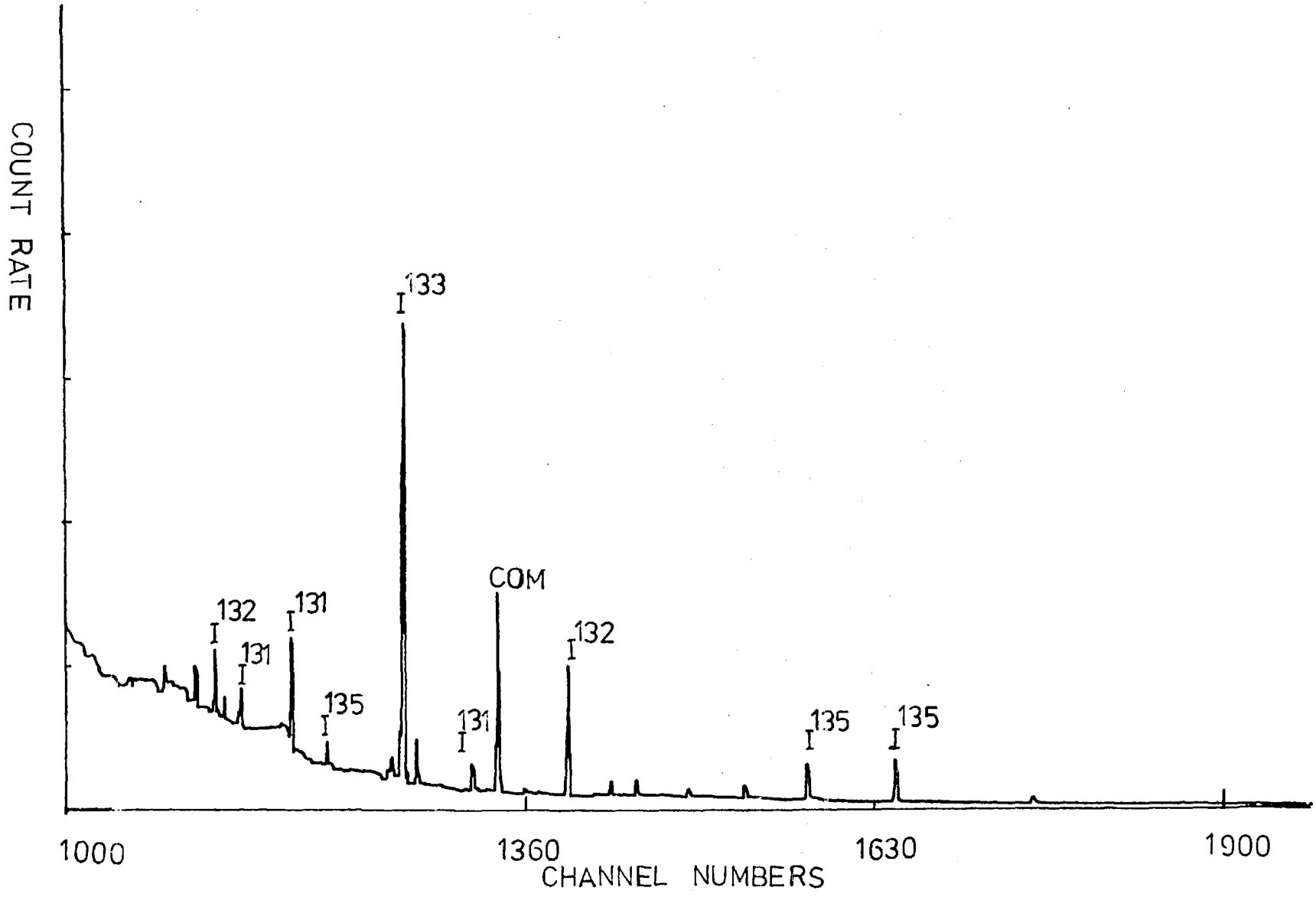

# Fig 3.3
# CALIBRATION CURVE

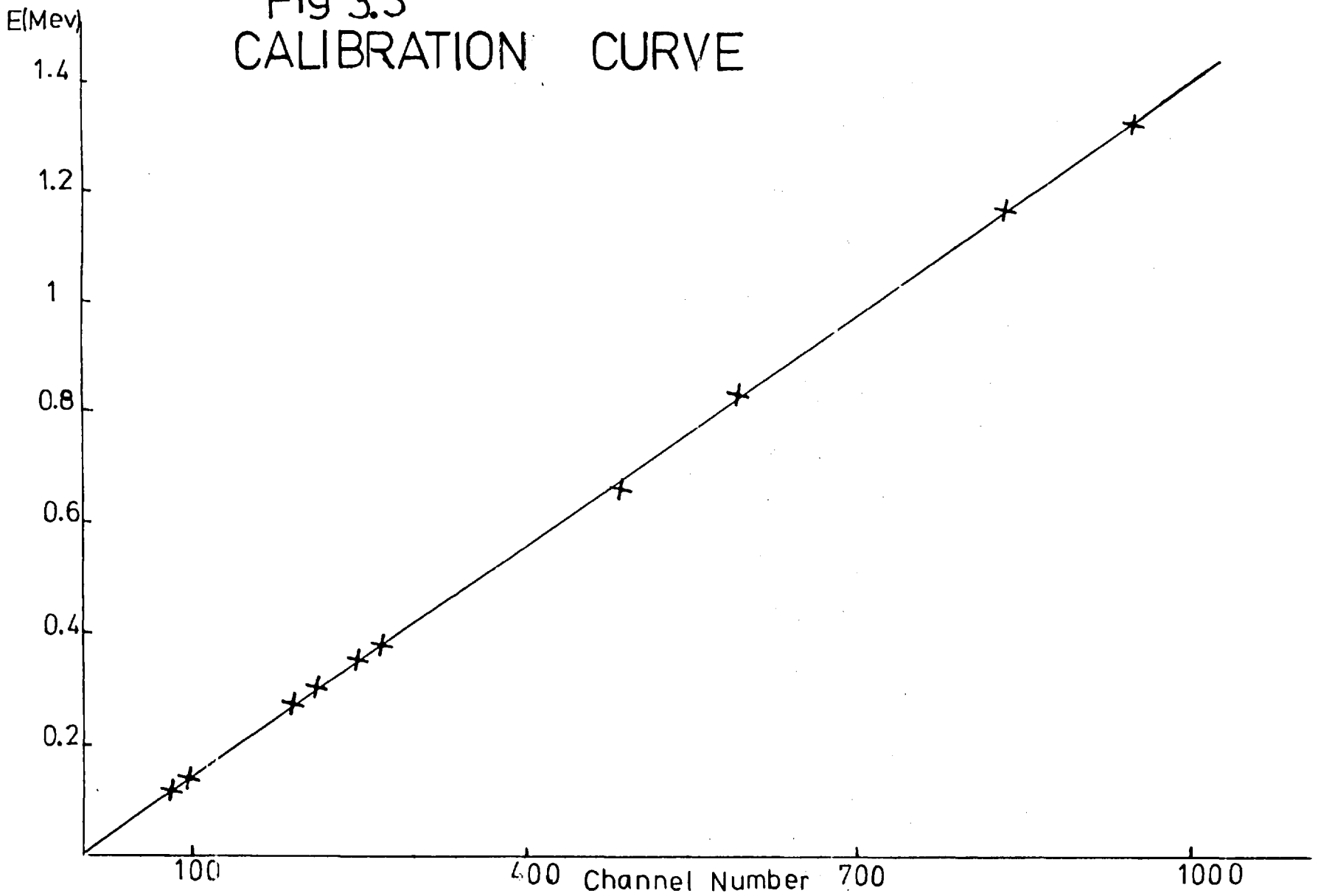

Table 3.5 The standard sources used for calibration

| Isotope | Half life | Principal photon energies (Mev) | % total disintegration | Channel no. |
|---|---|---|---|---|
| $^{57}Co$ | 270.5d | 0.122 | 85.2 | 78 |
| | | 0.136 | 11.1 | 88 |
| $^{133}Ba$ | 10.8y | 0.276 | 7.1 | 187 |
| | | 0.302 | 18.7 | 206 |
| | | 0.356 | 61.9 | 244 |
| | | 0.382 | 8.9 | 264 |
| $^{137}Cs$ | 30.1y | 0.662 | 85.1 | 478 |
| $^{54}Mn$ | 312.5d | 0.835 | 100 | 586 |
| $^{60}Co$ | 5.27y | 1.173 | 99.86 | 828 |
| | | 1.333 | 99.98 | 942 |

(A) Detection efficiency determination

Percentage detection efficiency of Ge detector for isotopes with energy range from 0.122 to 1.33 MeV were determined. Standard sources were used and they were counted at distances of 5 and 9cm from the crystal and also close to crystal. Curves of percentage detection efficiency against energy are shown in fig. 3.4. Samples were usually counted close to the detector. When samples had high activity, to prevent high deadtime, (although dead time correction was considered for each sample), they were placed at distances of 5 or 9cm from the crystal and then counted. Percentage detection efficiency (DE%) for the standard and iodine isotopes for different distances are shown in Table 3.6.; from this table it can be seen that as the distance increases the DE% decreases. All the liquid samples were counted in the same container where the correction for distance should be a constant factor. The efficiency curves plotted with standard sources did not represent the absolute efficiency of the liquid samples. However this was not required in the final analysis of the samples and would not affect the results, since it was a constant factor throughout.

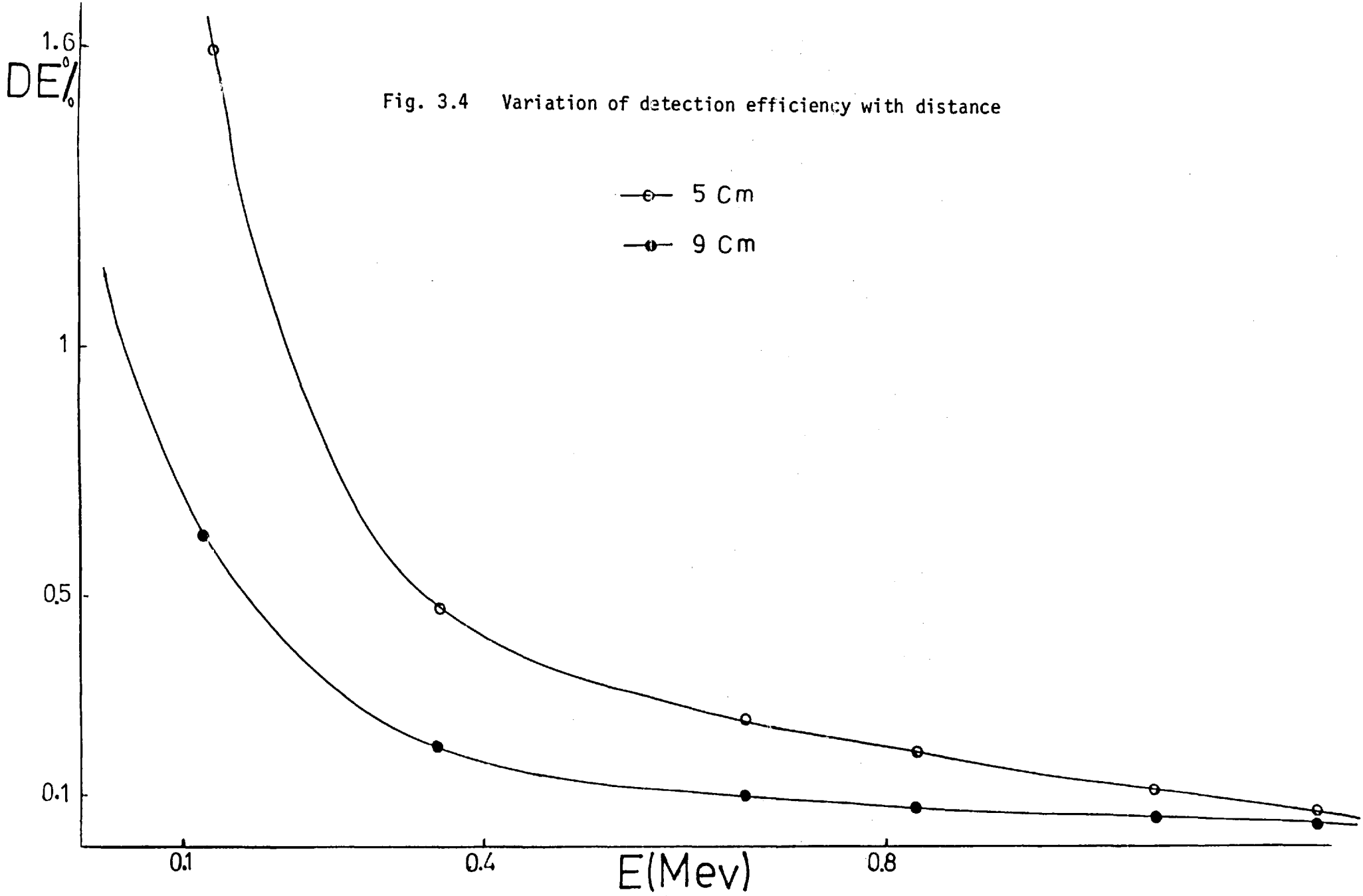


Fig. 3.4 Variation of detection efficiency with distance

Table 3.6 Percentage detection efficiency for different isotopes at different distances from the detector.

| Isotope | E(MeV) | DE% close to crystal | DE% 5cm from crystal | DE% 9 cm from crystal |
|---|---|---|---|---|
| $^{57}Co$ | 0.122 | 11.9 | 1.6 | 0.61 |
| $^{133}Ba$ | 0.356 | 3.05 | 0.45 | 0.19 |
| $^{137}Cs$ | 0.662 | 1.639 | 0.24 | 0.10 |
| $^{54}Mn$ | 0.835 | 1.4 | 0.18 | 0.08 |
| $^{60}Co$ | 1.17 | 0.902 | 0.1 | 0.06 |
| | 1.33 | 0.767 | 0.064 | 0.05 |
| $^{131}I$ | 0.364 | 3 | 0.46 | 0.19 |
| $^{133}I$ | 0.53 | 1.7 | 0.3 | 0.12 |
| $^{132}I$ | 0.77 | 1.3 | 0.2 | 0.08 |
| | 1.14 | 0.9 | 0.1 | 0.06 |
| | 1.28 | 0.8 | 0.07 | 0.05 |

3.12 Decay curves of the isotopes $^{131}I$, $^{132}I$, $^{133}I$ and $^{135}I$

In order to make sure that the isotopes used were correct and were isotopically pure, the decay curves were plotted for each isotope on log -linear graph paper. The decay curves for isotopes used in the experiments are shown in Fig. 3.5. The samples were counted at characteristic $\gamma$-ray energies as $I_2$ in $CCl_4$. No interference from other isotopes with similar $\gamma$-ray energies was detected.

3.13 Determination of the activity of iodine as iodide and iodate

The calculation required to find the distribution of the active iodine atoms between the iodide and iodate states, is divided into two sections.

(A) To find the experimental activity from the count rate.

The counts produced by $\gamma$-ray photons was recorded by the Ge detector were stored as an integer in a channel location whose position was determined by the photon energy. The peaks were analysed by the method of summing under the peak and subtracting the background compton effect. The latter was found by averaging the first and last channel number in the peak and multiplying by the number of channels used. Each iodine isotope has several peaks with different energy and percentage intensities, therefore for each isotope the peak with the highest intensity was chosen, as follows: 0.364Mev (82%) $^{131}I$, 0.53Mev (90%) $^{133}I$, 0.773Mev (89%) $^{132}I$ and 1.14Mev (37%) $^{135}I$. The determination of the DE% is described in the section 3.11A. Knowing the percentage intensity for each isotope and the DE% the activity for each particular isotope can be calculated as follows:

$$\lambda N = \frac{a}{DE\% \times int\%}$$

where a is (area of the peak-background)/counting time

It is usual to take the end of the irradiation as a reference point, and so all activities (apart from $^{132}I$) were worked out relative to this time using the following equation:

$$A = A_o \; e^{-\lambda t} \qquad (3.3)$$

For correction of the activity of $^{132}I$ see Appendix 2.

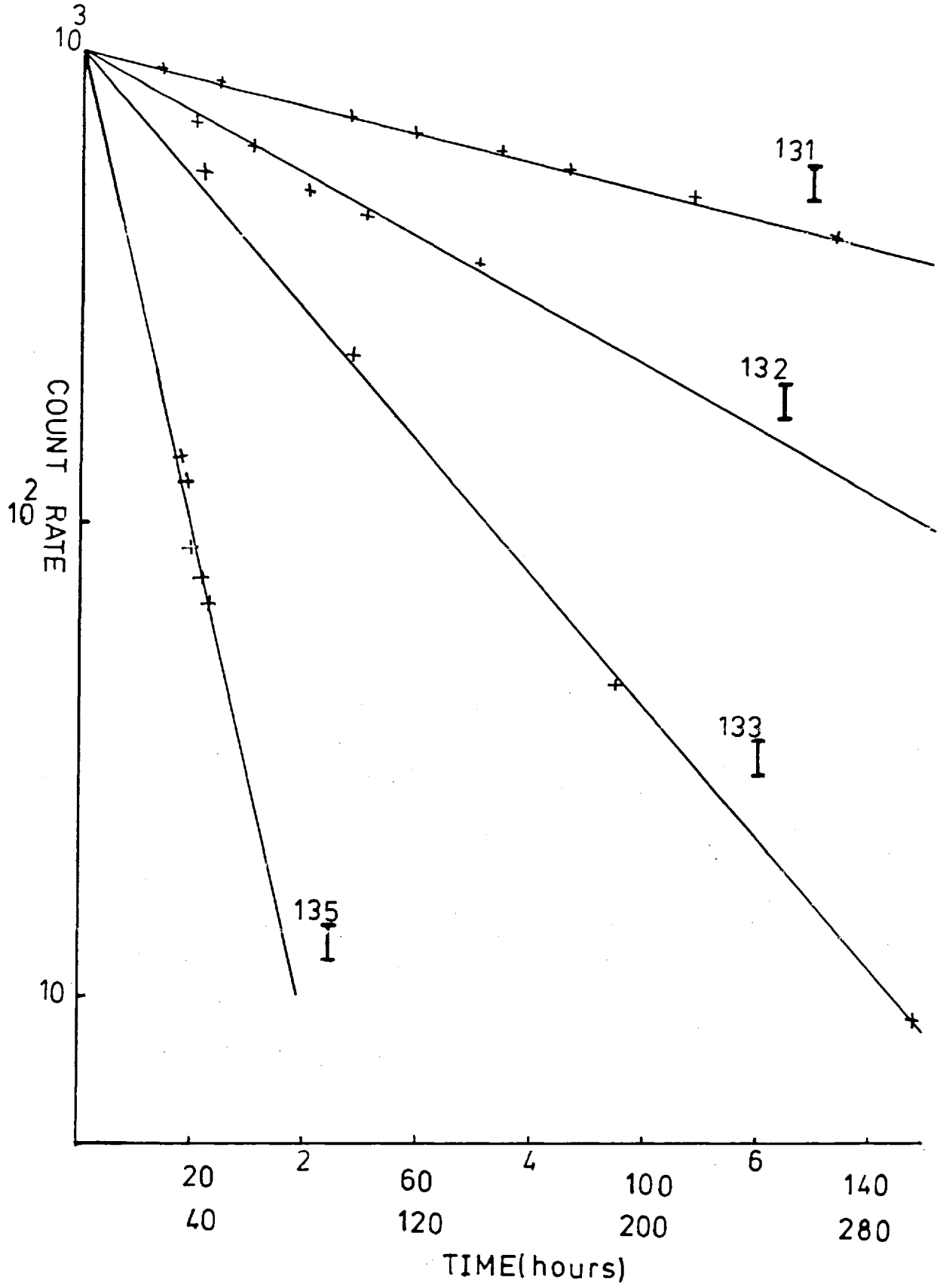


Fig. 3.5 Decay curves of the isotopes $^{131}I$, $^{132}I$, $^{133}I$ and $^{135}I$

(B) Specific and fractional activities

(I) Specific activities

The specific activity for each state is defined as the activity per gm of iodine in the carrier solution for each state. The activities in the two extracted solutions A and B were computed according to part (A) of this section. The activity in B was due entirely to iodate, and activity in A was due to iodide ions and a small amount of iodate ions. The activity was separated as described in Appendix 3.

(II) Fractional activities

The determination of the fractional activities for iodide and iodate for each isotope was carried out by dividing the activity of each state by the total activity of iodide and iodate.

(III) Computer program used for calculations

A computer program in Fortran was written to calculate the activity in each fraction (A and B), the specific activity and fractional activity for each state. The program and a typical output are shown in Appendix 3.

3.14 Thermal annealing of $K_2SO_4$ containing fission fragments

Thermal annealing of $K_2SO_4$ containing fission fragments was carried out at different temperatures and different times. Active samples containing fission fragments were mixed (see Appendix 1 for calculation of the range of fission fragments in $K_2SO_4$) and then transferred to a boat crucible and placed in a cool furnace. The active sample placed directly in a hot furnace was spread over the inside of the furnace, because of the thermal shock. To prevent this the active samples were placed in the cool furnace whose temperature was slowly raised. The furnace was connected to a temperature controller. Thermocouple was in good thermal contact with the boat crucible as near as possible to the active sample. Samples were annealed at 100, 200, 300, 350, 400 and 450$^{o}$C for different times. No change in the fractional activity of iodate has been observed at temperatures up to 300$^{o}$C

for annealing times as long as 1 hour. After this observation thermal annealing was carried out in a temperature range of 350 to 450 $^{o}$C.

To work out the time of annealing at certain temperatures, the time which the sample has been in the furnace was subtracted from the time that the furnace reaches 300$^{o}$C (since no change has been observed below this temperature). The sample was taken out from the furnace after annealing and left to cool to room temperature. The annealed samples were then analysed as described in Section 3.9.

3.15 Test on the release of active iodine during thermal annealing

The following experiment was carried out to check that no significant amount of radioiodine was released during thermal annealing. Sample of $K_2SO_4$ containing fission fragments was mixed and transferred to a boat crucible and placed in the furnace. The silica tube inside the furnace was connected to three tubes containing KOH solution; the third tube was connected via an empty bottle to a water pump, as shown in fig. 3.6. The silica tube on the right hand side was connected to the compressed air line. During thermal annealing a very slow flow of the air passed over the sample and the released iodine transferred by air was dissolved in the KOH (0.1M) solution (10ml in each tube), the second and third tube was used to ensure that all the iodine had been absorbed. During the annealing process the water pump was sucking air, over the sample and the empty bottle was used in case the water pump sucked back. After annealing the KOH solution from three test tubes was transferred to the glass container and the activity was measured. The experiments were carried out at different temperatures and times.

The KOH solution used for collecting the radioiodine was first tested for the effect of air flow on the release of iodine from the solution. 0.3172gm of iodine (inactive) was dissolved in 250ml KOH (0.1M), to 30ml of this solution 4ml of $H_2SO_4$ (2M) was added and then titrated with a solution

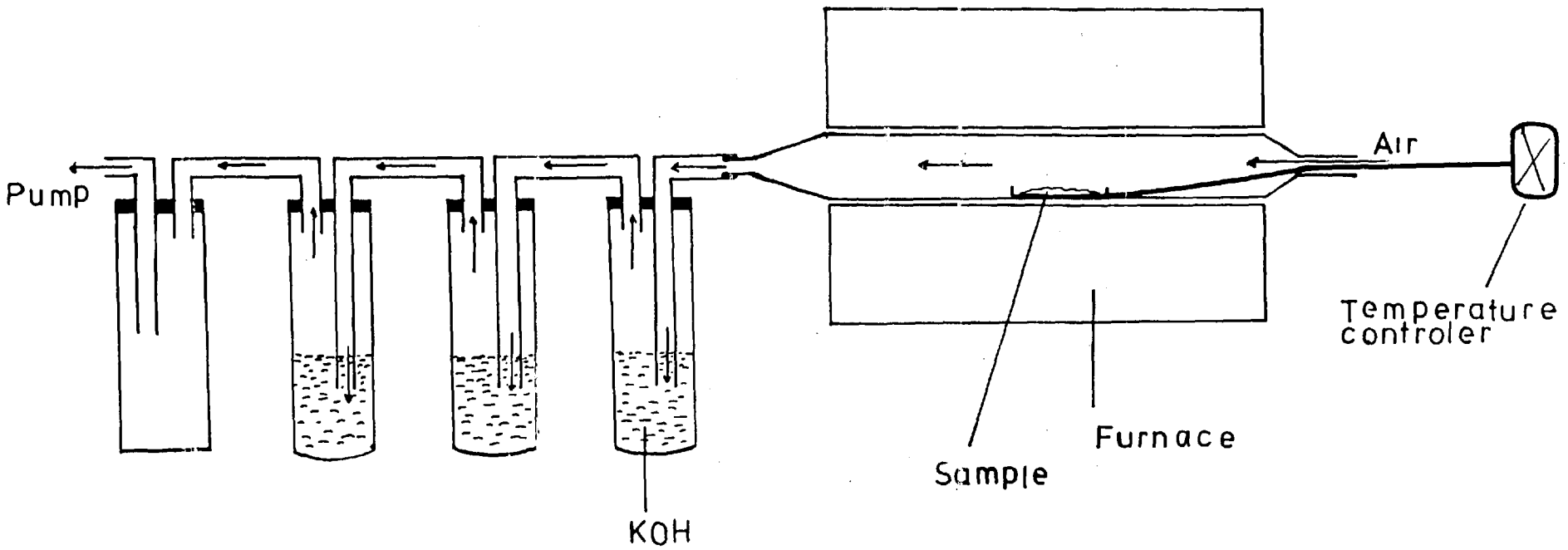


Fig. 3.6 System used for detection of radioiodine during thermal annealing

of $Na_2S_2O_3$ (0.01M). Titration was repeated twice and each time 29ml of $Na_2S_2O_3$ was used to reduced iodine. Another 30ml of KOH solution containing iodine was poured into the test tube and the air passed through for 3 hours, and then the titration was carried out as above. The amount of $Na_2S_2O_3$ used was exactly the same; this suggested that the flow of air did not cause any release of iodine from KOH solution.

3.16 Test of the effects of evacuation on $K_2SO_4$ sample

In order to see the effect of atmospheric oxygen and moisture on the fractional activity of reduced and oxidised form of fission fragment iodine in $K_2SO_4$, an attempt was made to irradiate a sample of $K_2SO_4$ in vacuum. The same assembly as described in Section 3.2 was used in this experiment. After, sealing the small polythene capsule containing $K_2SO_4$ and uranium oxide film, a small hole was made on the lid of the capsule in order to release the air from inside it during evacuation. The small polythene capsule was placed in a silica tube with a diameter of 2.5cm and 18cm length and was held in place by silica wool. The silica tube was connected to a vacuum system and evacuated for 2 hrs at $10^{-5}$mmHg. After evacuation the silica tube was sealed and sent to the reactor for irradiation. The tube was irradiated in the usual position in the core tube for 6.7 hours.

3.17 Test on the effects of dissolving the irradiated sample immediately after irradiation

To check if any annealing occurred during the time between the end of irradiation and measurement, irradiated sample of $K_2SO_4$ containing fission fragments was dissolved in the carrier solutions of iodide and iodate immediately after irradiation, but because of the very high activity of the dissolved sample the solution was kept in a glass tube container and analysed the day after irradiation.

## 3.18 Thermal decomposition of potassium iodate

Thermal annealing of $K_2SO_4$ containing fission fragments showed a significant decrease in the fractional activity of iodate. In order to make sure that this decrease in the iodate was not due to decomposition of $KIO_3$, an attempt was made to study the decomposition of iodate and determined the temperature at which $KIO_3$ started to decompose.

### (A) Thermogravimetric study of decomposition of $KIO_3$

Analar grade of $KIO_3$ (10mg) was used for this experiment. The sample after being dried (kept in a desiccator for a few days) was transferred to the small cup of the thermo balance. The apparatus used for this experiment was a Perkin-Elmer (TG-1) Thermobalance. The heating rate was $10^oC$ per minute. The machine was connected to a chart recorder, and the decrease in weight could be observed from the chart.

### (B) Thermal decomposition of $KIO_3$ after a long annealing time

Although the thermogravimetric study of the decomposition of $KIO_3$ gave results in agreement with the literature (64,65), attempts were made to see if $KIO_3$ does decompose at a temperature lower than that observed when they are annealed for a longer time. Iodide produced by the decomposition of $KIO_3$ was converted to iodine by dissolving the heated sample in an adequate amount of $H_2SO_4$, the iodine released was separated using $CCl_4$, excess KI solution was added to convert $I_2$ in $CCl_4$ to $I_3^-$. $I_3^-$ has an absorption band at 353μm, and can be measured spectrophotometrically. Two samples of $KIO_3$ (weight of each sample about 0.3gm) were heated for an hour at 480 and $500^oC$. Each heated sample was dissolved in 5ml (2M) $H_2SO_4$ and water, then the released iodine was separated by five portions of $CCl_4$ (each portion 10ml) and excess KI solution was added. To prepare the standard solution of iodine (59) 3.567gm of Analar grade $KIO_3$ were dissolved in water and diluted to one liter. 25ml of this solution was treated with an excess of pure KI (0.345gm), followed by 3ml of $H_2SO_4$ (2N). The amount of iodine

released can be calculated from the following equation (Standard solutions with different concentrations were prepared).

$$5KI + KIO_3 + 3H_2SO_4 \longrightarrow 3\ I_2 + 3K_2SO_4 + 3H_2O$$

The absorption of prepared samples and standards were measured in the spectrophotometer at 353μm, and a standard curve of absorbance against concentration was plotted.

3.19 Test of the effect of irradiation time on the observed valency states of fission fragment iodine in $K_2SO_4$

This experiment was carried out to see the effect of irradiation dose on the valency states of fission fragment iodine. Five samples of potassium sulphate with uranium oxide were irradiated with neutron at ICIS ($2 \times 10^{12}$ n $sec^{-1}cm^{-2}$) position for 10, 15, 30, 60 and 120 minutes. The irradiated samples were delivered to the College a few hours after irradiation. The samples were analysed on the same day because of the low activity of the samples(especially the samples with short irradiation time).

3.20 Post-irradiation of $K_2SO_4$ containing fission fragments

Several samples of potassium sulphate containing fission fragments were irradiated by electrons, in a Van de Graaff machine with different beam currents

Platinum discs were removed before irradiation.

(A) - Irradiation with high dose rate

The samples were irradiated by passing them under the electron beam using a moving belt. The beam current of the machine was 200μA. The dose for each pass was 0.838 Mrad per pass. The samples were under the beam for 11 sec in each pass, time for each pass was 22 sec, therefore the dose rate was 4.57.Mrad/min. Seven samples were irradiated at this condition for 5, 10, 20, 62, 142, 202 and 309 mins. The samples were under the electron beam just half of the above times. The samples after irradiation were analysed as described in Section 3.9.

(B) Irradiation with low dose rate

The beam current of the machine was set to 25μA. The dose rate at this setting was 0.49 Mrad/min. Three samples of $K_2SO_4$ containing fission fragments were irradiated with these conditions for 80, 240 and 390 minutes.

3.21 Pre-irradiation of $K_2SO_4$ with γ-rays before fission fragments injection

Seven samples of $K_2SO_4$ before sending to the reactor were irradiated in the centre of the cobalt source for 25, 48, 96, 120, 144, 167 and 237 hours with dose rate of 0.9Mrad/hr. After irradition, the uranium films were placed at the top of the irradiated samples and sent to the reactor with a control sample (not pre-irradiated) for irradiation. The samples after being irradiated by neutrons in the reactor were analysed as described in Section 3.9.

3.22 Pre-irradiation of $K_2SO_4$ with neutrons before fission fragments injection

Four samples of $K_2SO_4$ were sent to the reactor for irradiation. Samples were irradiated for 7.25, 14.5, 21.50 and 29 hours in the core tube number 2 position 6 with neutron flux of $0.7 \times 10^{12}$ n $sec^{-}$ $cm^{-2}$. The active samples were left to cool for 2 days and the uranium film was placed on the top of each sample and sent again to the reactor for further irradiation. Samples were irradiated in the same position for 7.17 hours. The $K_2SO_4$ samples containing fission fragments were analysed after cooling for 3 days.

3.23 Thermal annealing of $K_2SO_4$ containing fission fragments pre-irradiated by electron

Four samples of $K_2SO_4$ were irradiated by electrons using the Van de Graaff machine with a dose rate of 4.57 Mrad/min for 3 hours. The samples were then sent to the reactor for irradiation. After the irradiation they were annealed at a temperature of $400^{0}C$ for 3.5, 7 and 52 mins. They were then analysed in the usual way.

### 3.24 Observation of the colour change in irradiated $K_2SO_4$

All samples of $K_2SO_4$ after any type of irradiation were light pink to pink in colour. During thermal annealing the colour of the sample changed from pink through a succession of different hues to white. A sample of $K_2SO_4$ containing fission fragments was transferred to a boat crucible and placed in the cool furnace. Thermal annealing started at room temperature, between 180 to 320°C the colour of the sample changed very slowly to violet and at around 330°C it started to change to grey, at higher temperatures still the colour of the sample changed to very light grey and finally at about 370°C it became white.

### 3.25 Pre-thermal annealing of $K_2SO_4$ before fission fragments injection

Five samples of $K_2SO_4$ were heated for 1.5 hours at 300, 400, 500, 600 and 700°C respectively. The heated samples and a control ($K_2SO_4$ not being heated) were sent to the reactor for irradiation. The preheated samples containing fission fragments were white in colour, unlike the control which was light pink. But the surface of all samples was light yellow, which was an indication of fission fragment penetration. The samples were analysed in the usual way.

### 3.26 The effects of crushing of $K_2SO_4$ prior to injection of fission fragments

All the experiments described before were carried out with powdered $K_2SO_4$. In this experiment $K_2SO_4$ crystals were not ground to powder. The size of the crystal on average was about $0.5mm^3$ (sugar size). The assembly sent to the reactor for irradiation was as described in Section 3.2.

# CHAPTER FOUR

## Electron spin resonance of irradiated $K_2SO_4$

### 4.1 Introduction

Thermal annealing effect on the $K_2SO_4$ containing fission fragments is discussed in Chapter 5. The results obtained show a significant decrease in the fractional activity of the fission fragment iodine as iodate, and the experiment shows that as the temperature and time of the annealing increases the rate of the reduction of the iodate to the iodide increases. To explain the above observation, an attempt was made to investigate the irradiation products of $K_2SO_4$. Defused reflectance and infrared spectra of irradiated $K_2SO_4$ did not give any useful information. The only absorption band observed in defused reflectance was at 550 nm which was due to the colour of the sample and could not be related to any radical ion. The ESR of irradiated $K_2SO_4$ was carried out, since this method is very suitable for identification of the low concentration of the radical ions. Some work has been reported on the ESR of $\gamma$ and x-ray irradiated $K_2SO_4$, but no work has been reported on the ESR of neutron irradiated $K_2SO_4$ containing fission fragments. The ESR spectra of gamma, electron, and neutron irradiated $K_2SO_4$ were obtained and the results compared with the neutron irradiated $K_2SO_4$ containing fission fragments. Thermal annealing showed a significant decrease in the intensity of the radical ions. The concentration of $SO_3^-$ was measured in $\gamma$-irradiated $K_2SO_4$ and $K_2SO_4$ containing fission fragments. The results obtained in this chapter were used in Chapter 5 to explain the thermal annealing behaviour of iodine fission fragment in $K_2SO_4$.

### 4.2 Experimental

#### 4.2.1 Description of the ESR machine

The machine used in this work was a Varian E12 operating at about 9.2 GHz and the full operating power of the machine was 200 mW ≡ 0dB.

Samples were placed in round quartz tubes 12cm long cooled to -165°C using a Varian variable temperature controller to regular temperature of pure $N_2$ gas precooled in liquid nitrogen. Modulation frequency was 100 KHz.

4.2.2 Type of irradiation of $K_2SO_4$

(A) γ-irradiation

Potassium sulphate powder (0.3 gm) placed in a small polythene capsule (1 cm diameter and 0.5 cm height) was irradiated in the cobalt source with a dose rate of 0.9Mrad/hr for 40 hours. Samples after irradiation were mixed and transferred to the quartz tube (∿4mm diameter and 12cm height) especially made for the ESR machine. The tube was kept in the liquid nitrogen until transferred to the cavity of the machine. The sample was run at liquid nitrogen temperature (-165°C);keeping the sample after irradiation in liquid nitrogen and running at this low temperature was carried out in order to prevent any possible reactions of the radicals.

(B) Electron irradiation

Powder of $K_2SO_4$ (0.3 gm) was irradiated in the van de Graaff (at 200μAm) for one minute with a dose rate of 4.57 Mrad/min. The irradiated sample was mixed and transferred to the quartz tube and kept in liquid nitrogen for the ESR measurement. The sample was scanned at liquid nitrogen temperature.

(C) Neutron irradiation

Powdered $K_2SO_4$ (0.3gm) was placed in the polythene capsule (same size as experiment A) and sealed. The polythene capsule was placed in a second polythene capsule (7cm high and 2.5cm diameter) and sent to a reactor for neutron irradiation. The sample was irradiated in the core tube 2 position 6 for 7 hours at the neutron flux of $0.7 \times 10^{12}$ n $sec^{-1}$ $cm^{-2}$.

(D) Fission fragments irradiation

Assembly as described in Chapter 3 Section 2 was used, in the following experiments. Two samples of $K_2SO_4$ were irradiated for 7 hours (both in

the same capsule) in core tube 2 position 6 ($0.7 \times 10^{12}$ n $sec^{-1}$ $cm^{-1}$). Samples were left to cool for 48 hours and then they were mixed and transferred to the quartz tubes. The tubes were sealed with rubber stoppers and kept in liquid nitrogen for ESR experiments.

Sample (F1)

a) $K_2SO_4$ containing fission fragments was transferred from liquid nitrogen to the cavity of the ESR machine and scanned at liquid nitrogen temperature.

b) The sample was taken out from the cavity and warmed up to room temperature and was replaced in the cavity and again scanned at liquid nitrogen temperature.

c) The sample was taken out from the cavity, warmed up to room temperature, and replaced in the cavity and scanned at room temperature.

d) The sample was taken out from the cavity transferred to the furnace and annealed for 3 hours at 420°C. The annealed sample was scanned at room and liquid nitrogen temperatures.

Case a and c of the above experiment were repeated with another active sample (F2).

### 4.2.3 Quantitative measurement of $SO_3^-$ radical ion in unannealed and thermally annealed $K_2SO_4$ containing fission fragments

Four samples of $K_2SO_4$ enclosed with $U_3O_8$ films (assembly as discussed in Chapter 3.2) were placed in the same tube and sent to the reactor for irradiation. The samples were irradiated in core tube 2 position 6 for 7 hours at a neutron flux of $0.7 \times 10^{12}$ n $sec^{-1}$ $cm^{-2}$. The samples after irradiation were left to be cooled (at room temperature) for nearly 70 hours, then one of the samples (F3) was mixed and transferred to the quartz tube and sealed with a rubber stopper. The rest of the samples were transferred to three boat crucibles and annealed at400°C for 3, 5 and 7 minutes (sample F4, F5 and F6). The unannealed sample and annealed samples were kept at

room temperature for ESR measurements. A solution of copper chloride, 1mmol of $CuCl_2$ in 2M $NaClO_4$ and 0.01 M HCl (0.2066ml) was used as a standard. Care was taken in using equal volumes of standard solution and $K_2SO_4$ powder. All samples were scanned at liquid nitrogen temperature. The data was collected on tape and a computer program was used for calculating the g-values and integrals.

#### 4.2.4 Quantitative measurement of $SO_3^-$ radical ion in γ-irradiated $K_2SO_4$

Powdered $K_2SO_4$ (0.3 gm) was irradiated in the cobalt source (0.9Mrad/hr) for 71.8 hours. The sample was run at liquid nitrogen temperature. The concentration of $SO_3^-$ was determined as described in Section 4.2.3.

### 4.3 Results and discussion on ESR measurements

#### 4.3.1 Radicals observed in irradiated $K_2SO_4$

The g-value for the radical ions were calculated using the following formula (see Chapter 1.3 for more detail).

$$g = \frac{h\nu}{BH}$$

The g-values were calculated by taking DPPH as standard (g = 2.0036). The radicals of $SO_3^-$, $SO_4^-$ (two kinds), $SO_2^-$ and $O_3^-$ have been observed in all types of irradiated $K_2SO_4$. The spectra observed in all samples were almost the same. The g-values of the radicals observed were very similar to those reported in the literature (48-51). Spectra of $K_2SO_4$ containing fission fragments and electron irradiated $K_2SO_4$ are shown in figs. 4.1 and 4.2.

Operating parameter for the sample F2 were as follows:

| | |
|---|---|
| Scan range | ±200 Gauss |
| Field set | 3230 |
| Modulation amplitude | 1 |
| Receiver gain (I) | $2 \times 10^3$ |
| Receiver gain (II) | $2.5 \times 10^2$ |
| Receiver gain (III) | $5 \times 10^3$ |
| Power | 20dB (decibles) |
| Frequency | 9.224 |
| Temperature | $-165^oC$ |

Operating parameters for electron irradiated $K_2SO_4$ were as follows:

| | |
|---|---|
| Scan range | ±100 Gauss |
| Field set | 3230 |
| Receiver gain (I) | $2 \times 10^3$ |
| Receiver gain (II) | $1 \times 10^4$ |
| Modulation amplitude | 1 |
| Power | 20dB |
| Frequency | 9.225 |
| Temperature | -165°C |

As can be seen from figs. 4.1 and 4.2 the spectra were complex. They were resolved by running at different powers and gains. From the several spectra obtained for each sample the radicals identified and the g-values were calculated. The spectra obtained from $K_2SO_4$ containing fission fragments were slightly different compared with the other samples but the same radicals identified. The sample of $K_2SO_4$ containing fission fragments taken out from the cavity and warmed at room temperature for 5 minutes replaced again in the cavity and run at liquid nitrogen temperature, did not show any difference in the spectrum in comparison with the sample which remained in liquid nitrogen all the time. The spectrum obtained from the sample run at room temperature was not as clear as the sample in the liquid nitrogen.

(A) $SO_3^-$ radical ion

The most intense signal observed in all samples was due to $SO_3^-$ radical. As can be seen from figs. 4.1 and 4.2 signal G was identified to be $SO_3^-$ (12). $SO_3^-$ radical ion is isotropic and the g-values obtained from the spectra for four different irradiated $K_2SO_4$ were very close. The g-values are shown in Table 4.1.

(B) $SO_4^-$ radical ions

Two types of $SO_4^-$ radical ions have been observed in all samples. $SO_4^-$ radical is anisotropic and it has three g-values (12). The intensity of this radical ion was much smaller than the $SO_3^-$ radical. The two types of

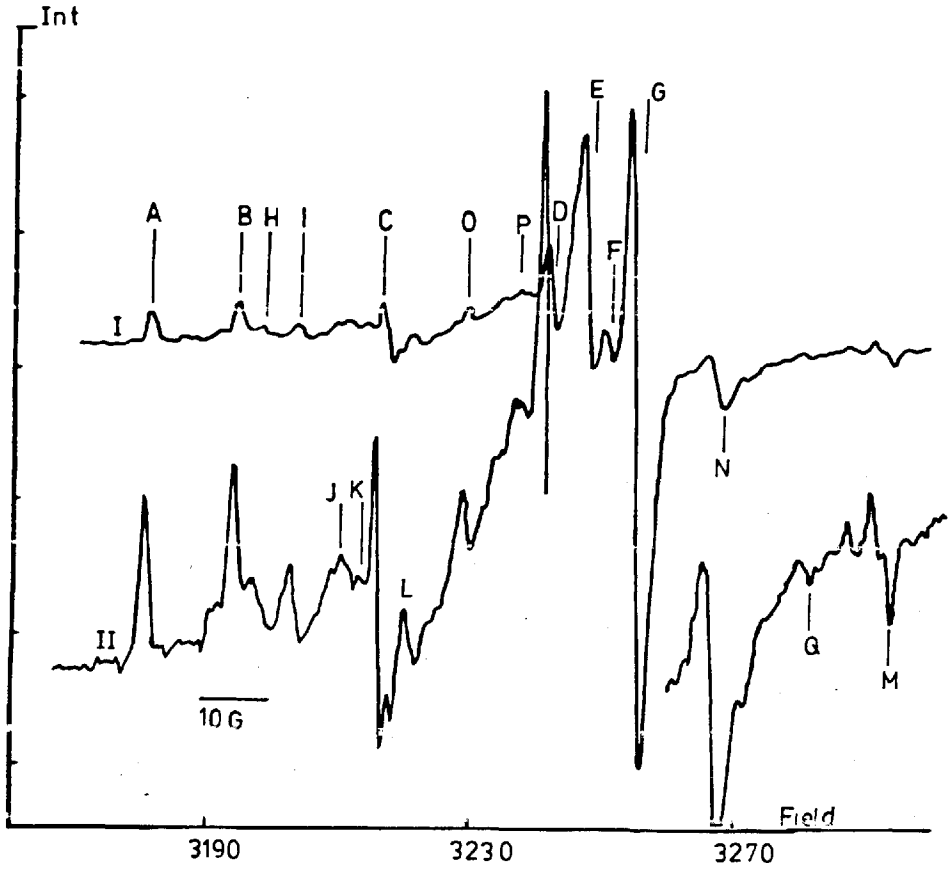


Fig. 4.1 ESR spectra of electron irradiated $K_2SO_4$

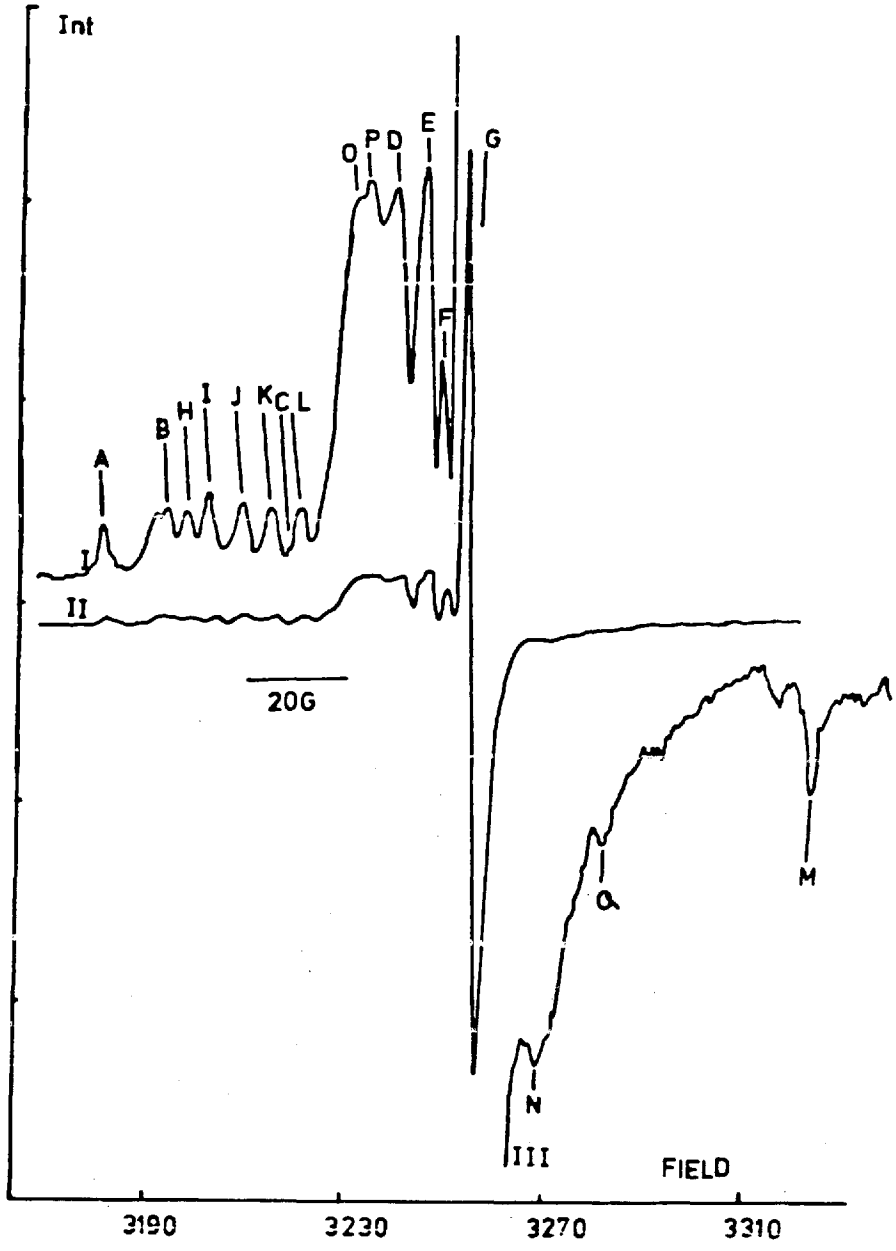


Fig. 4.2 ESR spectra of $K_2SO_4$ containing fission fragments

$SO_4^-$ radical had different g-values, the data are shown in Table 4.2. There are two non-equivalent sites for sulphate ion (50) and this was the reason for observing two kinds of $SO_4^-$ radical.

Table 4.1 The g-value of $SO_3^-$ radical in irradiated $K_2SO_4$

| Type of irradiation | g-value (isotropic) | signal |
|---|---|---|
| $\gamma$-irradiation | 2.0037 | G |
| electron irradiation | 2.0049 | ~ |
| neutron irradiation | 2.0035 | ~ |
| fission fragments (FI) | 2.004 | ~ |
| fission fragment (F2) | 2.0049 | ~ |

Table 4.2 The g-values of $SO_4^-$ (two types) in irradiated $K_2SO_4$

| Type of irradiation | g-value anisotropic | signals |
|---|---|---|
| $\gamma$ -irradiation | 2.050, 2.024, 2.0086<br>2.0416,2.0116,1.994 | A,C,E,<br>B,D,N |
| electron-irradiation | 2.0507,2.028,2.0101<br>2.042,2.0128,1.9955 | " |
| neutron irradiation | 2.0496,2.0244,2.0078<br>2.0414,2.0115,1.9944 | " |
| fission fragments (Fl) | 2.0505,2.026,2.0108<br>2.0418,2.0123,1.9957 | " |
| fission fragments (F2) | 2.0508,2.0268,2.0101<br>2.042,2.0129,1.9950 | " |

(C) $SO_2^-$ radical ions

The $SO_2^-$ radical ion with three principle g-values has been detected in all samples. $SO_2^-$ radical is anisotropic with three different g-values (12). The g-values for different types of irradiation are shown in Table 4.3.

(D) $O_3^-$ radical ions

The radical ion $O_3^-$ has been observed in all samples. $O_3^-$ radical ion is isotropic (12), the g-values are shown in Table 4.4. The signal D in figs. 4.1 and 4.2 belongs to $O_3^-$. Although its wings were masked by the other radicals, it could be identified very easily. Signal E is possibly a mixture of two signals which belong to $SO_2^-$ and $SO_4^-$. Signals H, I, O, P, J, K and M could not be identified.

Table 4.3 The g-values of $SO_2^-$ radical ions in irradiated $K_2SO_4$

| Type of irradiation | g-values anisotropic | signals |
|---|---|---|
| $\gamma$-irradiation | 2.0086,2.0061,1.979 | E,F,Q |
| electron irradiation | 2.0101,2.0076,1.9877 | ∿,∿,∿ |
| neutron irradiation | 2.0078,2.0066,1.9794 | ∿ ∿ ∿ |
| fission fragment (F1) | 2.0108,2.0068,1.9812 | ∿ ∿ ∿ |
| fission fragment (F2) | 2.0101,2.0074,1.9868 | ∿ ∿ ∿ |

Table 4.4 The g-value of $O_3^-$ radical in irradiated $K_2SO_4$

| Type of irradiation | g-value isotropic | signal |
|---|---|---|
| $\gamma$-irradiation | 2.0116 | D |
| electron irradiation | 2.0123 | ∿ |
| neutron irradiation | 2.0115 | ∿ |
| fission fragment (F1) | 2.0123 | ∿ |
| fission fragment (F2) | 2.0129 | ∿ |

### 4.3.2 Results of quantitative measurement of $SO_3^-$ radical ion in irradiated $K_2SO_4$

The results obtained from the experiments described in previous sections showed that the most intense signal observed in irradiated $K_2SO_4$ was due to $SO_3^-$ radical ions. Radicals $SO_3^-$ could play a significant role as an electron donor during the irradiation and particularly during thermal annealing, therefore an attempt was made to measure the concentration of $SO_3^-$ radical ions in $\gamma$-irradiated $K_2SO_4$ and $K_2SO_4$ in which fission fragments have penetrated.

#### (A) Measurement of concentration of $SO_3^-$ radical ion in $\gamma$-irradiated $K_2SO_4$

This experiment was carried out to compare the G-value (number of $SO_3^-$ ions produced per 100 eV of energy absorved) of $SO_3^-$ produced in $\gamma$-irradiated $K_2SO_4$ with the G-value of the fission fragments irradiated $K_2SO_4$. The concentration of the other signals were too small to measure. The experimental spectrum was smoothed with a five point least squares method, to reduce noise level prior to processing. This was not found to alter the shape of the spectrum but gives a more accurate final integrated intensity. The smoothed spectrum was fitted with a simulated curve using the method of Kneubühl (80) in order to give a better idea of the true shape of the $SO_3^-$ signal. In view of this the double integration was performed over a limited region as shown in figs. 4.3 and 4.4. The signal of $SO_3^-$ radical and first integrated signal are shown in figs. 4.3 and 4.4. respectively.

All the operations for smoothing, g-value calculation, drawing the calculated signal and fitting the calculated to the experimental spectrum were done on a graphics terminal using a computer program 82 . Since the ESR signal is a derivative of the actual signal, the double integration value was used for calculation of the concentration of $SO_3^-$ radical ion. The following formula was used for calculating the concentration of $SO_3^-$.

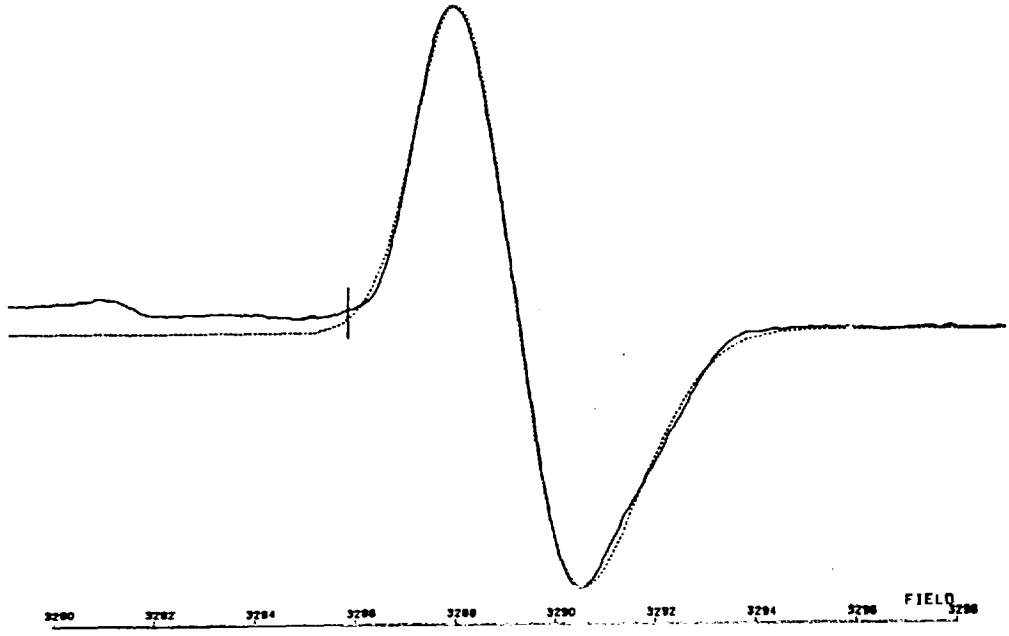


Fig. 4.3 ESR signal of $SO_3^-$ radical in γ-irradiated $K_2SO_4$ (doted lines represent the calculated signal)

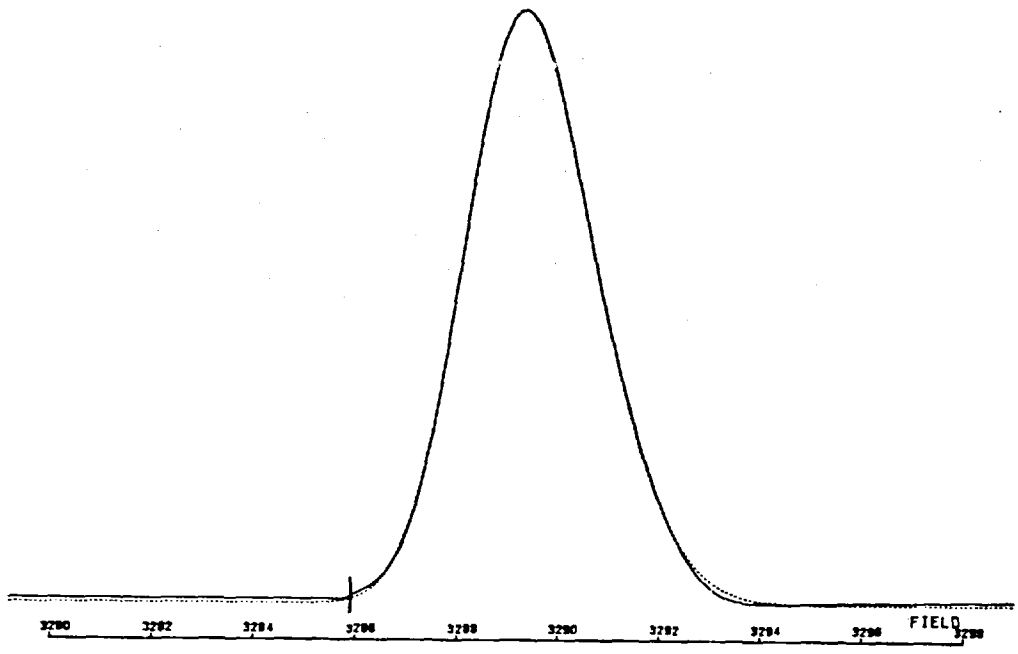


Fig. 4.4 First integrated signal of Figure 4.3

$$\left[SO_3^-\right]_\gamma = \frac{\left[\frac{(Int)^2}{modxRG}\, x(\Delta H)^2\right]_\gamma}{\left[\frac{(Int)^2}{modxRG}\, x(\Delta H)^2\right]_{cu}} x \left[\sqrt{a \log_{10}\left(\frac{P_\gamma - P_{cu}}{10}\right)}\right] x \frac{[CU] x V_{cu} x 1}{WK_2SO_4} \qquad (4.1)$$

where

$SO_3^-{}_\gamma$ is the concentration of $SO_3^-$ in mmole of spin/gm

int is the integral of the signal

mod is modulation amplitude

RG is receiver gain

$\Delta H$ is the field in Gauss

P is the power in decibels

$[CU]$ is the concentration of copper standard solution (in m mol/Lit)

$V_{cu}$ is the volume of the copper solution (Lit)

$W_{k_2SO_4}$ is the weight of the potassium sulphate (gm)

Experimental data for $\gamma$-irradiated $K_2SO_4$ sample

$(int)^2$ = 3.7292

mod = 1

RG = $3.2 \times 10^3$

$(\Delta H)^2$ = $(19.8)^2$ Gauss

P = 46 dB

$WK_2SO_4$ = 0.3 gm

Experimental data for copper standard solution

$(Int)^2$ = 2.1858

mod = 6.3

RG = $6.3 \times 10^2$

$(\Delta H)^2$ = $(1001.4)^2$ Gauss

$P_{cu}$ = 24dB

$V_{cu}$ = $0.2066 \times 10^{-3}$ lit

$[cu]$ = 1 mmoL/lit

The above values are used in equation (4 .1) to give

$\left[SO_3^-\right]_\gamma = 0.7172 \times 10^{-8}$ mole of spin/gm

Number of $SO_3^-$ pre gm sample would be

$0.7172 \times 10^{-8} \times 6.023 \times 10^{23} = 4.3197 \times 10^{15}$ no. of $SO_3^-$/gm

Samples were irradiated in cobalt source for 71.8 hours at a dose rate of 0.9Mrad/hr.

1 Rad = $6.242 \times 10^{13}$ ev/gm

received dose = $64.62 \times 10^6$ rad

$64.62 \times 10^6 \times 6.242 \times 10^{13} = 4.03 \times 10^{21}$ ev/gm

Using the above value $G(SO_3^-)$ could be calculated:

$$\frac{4.3197 \times 10^{15} \times 100}{4.03 \times 10^{21}} = 1.07 \times 10^{-4} \quad SO_3^-/100ev$$

$G(SO_3^-) = 1.07 \times 10^{-4}$ $SO_3^-$/100ev

(B) Measurement of concentration of $SO_3^-$ radials in $K_2SO_4$ containing fission fragments

In the section 3.4 the sensitivity of the $SO_3^-$ radical ion towards thermal annealing is discussed, and it is shown that the concentration of $SO_3^-$ radicals decreases as the time or temperature of annealing increases. Therefore it was necessary to know the initial concentration of $SO_3^-$ in order to compare it with the annealed sample. The second reason for measuring the concentration of $SO_3^-$ was to see if there was enough $SO_3^-$ radicals considered as an electron doner, available for the reduction of iodate (see Chapter 5 for thermal annealing effect on the oxidation state of iodine isotopes). Knowing the concentration of $SO_3^-$ produced in the sample, it is possible to calculate the number of $SO_3^-$ produced by fission fragments.

Experimental data for $K_2SO_4$ containing fission fragments

$(int)^2 = 4.0134$

mod = 1

RG = $1.25 \times 10^3$

$(\Delta H)^2 = (19.8)^2$ Gauss

$P_F$ = 46dB

$WK_{2SO_4}$ = 0.3gm

Experimental data for the copper standard solution were the same as the data used for calculation of $SO_3^-$ in $\gamma$-irradiated $K_2SO_4$ (see Part A of this section). Substituting the experimental data in equation 4.1 the $SO_3^-$ concentration can be calculated:

$$\left[SO_3^-\right]_f = 1.976 \times 10^{-8} \text{ mol of spin/gm}$$

$$1.976 \times 10^{-8} \times 6.023 \times 10^{23} = 1.19 \times 10^{16}$$

$$S_t = 1.19 \times 10^{16} \text{ no of } SO_3^- \text{ /gm}$$

where $S_t$ represents the total number of $SO_3^-$ produced per gram sample. Fig. 4.5 shows the signal of $SO_3^-$ in $K_2SO_4$ containing fission fragments.

### 4.3.3 Determination of the $G_f$(value) for $SO_3^-$ radical due to fission fragments

The LET (linear energy transfer) of fission fragments in $K_2SO_4$ is higher than that of neutrons and $\gamma$-rays. (reactor background radiation), therefore the G (value) of $SO_3^-$ radical is expected to be higher for fission fragments than for $\gamma$-rays and neutrons.

The volume of $K_2SO_4$ in which fission fragments have penetrated = 0.7154 $mm^3$

Density of $K_2SO_4$ = 2.66 $gm/cm^3$

Knowing the volume and density the weight of $K_2SO_4$ in which fission fragments have penetrated can be calculated:

$$M_f = 2.66 \times 0.7154 = 1.903 \times 10^{-3} \text{ gm}$$

Range of fission fragments in $K_2SO_4$, total number of fission fragments entering $K_2SO_4$ and total energy generated by fission fragments in $K_2SO_4$ are calculated and discussed in Appendix 1.

Total energy generated by fission fragments in $K_2SO_4$ ($E_f$) = $1.192 \times 10^{18}$ ev

Dividing $E_f$ by $M_f$ gives the energy per gm

$$\frac{E_f}{M_f} = \frac{1.912 \times 10^{18}}{1.903 \times 10^{-3}} = 1.005 \times 10^{21} \text{ ev/gm}$$

The following equation can be used to calculate the $G_f$ (value) of $SO_3^-$ due to fission fragments.

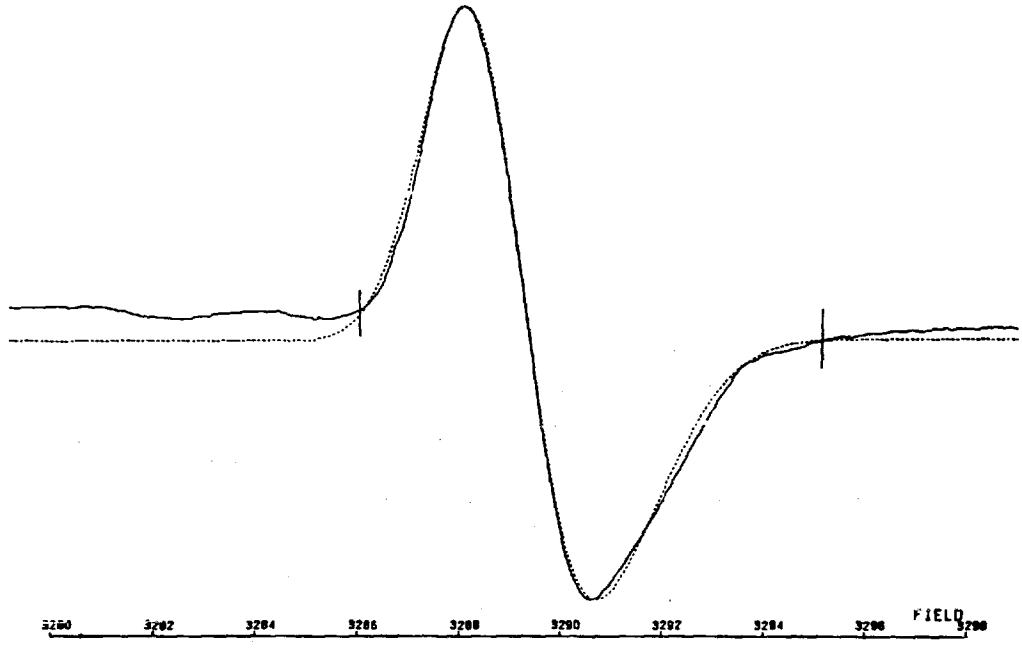


Fig. 4.5 ESR signal of $SO_3^-$ radical ion in $K_2SO_4$ containing fission fragments (doted lines represent the calculated signal).

$$S_t = \frac{E_f . G_f}{100} + \frac{E_\gamma . G_\gamma}{100} \qquad 4.2$$

where

$E_f$ is the energy of fission fragment (calculated above)

$G_f$ is the G(value) of $SO_3^-$ for fission fragments

$E_\gamma$ is the energy of the reactor radiation

$G_\gamma$ is the G(value) of $SO_3^-$ for $\gamma$-rays

$S_t$ is the total number of $SO_3^-$ in $K_2SO_4$ containing fission fragments

$G_\gamma$ and $S_t$ are calculated in part A and B of this section respectively.

In order to work out the value of $E_\gamma$ it is supposed that most of the reactor dose absorbed by $K_2SO_4$ was due to $\gamma$-rays. The latest calorimetric measurement (62) of the dose rate in the University of London Nuclear Reactor showed that for samples of Fe the dose was $8.06 \times 10^6$ Rad/hr. From this value the dose absorbed by $K_2SO_4$ can be calculated.

Electron density per gramme for Fe = $\frac{26}{56} = 0.4643$

Electron density per gramme for $K_2SO_4$ = $\frac{86}{176} = 0.4886$

Time of irradiation = 7 hours

$(8.06 \times 10^6 \times 7 \times 0.4886)/0.4643 = 5.937 \times 10^7$ Rad/hr

1 Rad = $6.242 \times 10^{13}$ ev/gm

$5.937 \times 10^7 \times 6.242 \times 10^{13} = 3.71 \times 10^{21}$ ev/gm

$E\gamma = 3.71 \times 10^{21}$ ev/gm

The values of $E_f$, $S_t$, $G_\gamma$ and $E_\gamma$ were substituted in equation 4.2 to give

$G_f = 7.89 \times 10^{-4}$ $SO_3^-$/100 ev

The above results show that the number of $SO_3^-$ ions produced by fission fragments (in 100 ev) is almost 8 times higher than that for $\gamma$-rays.

### 4.3.4 The effect of thermal annealing on the $SO_3^-$ radical ion in $K_2SO_4$ containing fission fragments

Preparation and annealing conditions for the samples used in these experiments are described in section 2.2D. All samples were run at liquid

nitrogen temperature. The signals of $SO_3^-$ obtained from the unannealed and annealed samples are shown in figs. 4.6, 4.7, 4.8 and 4.9. As can be seen from these figures, the concentration of $SO_3^-$ decreases as the time of annealing increases. When the samples were run at 10dB power signals possibly belonging to $SO_4^-$ and $SO_2^-$ have also been observed but with low intensity compared with $SO_3^-$. The concentration of $SO_3^-$ can be calculated using the following equation:

$$\left[SO_3^-\right]_X = \left[\frac{\left[SO_3^-\right]_N \cdot H_X . Mod_N . RG_N}{H_N \cdot Mod_X \cdot RG_X}\right] x \left[\sqrt{a \log_{10}\left(\frac{P_N - P_X}{10}\right)}\right] \qquad 4.3$$

where

N represents the unannealed sample

X represents the annealed sample

H is the height of signal

Mod is the modulation amplitude

RG is the receiver gain

The concentration of $\left[SO_3^-\right]_N$ is calculated in previous section in the unannealed $K_2SO_4$ containing fission fragments. Using this concentration and the experimental data for the annealed and unannealed samples, the concentration of $SO_3^-$ in the annealed samples can be calculated.

(I) Concentration of $SO_3^-$ in the sample annealed for 3 min at 400°C.

Experimental data for the unannealed sample

$Mod_N = 1$

$RG_N = 1.25 \times 10^3$

$P_N = 46$ dB

$H_N = 19.7$ cm

$\left[SO_3^-\right]_N = 1.1901 \times 10^{16}$ no $SO_3^-$/gm

Experimental data for the annealed sample:

$Mod_X$ = 1.6

$RG_X$ = $4 \times 10^3$

$P_X$ = 46dB

$H_X$ = 16.1 cm

Replacing the above data in equation 4.3, the concentration of $SO_3^-$ in annealed sample would be

$$\left[SO_3^-\right] = 1.8995 \times 10^{15} \quad \text{no. } SO_3^-/gm$$

This amount is 16% of the initial concentration.

(II) - Concentration of $SO_3^-$ in the sample annealed for 5 minutes at 400°C.

Experimental data for annealed sample

$Mod_X$ = 1.6

$RG_X$ = $4 \times 10^3$

$P_X$ = 46

$H_X$ = 12 cm

The concentration of $SO_3^-$ in annealed sample would be

$$\left[SO_3^-\right] = 1.4159 \times 10^{15} \quad \text{no. } SO_3^-/gm$$

This amount is 11.89% of the initial concentration.

(III) Concentration of $SO_3^-$ in the sample annealed for 7 minutes at 400°C

Experimental data for annealed sample

$Mod_X$ = 1.6

$RG_X$ = $4 \times 10^3$

$P_X$ = 46 dB

$H_X$ = 8.8 cm

Using the equation 4.3 the concentration of $SO_3^-$ would be:

$$\left[SO_3^-\right] \quad 51.0383 \times 10^{15} \quad \text{no. } SO_3^-/gm$$

This is 8.7% of the initial concentration.

The calculated concentration of $SO_3^-$ shows a significant drop in the first few minutes of the annealing, about 84% of the concentration of $SO_3^-$

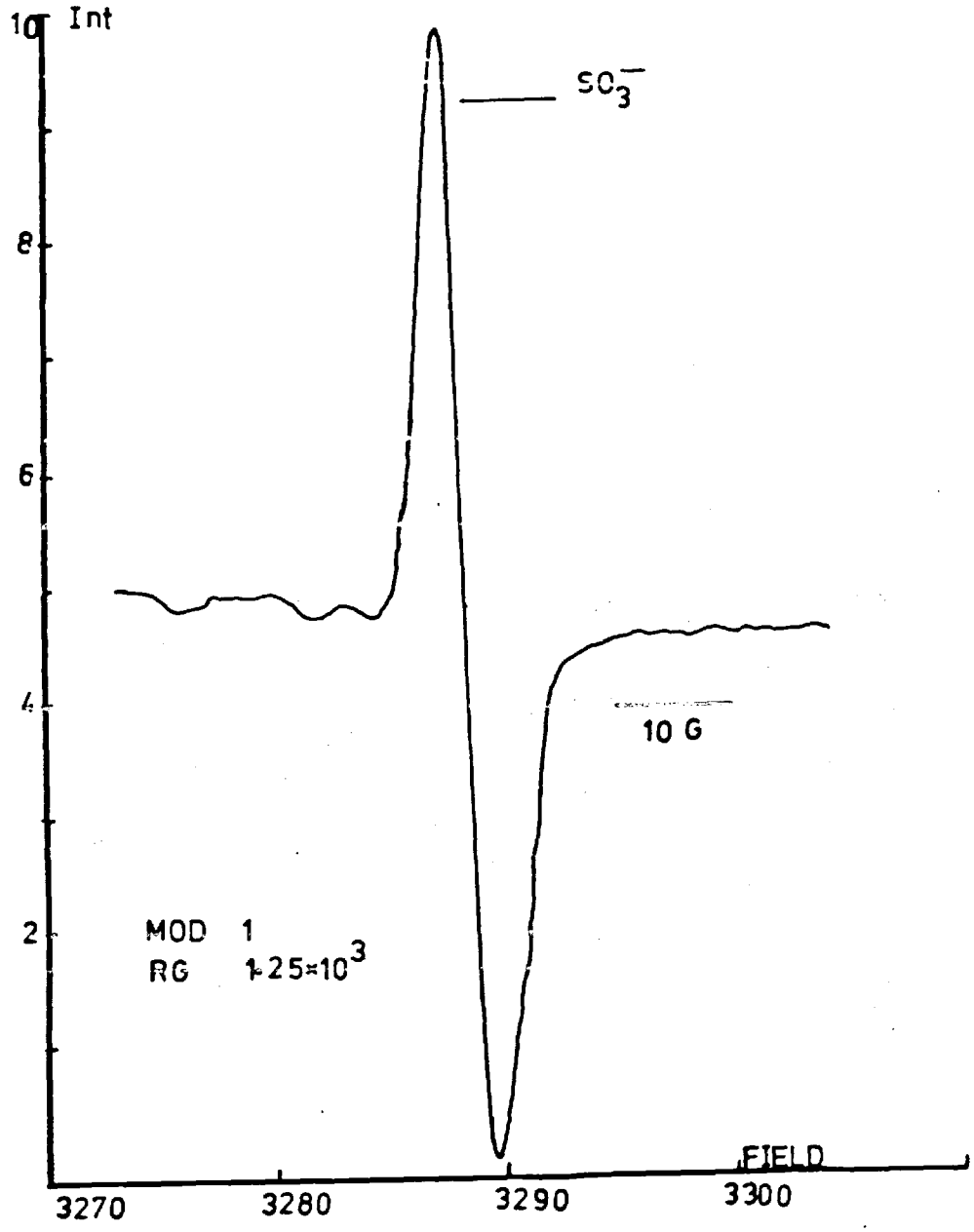


Fig. 4.6 ESR signal of $SO_3^-$ in unannealed sample of $K_2SO_4$ containing fission fragments (microwave frequency = 9.222 GC)

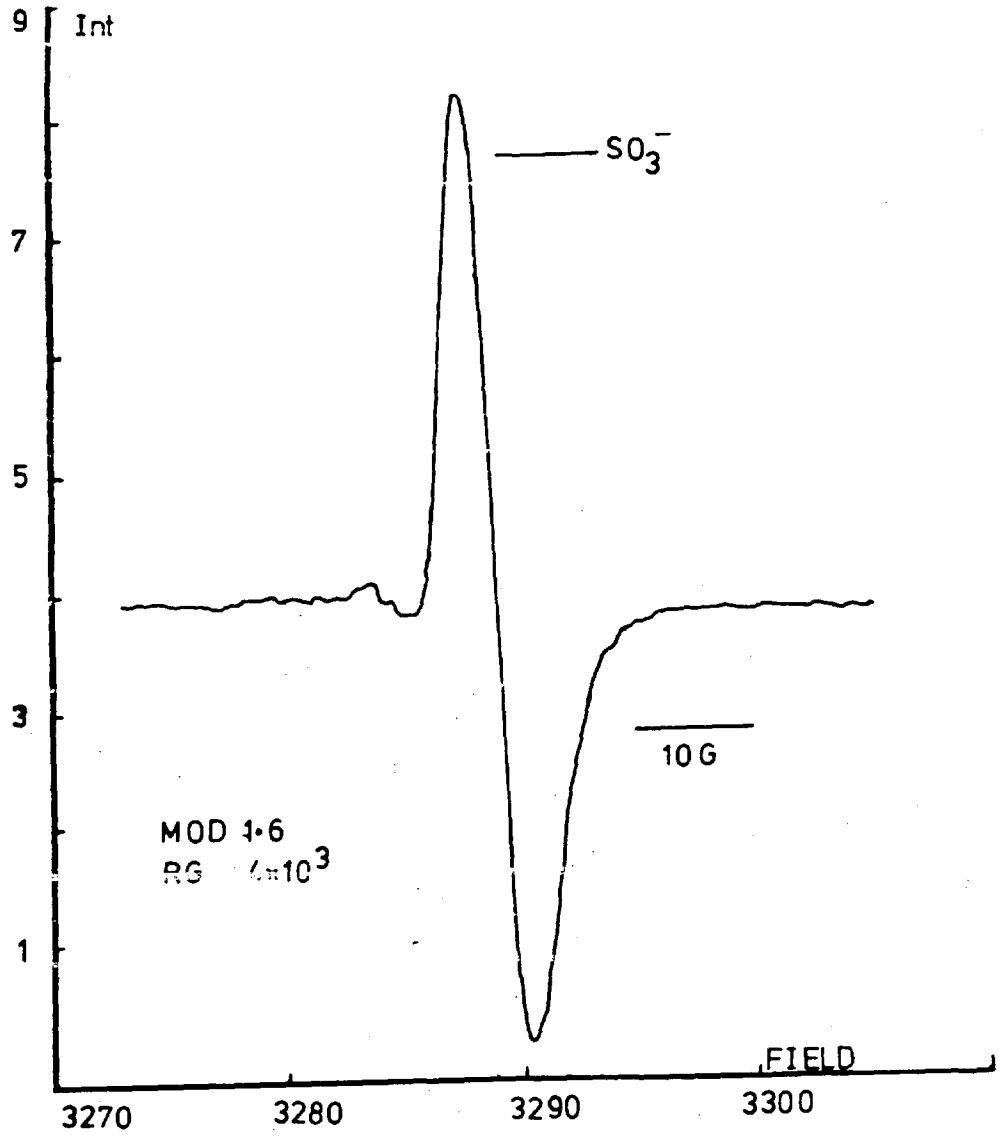


Fig. 4.7 ESR signal of $SO_3^-$ in $K_2SO_4$ containing fission fragments annealed at 400°C for 3 mins (microwave frequency = 9.226 GC)

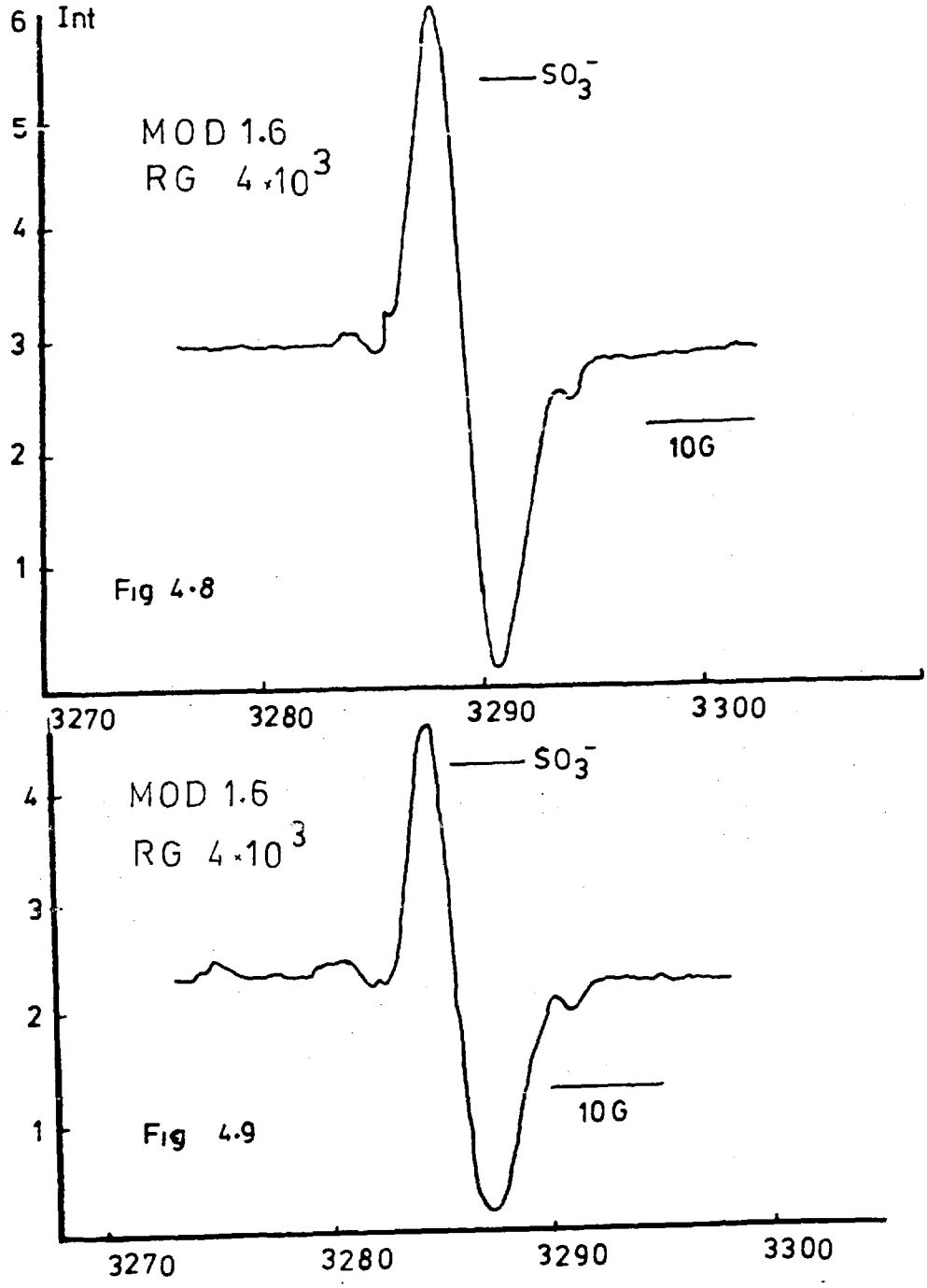


Fig. 4.8 ESR signal of $SO_3^-$ in $K_2SO_4$ containing fission fragments, annealed at 400°C for 5 mins (microwave frequency = 9.226 GC)

Fig. 4.9 ESR signal of $SO_3^-$ in $K_2SO_4$ containing fission fragments, annealed at 400°C for 7 mins (microwave frequency = 9.222 GC)

disappears at this stage. For longer annealing the drop is almost slow in comparison to the first few mintues. The ESR spectrum of the sample annealed for 3 hours at 420°C was very weak. The results of the annealing at 400°C are summarized in table 10 Chapter 5.

A graph of $SO_3^-$ against time of annealing is shown in Chapter 5, fig.5.4

4.3.5 Comparison of results with literature

No report could be found of the ESR of neutron, electron and fission fragments irradiated $K_2SO_4$, but ESR of γ and x-ray irradiated $K_2SO_4$ have been reported (see Chapter 2, Table 2). Since there were no considerable differences between the ESR spectra of $K_2SO_4$ irradiated in different ways, it is reasonable to compare the results obtained in this work with the results in the Literature. The detected radicals and their principle g-values are as found by Hariharan and Sobhanadri (50), but they did not observe radical $SO_2^-$. The radicals observed by Saskaki (51) in γ-irradiated $K_2SO_4$ are also the same as the present work. Gromov and Morton (48) have observed radicals of $SO_4^-$ and $SO_3^-$ in x-ray irradiated $K_2SO_4$. They detected just one type of $SO_4^-$ with principle g-values not similar to any of $SO_4^-$ observed in this work. Most of the ESR work reported so far (50, 48) has been carried out on the lightly irradiated $K_2SO_4$ except (51). Radicals $SO_2^-$ and $O_3^-$ not being observed (48, 49, 50) may well be because of the low dose of irradiation. Saskaki (51) has observed that the concentration of $SO_3^-$, $SO_4^-$ and $O_3^-$ radicals was increased with increasing the dose of irradiation.

# CHAPTER 5:

## RESULTS AND DISCUSSION OF THE BEHAVIOUR OF FISSION FRAGMENT IODINE IN $K_2SO_4$

5.1 Results of fractional activity of iodate in $K_2SO_4$ containing fission fragments.

(A) Analysing the samples three days after irradiation: Most of the $K_2SO_4$ samples containing fission fragments were left to cool for three days after irradiation. The average results and the standard deviation obtained for 15 samples analyzed at room temperature are shown in Table 5.1 for isotopes $^{131}I$, $^{133}I$ and $^{132}I$.

Table 5.1 Fractional activity of iodate in $K_2SO_4$ (powder) containing fission fragments.

| Sample | $^{131}I$ | $^{133}I$ | $^{132}I$ |
|---|---|---|---|
| $K_2SO_4$ (powder) | $0.524 \pm 0.02$ | $0.523 \pm 0.02$ | $0.62 \pm 0.02$ |

As can be seen from Table 5.1 the fractional activity of iodate is almost the same for isotopes $^{131}I$ and $^{133}I$, but for $^{132}I$ it is about 10% higher than $^{131}I$ and $^{133}I$. This difference in the oxidized form of iodine in $^{132}I$ could be due to its way of formation which is not the same as $^{131}I$ and $^{133}I$.

The independent fission yield for $^{132}I$ is very small compared with $^{131}I$ and $^{133}I$. $^{132}I$ is mainly produced after irradiation from the decay of $^{132}Te$ (77 hours half life) while $^{131}I$ and $^{133}I$ are spending less time as $^{131}Te$ and $^{133}Te$ (see Chapter 3 Table 3.4). The precursors for $^{131}I$ and $^{133}I$ should all have decayed away at the time of analysis, while the precursors of $^{132}I$ exist until the time of analysis. Since all the activity observed for $^{132}I$ at the time of analysis was formed by decay of $^{132}Te$, it is not unreasonable to conclude that $^{132}Te$ after irradiation exists mostly in its oxidized form, and this could be the reason for observing the higher oxidized form for $^{132}I$. A special correction was used in calculating the activity of $^{132}I$ at the end of irradiation (see Appendix 2 for details).

The precise condition of the iodine atom stopped in the $K_2SO_4$ lattice is unknown. The form of the iodine fission fragment that exchanged with the iodate carrier on dissolution is identified as $I^F$. In this thesis where the oxidised form of iodine is mentioned, that means the form of iodine ($I^F$) which is converted to iodate on dissolution.

(B) Dissolving the sample in carrier solution immediately after irradiation

$K_2SO_4$ containing fission fragments after the end of irradiation were dissolved (36 min after irradiation) in the 10ml of carrier solutions of $KIO_3$ and KI, the active solution in the small glass tube was sealed and analysed the day after irradiation. The results are shown in Table 5.2. As can be seen from this table the fractional activity of iodate for all three isotopes of iodine are the same. These results suggest that the isotopes of iodine after irradiation exist in almost the same fraction of oxidized form.

Table 5.2 Fractional activity of iodate in $K_2SO_4$, sample dissolved in carrier solution after irradiation.

| Sample | $^{131}I$ | $^{133}I$ | $^{132}I$ |
|---|---|---|---|
| $K_2SO_4$ powder | 0.52 | 0.51 | 0.51 |

Although $^{132}Te$ in the active sample dissolved in the carrier solution immediately after irradiation still decaying to $^{132}I$, but it is not clear why $^{132}I$ did not show higher oxidised form as it did in the samples analysed three days after irradiation. This experiment suggested that as $^{132}Te$ spends more time in the crystal after irradiation it is more likely to decay to the oxidised form of $^{132}I$. Unfortunately due to the high activity of the sample it could only be dissolved immediately after irradiation, and analysis could not be carried out until 24 hours later.

(c) Irradiation of $K_2SO_4$ in evacuated container

Preparation of the sample is described in Chapter 3 Section 16. This experiment was carried out to see the effect of moisture and atmospheric

oxygen on the $K_2SO_4$ prior to irradiation. The results obtained did not show any significant difference with those of the sample which was not evacuated. The results are shown in Table 5.3. They suggest that the atmospheric oxygen and moisture did not have any effect on the distribution of valency states of iodine fission fragment .

Table 5.3 Fractional activity of iodate in vacuum irradiation of $K_2SO_4$

| Sample | $^{131}I$ | $^{133}I$ | $^{132}I$ |
|---|---|---|---|
| $K_2SO_4$ (powder) | 0.49 | 0.48 | 0.60 |

(D) Uncrushed $K_2SO_4$

The uncrushed sample of $K_2SO_4$ after irradiation was white in colour unlike powdered $K_2SO_4$ which was pink.

The results observed were almost the same as those of the crushed $K_2SO_4$ (powder). The results suggested that crushing has no effect on distribution of iodine fission fragment .

5.2 Results of test on the release of active iodine during thermal annealing

The activity of the released iodine was very low, therefore the results could have an error of about 10% due to low counting rate. The collection of iodine was carried out at different temperatures and times. The results are shown in Table 5.4. In the unannealed sample the iodine atoms in the crystal when dissolved in the carrier solution converted to iodide. After thermal annealing the annealed sample was analysed and the total activity of the iodide was calculated. The activity of released iodine was worked out as a percentage of the total iodide activity. As can be seen from Table 5.4 , the percentage of the iodine released is less than 2% of the total iodide activity and does not depend on the temperature of the annealing. These results suggested that the iodine atoms are released in the first few minutes of annealing. From this experiment it was concluded that the released of the iodine atoms during thermal annealing was negligible.

Table 5.4 Iodine released as a percentage of the total iodide

| Temperature of annealing<br>Time of annealing | $^{131}I$ (%) | $^{133}I$ (%) |
|---|---|---|
| 310°C<br>7 min | 1.74 | 1.8 |
| 350°C<br>7 min | 0.83 | 0.8 |
| 400°C<br>7 min | 1.8 | 0.5 |
| 400°C<br>2 hrs | 0.95 | 0.6 |
| 400°C<br>4 hrs | 1.45 | 1.04 |

## 5.3 Result of thermal decomposition of $KIO_3$

### (A) Thermogravimetric results

This experiment was carried out to make sure that the annealing processes observed in $K_2SO_4$ containing fission fragments are not due to thermal decomposition of $KIO_3$. Thermogravimetric study showed that $KIO_3$ started to decompose at about 513°C. The results obtained in this work are in good agreement with the work reported by Breusov et al (64). They have reported the value of 515°C for decomposition of $KIO_3$. Simon et al (65) also studied the thermal decomposition of $KIO_3$ and they found the decomposition temperature of 540°C. The result obtained from this experiment suggested that the decrease in the fractional activity observed in the thermal annealing of $K_2SO_4$ containing fission fragments are not due to thermal decomposition of iodate.

### (B) Thermal decomposition of $KIO_3$ at 480 and 500°C after one hour of annealing

The weight of the iodine (see Chapter 3 section 18(B) for detail) were measured from the standard graph shown in fig. 5.1 (The values obtained from

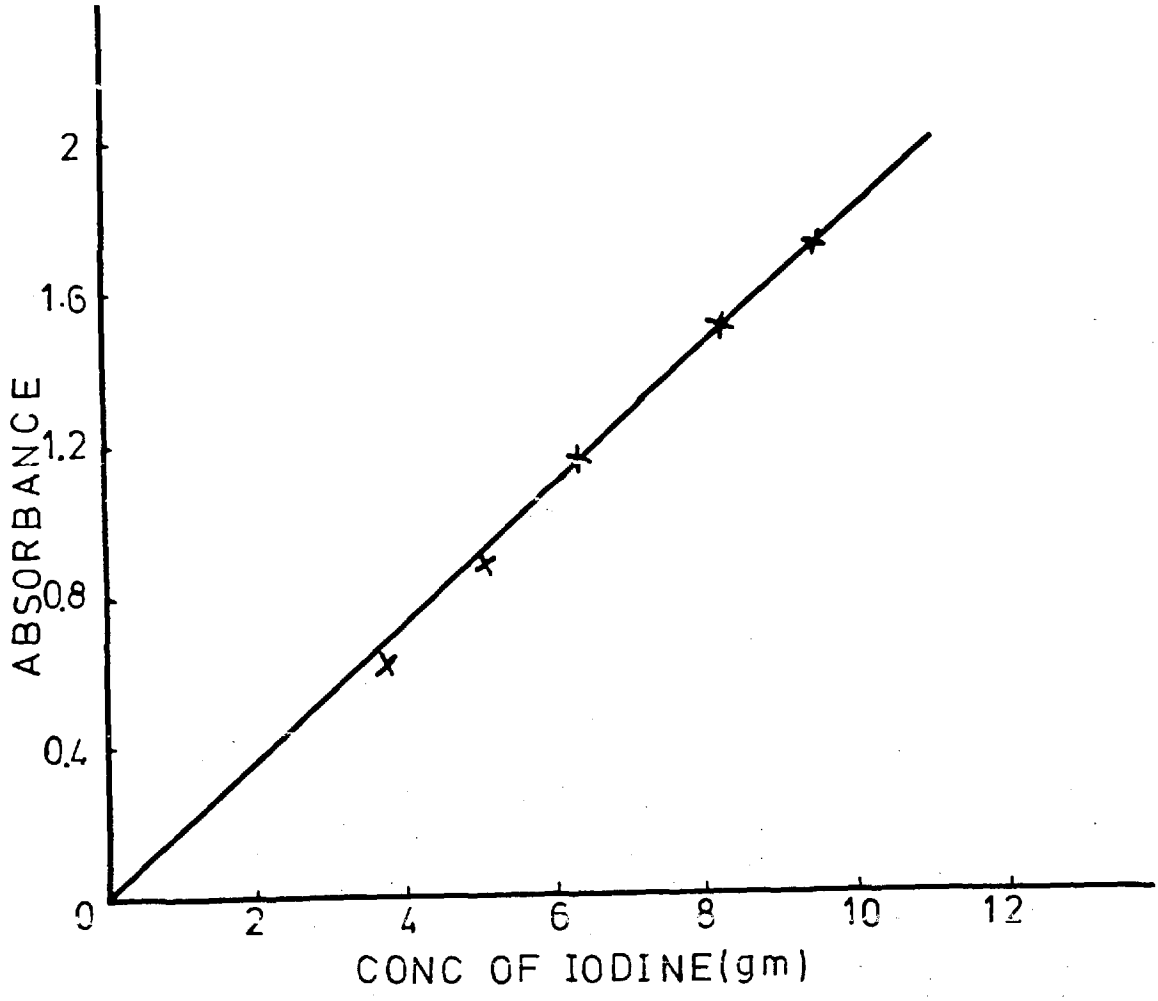


Fig. 5.1 Spectrophotometric measurements of iodine in thermally annealed $KIO_3$

the graph were corrected for dilution). From the weight of iodine the weight of iodate was calculated since the initial weight of $KIO_3$ was known, the percentage of the iodate decomposed at 480°C and 500°C after an hour were calculated and are shown in Table 5.5.

Table 5.5 Percentage of $KIO_3$ decomposed at 480 and 500°C after an hour of annealing.

| Annealing temperature (C°) | % of iodate decomposed |
|---|---|
| 480 | 1.1 |
| 500 | 1.9 |

The results obtained in this experiment suggested that the decomposition of $KIO_3$ below 480°C is negligible.

## 5.4 Thermal annealing of $K_2SO_4$ containing fission fragments

Thermal annealing of $K_2SO_4$ containing fission fragments was carried out at different temperatures and times. No change in distribution of iodine as iodide and iodate have been observed below 300°C, although the colour of the samples changed from pink to white.

A small decrease in the fractional activity of iodate has been observed at 350°C. After this observation, thermal annealing was carried out at temperatures of 380, 400 and 450°C. The annealing results showed a significant decrease in the fractional activity of iodate in the first few minutes. The rate of decreased became very slow after a few minutes of annealing. The samples used for annealing at certain temperatures had been irradiated in the same polythene capsule with an extra sample as a control. The control for each set of annealing was analysed at room temperature. The Fractional activity obtained for each annealed sample was normalized as follows:

$$\text{Normalized fractional activity} = \frac{(A)_{ob}\ (A)_{av}}{(A)_{con}}$$

where

$(A)_{ob}$ is the observed fractional activity

$(A)_{av}$ is the average fractional activity of 15 samples which were analysed at room temperature.

$(A)_{con}$ is the fractional activity of iodate of the control.

Thermal annealing results for four different temperatures are shown in Tables 5.6, 5.7, 5.8, and 5.9. The results shown in these tables are the normalized fractional activity. Curves of fractional activity against time of annealing are also shown in Figs. 5.2 and 5.3 for isotopes of $^{131}I$ and $^{133}I$ respectively.

Table 5.6 Fractional activity of iodate in thermal annealing of $K_2SO_4$ containing fission fragments at 350°C

| Sample No. | Time of annealing | $^{131}I$ | $^{133}I$ |
|---|---|---|---|
| 1 (control) | - | 0.524 | 0.523 |
| 2 | 4 min | 0.514 | 0.513 |
| 3 | 7 min | 0.496 | 0.50 |
| 4 | 8 min | 0.487 | 0.492 |
| 5 | 12 min | 0.482 | 0.487 |
| 6 | 22 min | 0.477 | 0.474 |
| 7 | 69 min | 0.457 | 0.455 |
| 8 | 292 min | 0.435 | 0.45 |
| 9 | 21 hrs and 22 min | 0.438 | 0.436 |

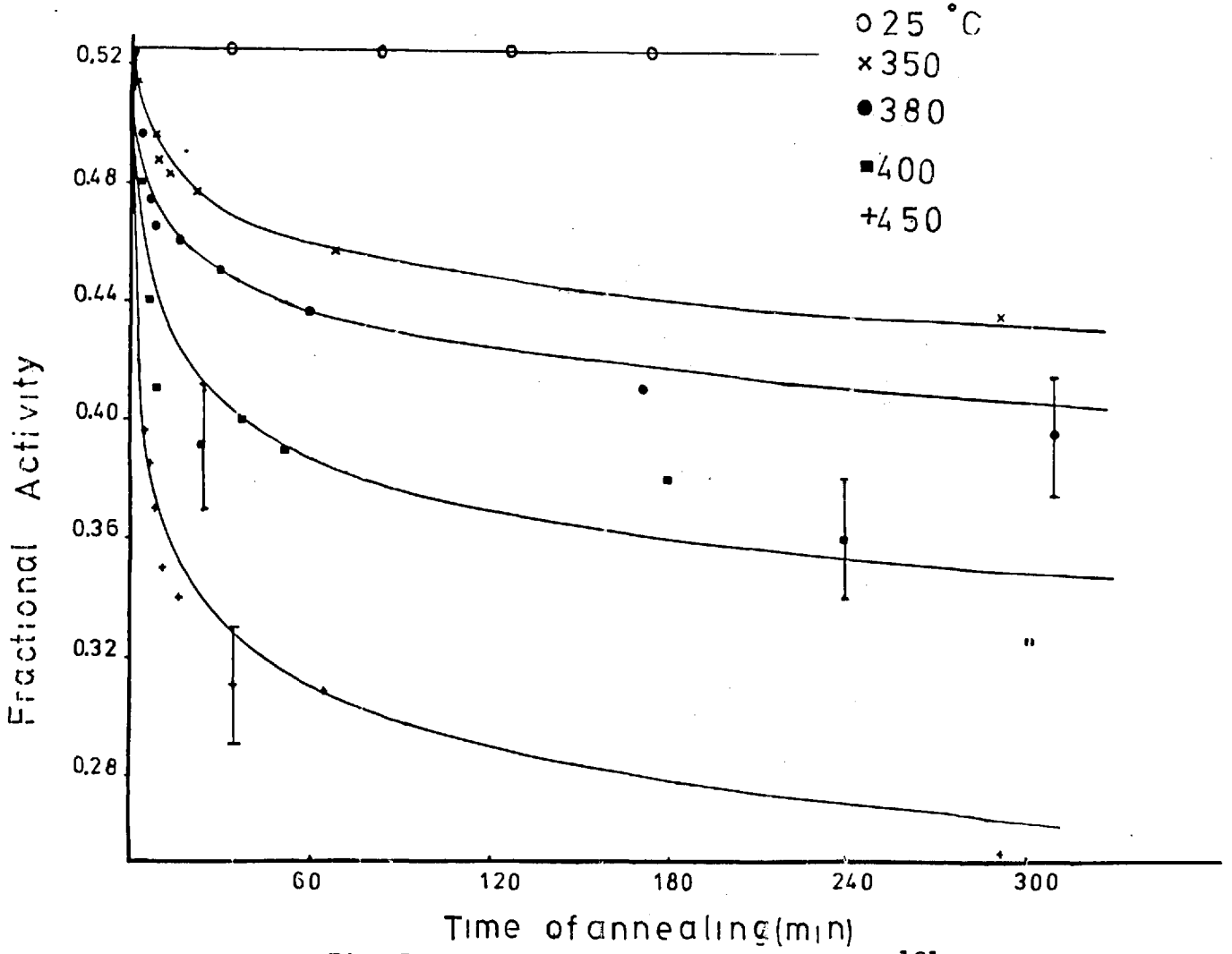


Fig. 5.2 Thermal annealing curves for $^{131}I$

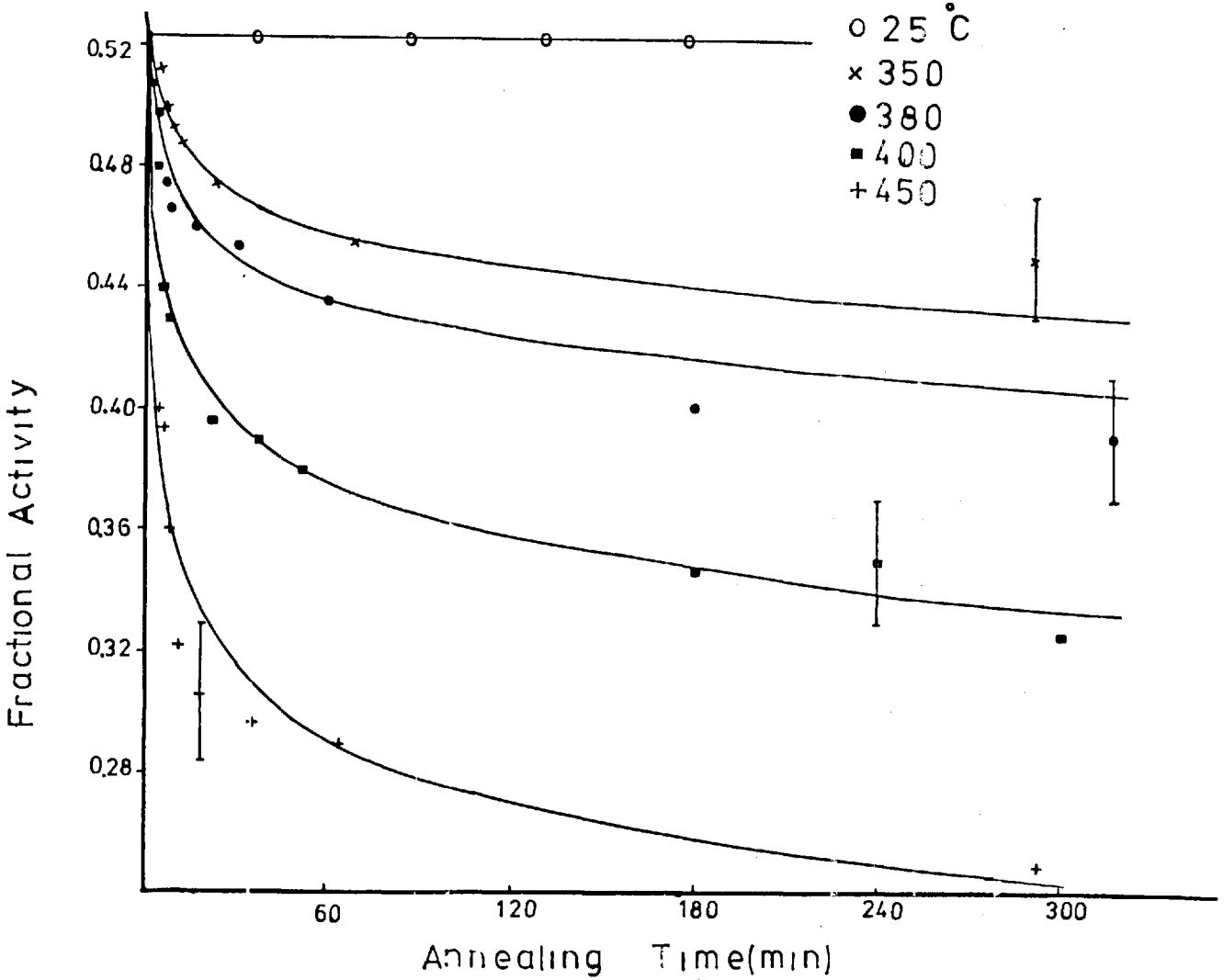


Fig. 5.3 Thermal annealing curves for $^{133}_{I}$

Table 5.7 Fractional activity of iodate in thermal annealing of $K_2SO_4$ containing fission fragments at 380°C

| Sample No. | Time of annealing | $^{131}I$ | $^{133}I$ |
|---|---|---|---|
| 1 (control) | - | 0.524 | 0.523 |
| 2 | 2 min | 0.51 | 0.508 |
| 3 | 3.5 min | 0.497 | 0.498 |
| 4 | 5 min | 0.474 | 0.474 |
| 5 | 7 min | 0.465 | 0.464 |
| 6 | 16 min | 0.46 | 0.461 |
| 7 | 30 min | 0.45 | 0.454 |
| 8 | 60 min | 0.437 | 0.436 |
| 9 | 172 min | 0.405 | 0.397 |
| 10 | 317 min | 0.395 | 0.39 |

Table 5.8 Fractional activity of iodate in thermal annealing of $K_2SO_4$ containing fission fragments at 400°C

| Sample No. | Time of annealing | $^{131}I$ | $^{133}I$ |
|---|---|---|---|
| 1 (control) | - | 0.524 | 0.523 |
| 2 | 3.5 min | 0.48 | 0.48 |
| 3 | 5 min | 0.44 | 0.44 |
| 4 | 7 min | 0.41 | 0.41 |
| 5 | 22 min | 0.39 | 0.396 |
| 6 | 37 min | 0.40 | 0.39 |
| 7 | 52 min | 0.39 | 0.38 |
| 8 | 3 hrs | 0.38 | 0.347 |
| 9 | 4 hrs | 0.36 | 0.352 |
| 10 | 5 hrs | 0.325 | 0.325 |
| 11 | 17 hrs | 0.30 | 0.33 |

Table 5.9 Fractional activity of iodate in thermal annealing of $K_2SO_4$ containing fission fragments at 450°C

| Sample No. | Time of annealing (min) | $^{131}I$ | $^{133}I$ |
|---|---|---|---|
| 1 (control) | - | 0.524 | 0.523 |
| 2 | 4 | 0.396 | 0.40 |
| 3 | 5.5 | 0.385 | 0.395 |
| 4 | 7 | 0.37 | 0.36 |
| 5 | 10 | 0.35 | 0.322 |
| 6 | 16 | 0.34 | 0.306 |
| 7 | 34 | 0.304 | 0.296 |
| 8 | 64 | 0.308 | 0.29 |
| 9 | 292 | 0.252 | 0.25 |

The curves reveal an initial decrease in the iodate fraction in the first few minutes of annealing, followed by very slow decrease after almost 30 minutes up to several hours. As can be seen from figs. 5.2 and 5.3 the decrease in the fractional activity of iodate for isotopes $^{131}I$ and $^{133}I$ are very similar. The results obtained for $^{132}I$ were too scattered to be meaningful.

In order to find out the reasons for decrease in the oxidised form of the fission product iodine in $K_2SO_4$ during thermal annealing, electron spin resonance (ESR) of $K_2SO_4$ containing fission fragments were carried out as described in Chapter 4. ESR of gamma, electron, and neutron irradiated $K_2SO_4$ (without fission fragments) were also studied to see if they were different compared to $K_2SO_4$ containing fission fragments. The species detected in all types of irradiated $K_2SO_4$ were $SO_3^-$, $SO_4^-$ (two types), $SO_2^-$ and $O_3^-$. The spectra observed were almost similar in all types of irradiation. The most intense radical ion observed was due to the $SO_3^-$ radical and the other radicals were relatively much lower in intensity. The annealing behaviour of

radical $SO_3^-$ is discussed in relation to the reduction of iodate during the thermal annealing. Three samples of $K_2SO_4$ containing fission fragments were annealed at 400°C for 3, 5 and 7 minutes. The concentration of the $SO_3^-$ of annealed samples and unannealed sample were measured quantitatively by ESR. A curve of concentration of $SO_3^-$ (y) against time of annealing is shown in Fig. 5.4. The results show a significant decrease in the concentration of $SO_3^-$ in the annealed sample, and greater decrease was observed with increasing the time of annealing (see Table 5.10). The above observations suggest that radical $SO_3^-$ is likely to be responsible for the reduction of the fission fragment iodine ($I^F$).

Table 5.10. Concentration of $SO_3^-$ radical ion in annealed samples (at 400°C) of $K_2SO_4$ containing fission fragments.

| Time of annealing (minutes) | Number of $SO_3^-$ in gram sample | Concentration of $SO_3^-$ in percentage |
|---|---|---|
| Room temperature | $1.19 \times 10^{16}$ | 100 |
| 3 | $1.8995 \times 10^{15}$ | 16 |
| 5 | $1.4159 \times 10^{15}$ | 11.89 |
| 7 | $1.0383 \times 10^{15}$ | 8.7 |

During thermal annealing an $SO_3^-$ radical could release an electron as follows:

$$SO_3^- \xrightarrow{\text{heat}} SO_3 + e^-$$

The released electrons react with $I^F$ (see Section 5.1) to reduce it to $I^-$. The number of iodine atoms in the $K_2SO_4$ containing fission fragments were $\sim 10^{10}$ atoms (see appendix 1 for calculation). It can be seen that the number of $SO_3^-$ ions produced are much higher than the number of iodine atoms. The decrease in the concentration of $SO_3^-$ after 3 minutes annealing at 400°C was about 8 4% while the reduction of iodate at the same temperature for

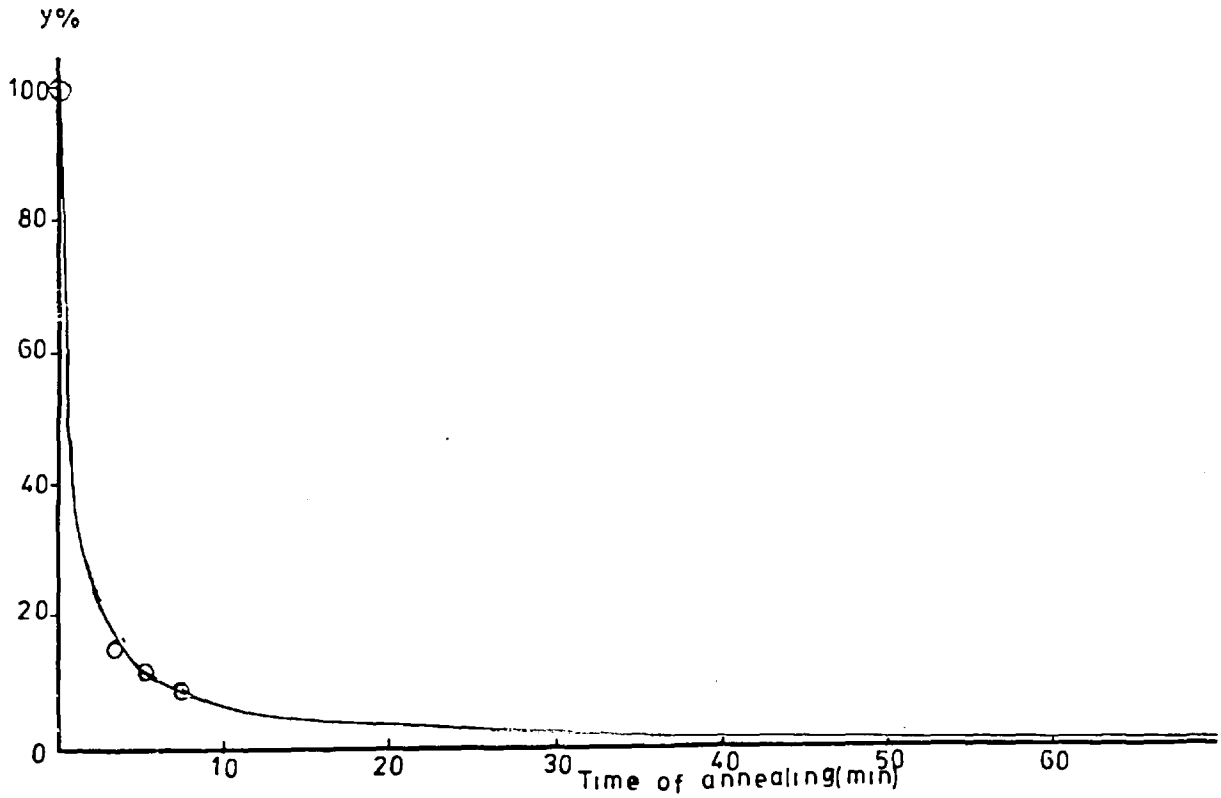


Fig. 5.4 Thermal annealing of $SO_3^-$ radical ion at 400°C in irradiated $K_2SO_4$ containing fission fragments

3.5 mins annealing was about 4.5%. The above comparison suggested that $SO_3^-$ could react with itself or other species as well as $I^F$.

$$SO_3^- + SO_3^- \longrightarrow SO_4^= + SO_2 \qquad (A)$$

$$SO_4^- + SO_3^- \longrightarrow SO_4^= + SO_3 \qquad (B)$$

$$SO_3^- + SO_2^- \longrightarrow SO_3^= + SO_2 \qquad (C)$$

since the concentrations of $SO_4^-$ and $SO_2^-$ were much smaller than $SO_3^-$, reaction (A) is more likely to occur. It can be seen from Figs. 5.2 and 5.3 that after about 10 minutes of annealing the decrease of iodate becomes very slow, and also ESR spectrum of the sample annealed for 7 minutes at the same temperature showed that only 8% of the initial concentration of $SO_3^-$ was present and 92% had disappeared. The above observation suggests that as the concentration of $SO_3^-$ radicals becomes smaller, the decrease in the Fractional activity of iodate becomes insignificant. The reduction of iodate due to $SO_3^-$ is based on a model which is discussed in the following section. The continuous lines shown in figures 5.2 and 5.3 are theoretical lines based on this model.

5.4.1 Theoretical model for thermal annealing processes

It is assumed that $SO_3^-$ radical ion is disappearing by two electron transfer processes in the lattice of sulphate ions.

(I) Reaction of $SO_3^-$ with itself

e.g. $SO_3^- + SO_3^- \longrightarrow SO_{4(aq)}^{2-} + SO_{2(g)}$ (A) $\Delta H_f = 287.86$ Kcal mol$^{-1}$

or $SO_3^- + SO_3^- \longrightarrow SO_{3(aq)}^{2-} + SO_{3(g)}$ (B) $\Delta H_f = 243.65$ Kcal mol$^{-1}$

As can be seen from the heat of formation, reaction (A) leads to more stable prodcuts and is thermodynamically more probable.

(II) Release of electrons by thermal annealing. The released electrons (as discussed in previous section) diffusing in the lattice, reacts with the fission fragment iodine ($I^F$) and reduces it to iodide. As discussed in section 5.1, the precise condition of iodine atoms in the $K_2SO_4$ is unknown, and $I^F$ represents the form of iodine that converts to iodate on dissolution.

The reduction of $I^F$ during thermal annealing could be written as follows:

$$SO_3^- \xrightarrow{\text{heat}} SO_3 + e^-$$

$$I^F + e^- \longrightarrow I^-$$

Let the concentration of $SO_3^-$ after annealing be y and fractional activity of iodate be x. The reaction rate for decrease of iodate (x) and disappearance of $SO_3^-$ (y) can be written as follows:

$$\frac{dx}{dt} = -K_1 yx \qquad (5.1)$$

$$\frac{dy}{dt} = -K_2 y^2 \qquad (5.2)$$

From equation (5.2) the value of y can be obtained as follows:

$$\frac{dt}{dy} = -\frac{1}{k_2 y^2}$$

After integration

when $t = 0 \quad y = y_0$

$$y = \frac{y_0}{(k_2 y_0 t + 1)} \qquad (5.3)$$

where $y_0$ is the initial concentration of $SO_3^-$

t is the time of annealing

The value of y from equation (5.3) is substituted in equation (5.1) to give:

$$\frac{dx}{dt} = -\left[\frac{k_1 y_0}{(k_2 y_0 t + 1)}\right] x$$

After integration when $t = o \quad x = x_o$

$$\text{Ln}\ \frac{x}{x_0} = -\frac{k_1}{k_2}\left(\text{Ln}\ (k_2 y_0 t + 1)\right) \qquad (5.4)$$

$$x = x_0 \exp\left(-k_1/k_2\ (\text{Ln}\ (k_2 y_0 t + 1))\right) \qquad (5.5)$$

The equation 5.5 was used (as described in the next sections) to calculate the rate constants ($k_1$ and $k_2$) and also to draw the theoretical annealing curves.

(A) Calculation of the rate constants

From equation (5.3) the value of $k_2$ can be calculated. The value of $y_0$ and y for different annealing times at 400°C is known from ESR experiments (see Table 5.10). To check whether equation 5.3 agrees with the experimental results, the values of y were calculated for different times using the initial concentration of $SO_3^-$ ($y_0$) and calculated value of $k_2$ (0.015/min). A curve of $SO_3^-$ concentration (y) against time of annealing is shown in figure 5.4. The continuous line shown in this figure is the theoretical line based on equation 5.3., and circles represent the experimental values. The value of $k_1$ can be calculated from equation (5.4.). The values of $x_0$ (average of fractional iodate activity of 15 room temperature results) and x for isotopes of $^{131}I$ and $^{133}I$ at 400°C for different times of annealing are shown in Table 5.8. The values of $x_0$, x, $k_2$, $y_0$ and t are substituted in equation 5.4 to give:

$k_1$ = 0.0010 $min^{-1}$ for $^{131}I$ and $k_1$ = 0.0011 $min^{-1}$ for $^{133}I$ at 400°C

(B) Theoretical annealing curves

Equation (5.5) was used to plot curves of theoretical fractional activity of iodate against time of annealing (annealing temperature 400°C) for isotopes of $^{131}I$ and $^{133}I$. The values of $x_0$, $y_0$ are known experimentally and $k_1$ and $k_2$ are calculated in the previous section. Therefore the values of x for different times of annealing can be calculated. Curves of x against t are shown in figs. 5.2 and 5.3. The continuous lines are the theoretical curves. Since the concentration of $SO_3^-$ ions were only measured at 400°C annealing temperature, it was not possible to work out the values of $k_2$ from equation (5.3) for 350, 380 and 450°C annealing temperatures. The values for $k_2$ were chosen ($k_1$ was calculated from equation 5.4) to give the best fit of the theoretical curves to the experimental results (see fig. 5.2 and 5.3). The values of $k_2$ and $k_1$ are shown in Tables 5.11 and 5.12 for isotopes of $^{131}I$ and $^{133}I$. Fractional activity of iodate obtained from the sample dissolved in the carrier solution immediately after irradiation and

analysed the day after irradiation, did not show any difference (with the exception of $^{132}I$) compared with the samples analysed three days after irradiation (see Section 5.1B). To check this experimental observation with the theoretical model, the values of $k_1$ and $k_2$ for room temperature annealing (during cooling time) were obtained from Figs. 5.5 and 5.6 by back extrapolation of the straight lines. The values of $k_1$ ($2\times10^{-12} min^{-1}$), $k_2$ ($2.2 \times 10^{-9}$ $min^{-1}$) and x were substituted in equation (5.5) and the value of $x_0$ (fractional activity of iodate in the sample not being annealed at room temperature) was calculated. The value of $x_0$ obtained was the same as x (fractional activity of iodate, for the sample left in room temperature for three days). These results suggest that no annealing has occurred at room temperature for a cooling time of three days.

Table 5.11 Rate constants of the thermal annealing process at different temperatures for isotope $^{131}I$

| T (temperature) | $\frac{1}{T} \times 1000$ | $k_2$ | $Lnk_2$ | $k_1$ | $Lnk_1$ |
|---|---|---|---|---|---|
| 350 | 1.605 | 0.005 | -5.3 | $0.19\times10^{-3}$ | -8.6 |
| 380 | 1.53 | 0.01 | -4.6 | $0.44\times10^{-3}$ | -7.7 |
| 400 | 1.486 | 0.015 | -4.2 | 0.0010 | -6.9 |
| 450 | 1.383 | 0.035 | -3.35 | 0.0034 | -5.7 |

Table 5.12 Rate constants of the thermal annealing process at different temperatures for isotope $^{133}I$

| $T(C^o)$ temperature | $\frac{1}{T} \times 1000$ | $k_2$ | $Lnk_2$ | $k_1$ | $Lnk_1$ |
|---|---|---|---|---|---|
| 350 | 1.605 | 0.005 | -5.3 | $0.19\times10^{-3}$ | -8.6 |
| 380 | 1.53 | 0.01 | -4.6 | $0.44\times10^{-3}$ | -7.73 |
| 400 | 1.486 | 0.015 | -4.2 | 0.0011 | -6.8 |
| 450 | 1.383 | 0.035 | -3.35 | 0.0038 | -5.57 |

(C) Remarks on the theoretical model

The theoretical model developed for the annealing processes does not explain all the possible reactions which might have occurred.

(I) The theoretical model is based on the reduction of iodate due to $SO_3^-$ radical ion and the disappearances of $SO_3^-$ by itself. In this model the effects of the other radical ions ($SO_4^-$, $SO_2^-$ and $O_3^-$) with fission fragment iodine and also with $SO_3^-$ are not taken into consideration because of their small concentrations. One cannot be certain that they are not playing a role in the annealing processes, although the evidence suggests that their effect is not very significant.

(II) Possible production of iodate by reaction of iodide with oxygen is not taken into consideration. Cleary et al (63) have studied the effect of heat on neutron irradiated $NaIO_3$. They found that the retention of iodate increased with thermal annealing. This possibility was rejected in this work. Let us suppose that the plateau in the annealing curves (figs. 5.2, 5.3) is a steady state, resulting from the iodate being produced by iodide, and also iodate being reduced to iodide at the same rate. According to our ESR investigation most of the paramagnetic species had disappeared after almost an hour of annealing (see Fig. 5.4). The reduction of iodate by paramagnetic species after a long annealing time is very slow (due to the small concentration of $SO_3^-$ present) so that at this stage the fractional activity of iodate should increase with time of annealing (if it is being produced by iodide). The annealing curves did not show such behaviour, so the production of iodate by iodide is not fully supported by the experimental results in this work. Finally one could assume that the rate of this back reaction is possibly very slow.

(III) Before accepting this model, an attempt was made to write a model that showed $SO_3^-$ radical ions are disappearing according to the following equation:

$$dx/_{dt} = -k_1 yx \qquad (a)$$

$$\frac{dy}{dt} = -k_2 y \qquad (b)$$

$$y = y_0 e^{-k_2 t} \qquad (c)$$

A curve of calculated values of y according to equation (c) was plotted against time of annealing, but the experimental values of $SO_3^-$ concentration did not fit with this exponential curve, so that the above model was rejected.

## 5.5 Activation energies of the thermal annealing processes

The activation energies of the reduction of iodate and the disappearance of $SO_3^-$ can be calculated using Arrhenius' equation:

$$K = A \exp(-Ea/_{RT}) \qquad (5.6)$$

where K is the rate constant

A is a constant

Ea is activation energy

R = 1.986 KCaL $K^{-1}$ $moL^{-1}$ is the gas constant

T is in $k^o$

The values of $k_1$, $k_2$ and related temperatures are shown in Tables 5.11 and 5.12 for isotopes of $^{131}I$ and $^{133}I$. The activation energy calculated for the rate constants $k_1$ and $k_2$ for isotopes of $^{131}I$ and $^{133}I$ are shown in Table 5.13.

Table 5.13 Activation energy for rate constants $k_1$ and $k_2$

| $E_a$ | $^{131}I$ kcal/mol(Kjoules/mole) | $^{133}I$ kcal/mole(K joules/ mole) |
|---|---|---|
| $E_a(K_1)$ | 25.7±2.03(107.6) | 26.65±2.96 (111.5) |
| $E_a(K_2)$ | 17.7±0.93 (74.1) | 17.77±0.85 (74.4) |

Graphs of $Lnk_1$ and $Lnk_2$ against $^1/T$ are plotted for isotopes of $^{131}I$ and $^{133}I$ and are shown in figs. 5.5, 5.6. The activation energies calculated

Fig. 5.5 Arrhenius plot ($-\ln k_1$ vs $1000/T\ ^{o}K^{-1}$)

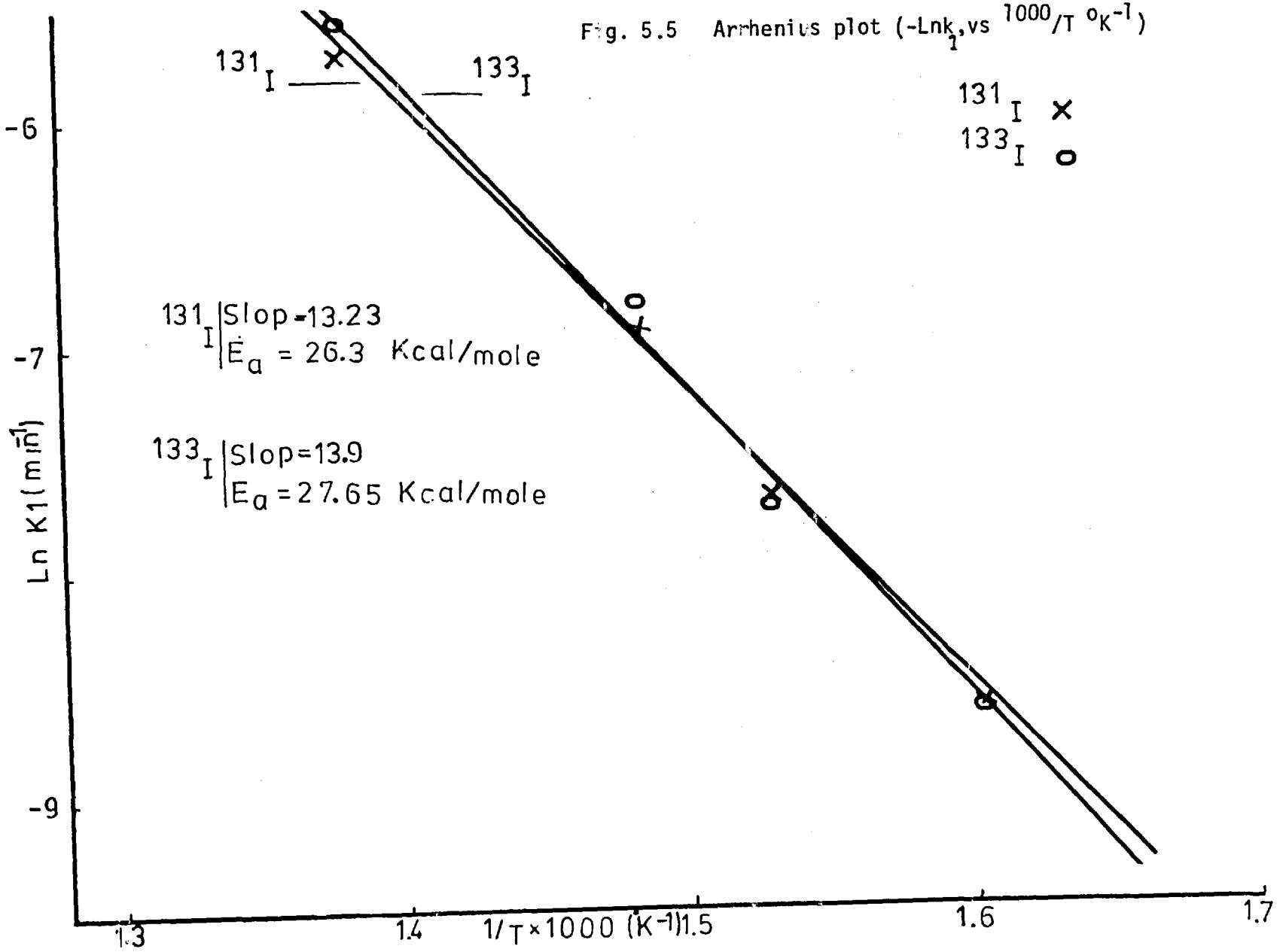

Fig. 5.6 Arrhenius plot ($-Lnk_2$ vs $^{1000}/_T\ ^oK^{-1}$)

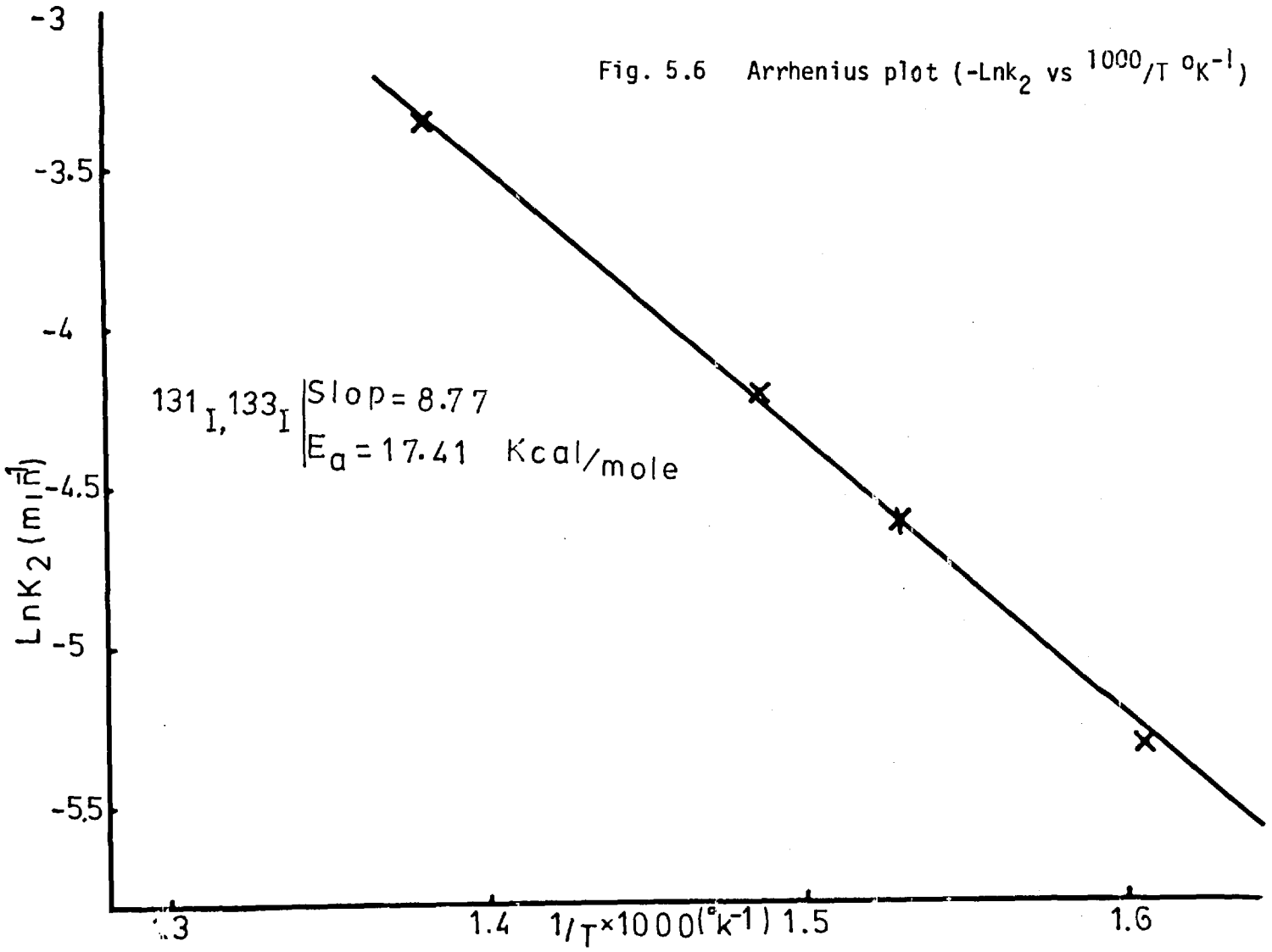

from the slope of the straight lines are shown in figs. 5.5 and 5.6. As can be seen from Table 5.13 there are no significant differences in the activation energies for the two isotopes. The lower activation energy for $SO_3^-$ suggest that this radical disappears more readily than the iodate.

## 5.6 Results of tests on the effects of irradiation time on the valency states of fission fragment iodine in $K_2SO_4$

The results of the fractional activity of iodate for isotopes $^{131}I$ and $^{133}I$ are shown in Table 5.14. These results are the average of two measurements. As can be seen from this table the fractional activity of the iodate decreases with increasing time of irradiation and after 60 minutes irradiation the fractional activity of iodate remained almost unchanged. Curve of the fractional activity against time of irradiation are shown in fig. 5.7. The higher percentage of oxidised form of fission fragment iodine in the short irradiation times suggests that the iodine atoms after losing their kinetic energy due to nuclear interaction in $K_2SO_4$ are present in higher valency states and are only converted to the reduced state by further irradiation up to a limiting dose.

Table 5.14 Effects of time of irradiation on the fractional activity of iodate (neutron flux = $2 \times 10^{12}$ n $sec^{-1}$ $cm^{-2}$)

| Sample no. | Time of irradiation (min) | ($I^{131}$) | ($I^{133}$) |
|---|---|---|---|
| 1 | 10 | 0.625 | 0.62 |
| 2 | 15 | 0.61 | 0.60 |
| 3 | 30 | 0.59 | 0.58 |
| 4 | 60 | 0.558 | 0.555 |
| 5 | 120 | 0.553 | 0.556 |

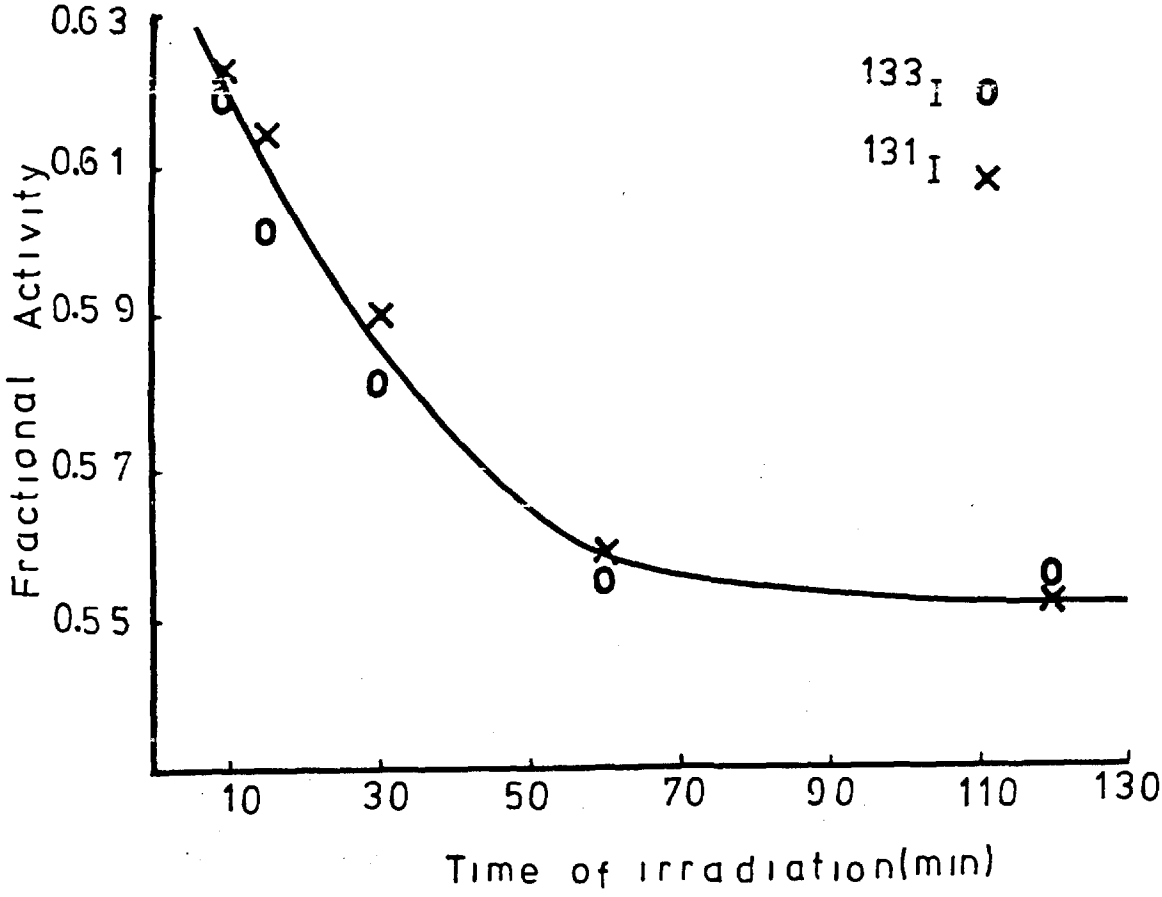


Fig. 5.7 Variations of the fractional activity of iodate with the the irradiation time

## 5.7 Results of post electron irradiation of $K_2SO_4$ containing fission fragments

Post electron irradiation of potassium sulphate containing fission fragments showed a significant decrease in the fractional activity of the iodate. The results of two groups of samples which have been irradiated in the van de Graaff machine with different beam currents (200 $\mu$A and 25 $\mu$A) are shown in Tables 3.15 and 3.16. Curves of fractional activity of iodate against received dose for isotopes $^{133}I$, $^{131}I$ and $^{132}I$ are shown in figures 5.8 (a), 5.8 (b) and 5.8 (c) respectively, the crosses represent irradiation at the high dose rate and the points represent irradiation at the low dose rate. As can be seen from these figures the low dose rate results are very similar to those for the high dose rate. Therefore no dose rate effect was observed. The behaviour of the fission fragment iodine towards post electron irradiation is very similar to that of thermal annealing. In the post irradiation from about 200 Mrad the decrease in the fractional activity of iodate became very slow. To explain these observations the following possibility is considered:

The $I^F$ is reduced to iodide by the electron beam and electron trapped species (such as $SO_3^-$), as follows:

$$SO_3^- \xrightarrow{\text{irradiation}} SO_3^{*-} \longrightarrow SO_3 + e^-$$

$$I^F + e^- \longrightarrow I^-$$

If this hypothesis is true, the iodate should continue to decrease at a constant rate until all the iodate has been used. However it was observed that the rate decreased rapidly after a certain dose. The slow reduction of iodate suggested that some oxidising species came into action at this stage and prevented rapid decrease in the iodate. Unfortunately it was not possible to continue ESR studies on the post irradiated samples. The ESR work could lead to a much clearer understanding of the observed results.

Table 5.15 Fractional activity of iodate in post electron irradiated $K_2SO_4$ containing fission fragments (dose rate 4.57 Mrad/min)

| Sample No. | Time of * irradiation (min) | Received dose (M rad) | ($^{131}I$) | ($^{133}I$) | ($^{132}I$) |
|---|---|---|---|---|---|
| control | – | – | 0.524 | 0.523 | 0.62 |
| 1 | 5 | 11.5 | 0.49 | 0.52 | 0.58 |
| 2 | 10 | 22.8 | 0.46 | 0.47 | 0.557 |
| 3 | 20 | 46 | 0.46 | 0.465 | 0.538 |
| 4 | 62 | 142 | 0.42 | 0.416 | 0.488 |
| 5 | 142 | 324 | 0.376 | 0.387 | 0.469 |
| 6 | 202 | 462 | 0.38 | 0.378 | 0.454 |
| 7 | 309 | 706 | 0.36 | 0.368 | 0.46 |

For half of this time the samples were under the beam

Table 5.16 Fractional activity of iodate in post electron irradiated $K_2SO_4$ containing fission fragments (dose rate 0.49 Mrad/min)

| Sample No. | Time of irradiation (min) | Received dose (M rad) | ($^{131}I$) | ($^{133}I$) | ($^{132}I$) |
|---|---|---|---|---|---|
| control | – | – | 0.524 | 0.523 | 0.62 |
| 1 | 80 | 20 | 0.504 | 0.497 | 0.55 |
| 2 | 240 | 59 | 0.457 | 0.464 | 0.52 |
| 3 | 390 | 95 | 0.438 | 0.437 | 0.50 |

## 5.8 Results of preheating and pre-irradiation

Samples of $K_2SO_4$ preheated at a temperature range of 300 to 700°C for 1.5 hours did not show any change in the distribution of the iodine fission fragment as iodide and iodate. Samples of $K_2SO_4$ pre-irradiated by neutron and gamma rays also did not show any effect on the fractional activity of iodate and iodide. It must be pointed out that all the pretreated samples after irradiation in the reactor with $U_3O_8$ film were analysed without further treatment. Results obtained from these experiments suggested that defects

Fig. 5.8 Effects of post irradiation on the fractional activity of iodate, $^{133}I(a)$, $^{131}I(b)$, $^{132}I(c)$

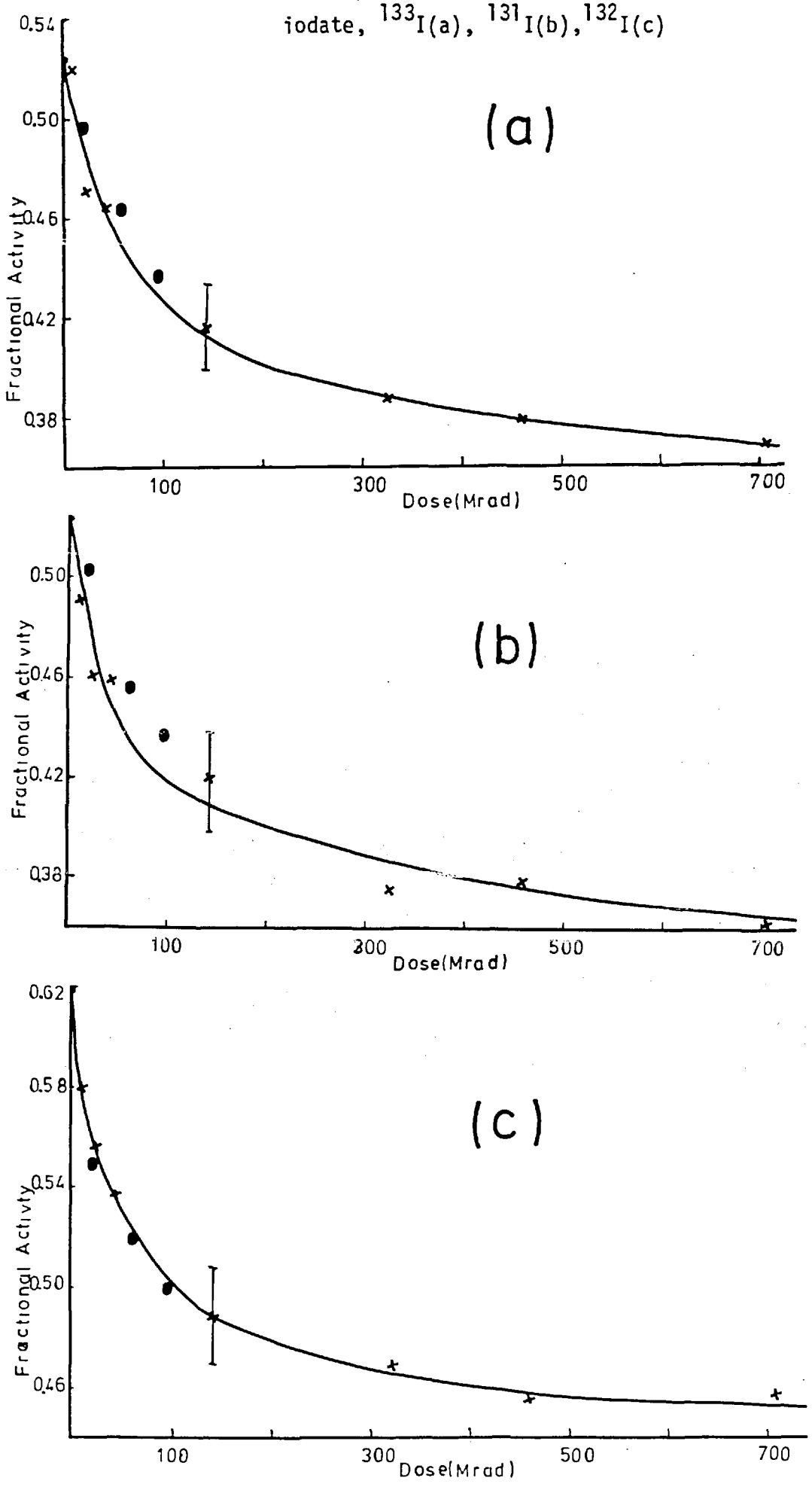

produced prior to fission fragments irradiation had no effect on the initial distribution of the valency states of the iodine fission fragment.

## 5.9 Thermal annealing results of pre irradiated $K_2SO_4$

The annealing of the pre-irradiated $K_2SO_4$ containing fission fragments showed a similar thermal annealing curve compared with samples which had not been pre-irradiated, but with a smaller decrease in the iodate. The results are shown in Table 5.17. Curves of the fractional activity against time of annealing are shown in figure 5.9 for isotope $^{131}I$ (the same behaviour has been observed for $^{133}I$). It should be noted that the given curve would obviously be improved with a greater number of experimental points. Curve (B) in figure 5.9 is the annealing curve of $K_2SO_4$ containing fission fragments which have not been pre-irradiated. As can be seen from these figures there is a shift of the annealing curve for pre-irradiated samples while the shape of the curve remained the same. The results obtained suggested that there was less $SO_3^-$ available to react with the iodate during thermal annealing. One would expect to see more $SO_3^-$ present in the pre-irradiated $K_2SO_4$. To explain these results it was assumed that the rate of reaction of $SO_3^-$ with itself was higher than that calculated (see section 5.4.1) for non pre-irradiated $K_2SO_4$. According to this hypothesis there was less $SO_3^-$ available to reduce $I^F$. An attempt was made to see if the thermal annealing model described in Section 4 agreed with the above assumption. Equation 5.5 was used to calculate the value of x (fractional activity of iodate) for different times of annealing, using the same value of $K_1$, calculated at the annealing temperature of 400°C (see Table 3.11 and 3.12). The value of $K_2$ increased until the best theoretical curve fitted the experimental results. The solid lines in fig. 5.9 are the theoretical curves. Since the calculated annealing curve fits the experimental results sufficiently well, the above hypothesis is reasonable.

Table 5.17 Fractional activity of iodate after thermal annealing of the pre-irradiated $K_2SO_4$ containing fission fragments. (Received dose in pre-irradiation 411 Mrad, and dose rate 4.57 Mrad/min)

| Sample No. | Time of annealing (min) | Fractional activity of iodate ($^{131}I$) | Fractional activity of iodate ($^{133}I$) |
|---|---|---|---|
| control | - | 0.55 | 0.54 |
| 1 | 3.5 | 0.52 | 0.52 |
| 2 | 7 | 0.47 | 0.47 |
| 3 | 52 | 0.45 | 0.45 |

Fig. 5.9 Thermal annealing of $K_2SO_4$ containing fission fragments ($^{131}I$)

(A) Samples irradiated with electrons prior to fission fragments injection

(B) No pretreatment prior to fission fragments injection

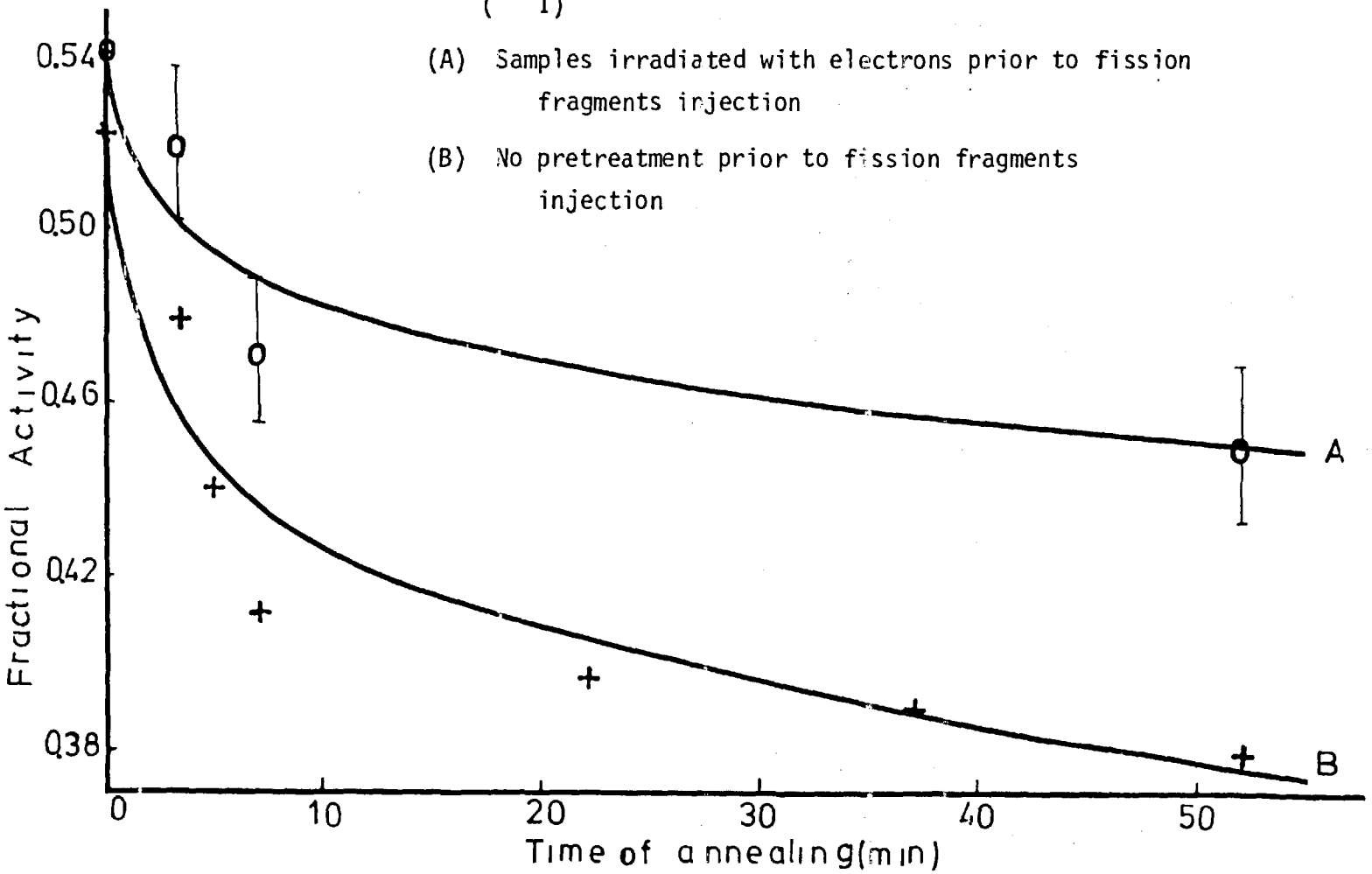

# CHAPTER 6

## Influence of the cationic dopants on the valency states of fission fragment iodine in $K_2SO_4$

### 6.1 Introduction

The effects of cation impurities on the valency states of fission fragment iodine in $K_2SO_4$ is discussed in this chapter. Potassium sulphate doped with sulphates of $Li^+$, $Cs^+$, $Mg^{2+}$, $Cu^{2+}$, $Fe^{2+}$ and $Al^{3+}$ have been investigated. The cations with one, two and three valency states were used to see if impurities with different charges behave differently on the valency states of fission fragments iodine.

### 6.2 Experimental

All the samples used in this investigation were irradiated in the core tube number 2 position 6 of the reactor, with a neutron flux of $0.7 \times 10^{12}$ n $sec^{-1}$ $cm^{-2}$. The assembly used for irradiation was the same as described in Chapter 3 section 3.2. The irradiated samples were delivered to College the day after irradiation and analysed three days after irradiation. The samples containing fission fragments were analysed and the activity of iodine as iodide and iodate were calculated as described in Chapter 3 sections 3 and 13. For each series of doping a control sample of $K_2SO_4$ were prepared exactly in the same condition as the doped samples.

#### 6.2.1 Preparation of the doped samples

All the material used for preparation of the doped samples were analar grade. The doping of $K_2SO_4$ with sulphates of $Li^+$, $Cs^+$, $Cu^{2+}$, $Fe^{2+}$ $Mg^{2+}$ and $Al^{3+}$ were carried out by dissolving known amounts of dopant sulphate in solutions of $K_2SO_4$ and solutions were heated in the oven at different temperatures to complete dryness. The doped $K_2SO_4$ was then ground to powder and kept in a desiccator before irradiation.

(A) Preparation of $K_2SO_4$ doped with $Li_2SO_4$

Amounts of 5.8, 10.2, 19.5, 33.5, 53 and 67.1 mgs of $Li_2SO_4.H_2O$ were added to six 100 mls beakers;each contained 1.5 gm $K_2SO_4$ dissolved in 30 mls distilled water. The solution was heated in the oven at 100°C to complete drynes

( 24 hours). When the samples reached constant weight they were ground to powder and kept in a desiccator. A solution of $K_2SO_4$ was recrystallised exactly in the same conditions and used as a control. The samples, each in a small polythene capsule were placed in a large capsule (6 cm height and 2.5 cm diameter) and sent to the reactor for irradiation.

(B) Preparation of $K_2SO_4$ doped with $Cs_2SO_4$ and $MgSO_4$

The same procedure as described in Part B was carried out. The amounts of $Cs_2SO_4$ used were 10.4, 23.4, 38.9, 60.8, 127.2 and 174.9 mgs and for $MgSO_4$ were 10, 19.6, 84.1, 126.3 and 206.2 mgs.

(C) Preparation of $K_2SO_4$ doped with $CuSO_4$, and $Al_2(SO_4)_3$

The same procedure was used for preparation of $K_2SO_4$ doped with $Cu^{2+}$ and $Al^{3+}$. The samples of $K_2SO_4$ doped with $Cu^{2+}$ were placed in the oven at $50^oC$ for 16 hours, and then at $100^oC$ for 24 hours, and finally constant weights were obtained when the samples were heated at $160^oC$ for 4.5 hours. The colour of the doped samples was light blue. The solutions of $K_2SO_4$ doped with $Al^{3+}$ were placed in the oven at $160^oC$ for 24 hours (to constant weight). The concentration of Al in the doped samples was measured by optical emission spectroscopy using an inductive coupled argon plasma.

(D) Preparation of the samples of $K_2SO_4$ doped with $FeSO_4$ in the vacuo.

For the preparation of samples of $K_2SO_4$ doped with $FeSO_4$ special care was taken to prevent oxidation of FeSO4. It is well known that $FeSO_4$ oxidises very easily with atmospheric oxygen, and heat (68). In order to prevent oxidation of the $FeSO_4$, the doped samples were prepared in a vacuum. The assembly used for the preparation of the samples is shown in Fig. 6.1. Potassium sulphate (1.5 gms) was added to 30 mls of the deoxygenated water (deoxygenated water was prepared by boiling the distilled water for an hour) in a conical flask (A) and dissolved. A known amount of $FeSO_4.7H_2O$ was added to the $K_2SO_4$ solution and quickly connected to the vacuum system. The flask was shaken very gently in order to dissolve $FeSO_4$. The flask was

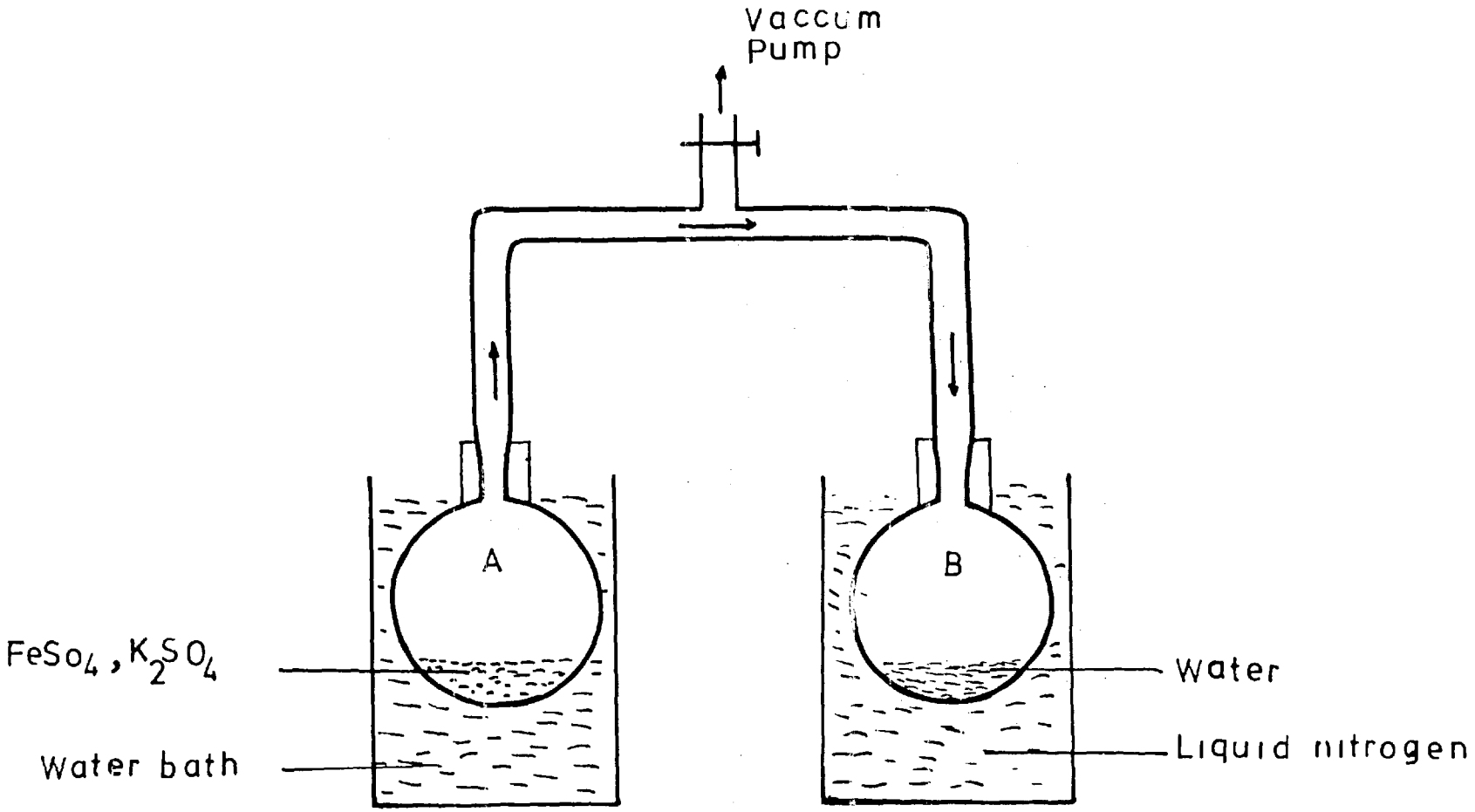


Fig. 6.1 Apparatus used for preparation of the samples of the $Fe^{2+}$-doped $K_2SO_4$

placed in a water bath (temperature of the bath was about 20°C) and evaporated water was collected in flask (B), which was kept in the liquid nitrogen. The samples were kept under vacuum until it was completely dry. Four samples were prepared in this way with 9.7, 19.9, 29.9 and 49.6 mgs of $FeSO_4.7H_2O$ respectively. A control of $K_2SO_4$ was also prepared with these conditions. The samples were kept in a desiccator before sending to the reactor. The concentration of Fe in the doped crystal was measured by the atomic absorption method.

## 6.3 Results

Doping of $K_2SO_4$ with monovalant cations ($Li^+$, $Cs^+$) did not show any change in the distribution of iodine fission fragment as iodide and iodate. $K_2SO_4$ doped with $Cu^{2+}$, $Mg^{2+}$, $Fe^{2+}$ and $Al^{3+}$ showed significant decrease in the fractional activity of iodate. The largest decrease was observed in $K_2SO_4$ doped with Al. The rate of decrease in the iodate fraction was proportional to the concentration of the dopant up to a few atoms % and after that the decrease in the iodate became much slower. Curves of fractional activity of iodate against concentration of dopant (in atom %) are shown in figs. 6.2 and 6.3, for isotopes $^{131}I$ and $^{132}I$. The same behaviour has been observed for isotope $^{133}I$. Fractional activities of iodate for $^{131}I$, $^{133}I$ and $^{132}I$ in $K_2SO_4$ doped with $Li^+$, $Cs^+$, $Mg^{2+}$, $Cu^{2+}$, $Fe^{2+}$ and $Al^{3+}$ are shown in Tables 6.1, 6.2, 6.3, 6.4, 6.5, 6.6 respectively. The concentration (in atom %) of the dopant of Li, Cs, Mg and Cu were calculated assuming that all the dopant materials have been taken up by the $K_2SO_4$. For $K_2SO_4$ doped with Fe and Al, the concentration of the Fe and Al were measured by atomic absorption and plasma emission spectroscopy. In both cases the results showed that there were no significant losses and that all the dopant material had been absorbed by the $K_2SO_4$.

Fig. 6.2 Variations of the fractional activity of iodate as a function of the dopant concentration ($^{131}I$)

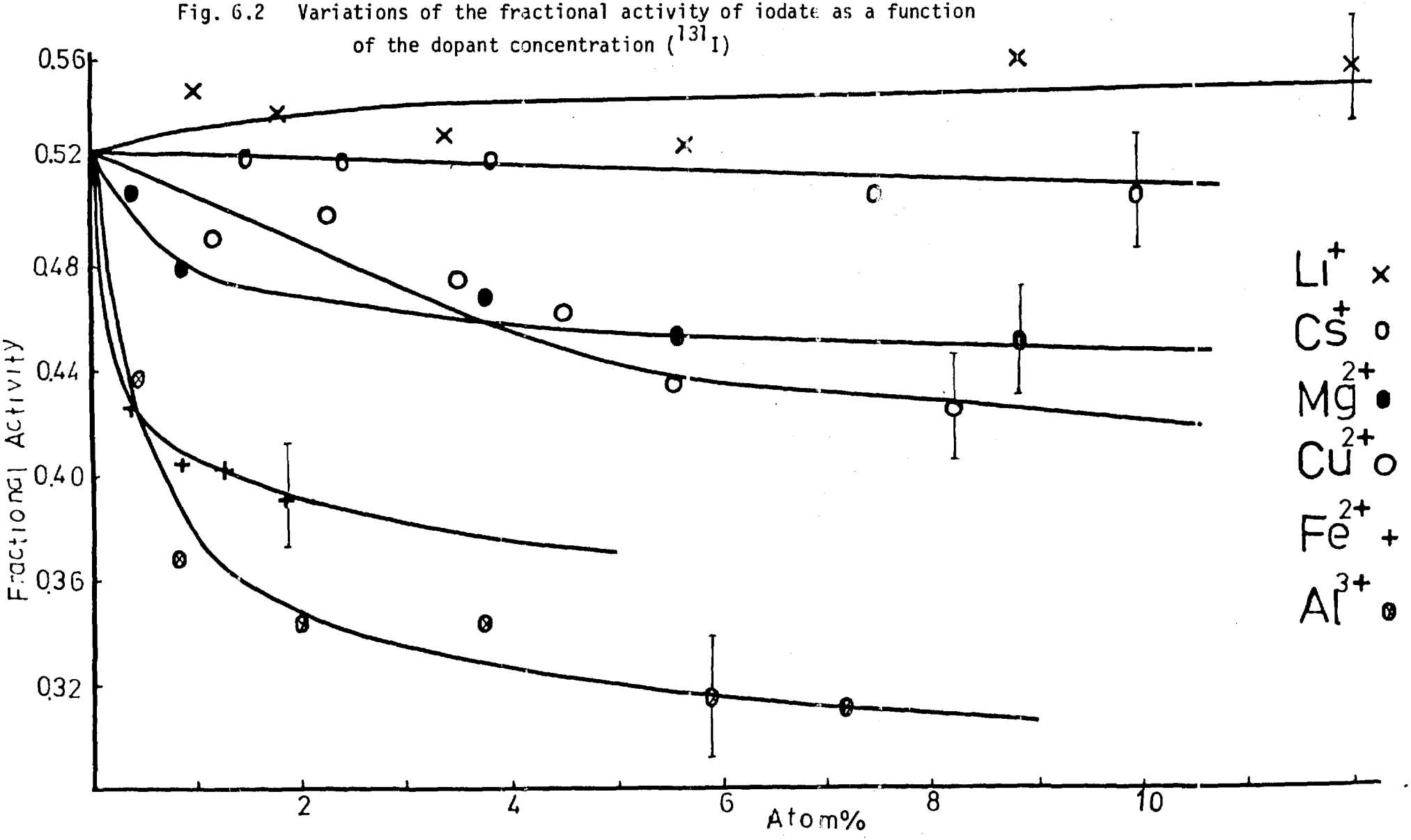

Fig. 6.3 Variations of the fractional activity of iodate as a function of the dopant concentration ($^{132}I$)

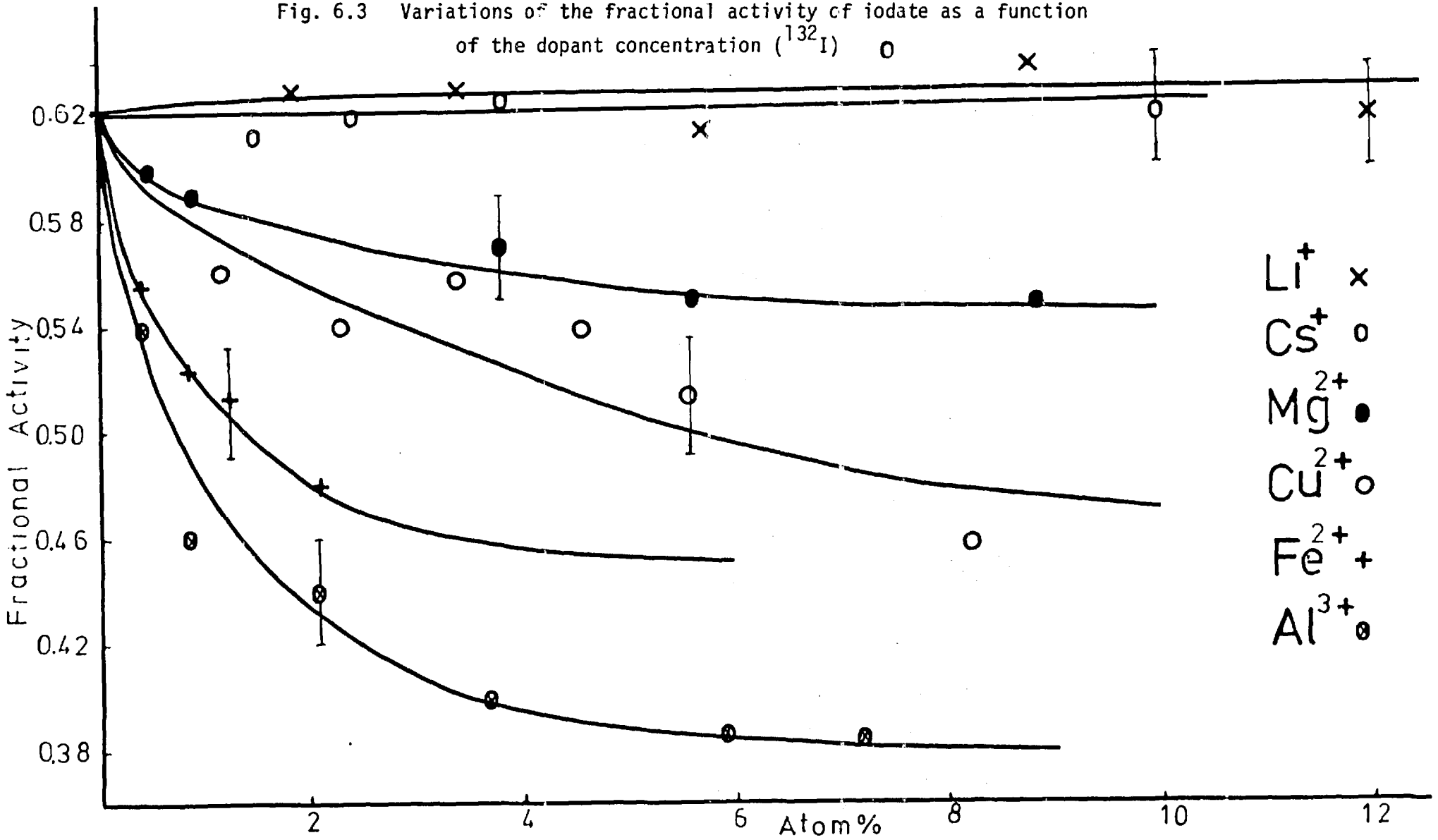

## 6.4 Discussion

The decrease in the fractional activity of iodate in the doped $K_2SO_4$ can be explained in terms of cation vacancies produced by the dopant and migration of the holes in the damaged crystal. Several ESR studies on the dopant impurities in $K_2SO_4$ and $K_2SeO_4$ (19, 20, 21, 27) lend support to the hypothesis that the impurity enters a $K^+$ site producing $K^+$-vacancy, $\square K_+$. In general the production of vacancies by cation impurity (M) before irradiation can be written as follows:

$$M^{n+} \longrightarrow M_{k+}^{n+} + (n-1)\,\square K_+ \qquad 6.1$$

Irradiation of doped $K_2SO_4$ by fission fragments creates donor/acceptor species. In the ESR study of irradiated $K_2SO_4$ (as discussed in Chapters 4 and 5) radical $SO_3^-$ has been identified as a major electron donor in the thermal annealing processes. Here it is assumed that the behaviour of the $SO_3^-$ radical ion is the same as the pure $K_2SO_4$, and it is acting as a hole capture during the irradiation. Cation vacancies are able to capture the holes with high efficiencies.

$$\square k_+ + h \longrightarrow \boxdot k_+ \qquad 6.2$$

The species capable of producing the hole are cation impurities and $I^F$ (The form of iodine which converts to iodate on dissolution)

$$M_{k+}^{n+} \rightleftharpoons M_{K+}^{(n-1)} + (+h) \rightleftharpoons M_{K+}^{(n-2)} + (+h) \qquad 6.3$$

For example for $Al^{3+}$

$$Al_{k+}^{3+} \rightleftharpoons Al_{k+}^{2+} + (+h) \rightleftharpoons Al_{K+}^{1+} + (+h) \qquad 6.4$$

and for $I^F$

$$I^F \xrightarrow{\text{defects}} I^{-1} + (+h) \qquad 6.5$$

since the concentration of $I^F$ is very small compared with cation vacancies and cation impurities the major competition exists between $M_{k+}^{n+}$ (hole donor) and $\square k_+$ (hole acceptor). It is assumed that the reduction of $I^F$ (according

to equation 6.5)in doped $K_2SO_4$ is due to irradiation and more likely due to defects in the crystals. Since the role of the $SO_3^-$ radical is the same (it was assumed) in the pure and the doped crystal and the radiation dose is also the same, therefore the role which is played by cation vacancy and cation impurity must be taken into consideration. The decrease of iodate in the doped samples suggested that the efficiency of the cation vacancies for capturing the holes (releasing electrons) is higher than the efficiency of the cation impurities for releasing the holes (capturing electron). Therefore equation 6.2 is more efficient than equation 6.3. The unchanged ratio of the iodate/iodide in the $K_2SO_4$ doped with monovalant cations ($Li^+$, $Cs^+$) is not unreasonable, since no cation vacancies exist in these doped samples. The efficiencies of the impurities for reduction in the iodate fractional activity are in the order of $Al^{3+} > Fe^{2+} > Mg^{2+}$, $Cu^{2+}$. The smaller decrease of the iodate in $K_2SO_4$ doped with divalant cations can be explained by the lower number of the cation vacancies that they introduced in the lattice as compared to that of Al. $K_2SO_4$ doped with $Fe^{2+}$ showed the higher decrease in the fractional activity of iodate compared with $Cu^{2+}$ and $Mg^{2+}$. Since the number of cation vacancies are the same for $Mg^{2+}$, $Cu^{2+}$ and $Fe^{2+}$, one would expect to see the same reduction in the iodate. To explain this exceptional behaviour of $Fe^{2+}$, it was assumed that equation 6.3 is more likely to go to the left in $K_2SO_4$ doped with $Fe^{2+}$ than it is for $Cu^{2+}$ and $Mg^{2+}$. This means less hole would be introduced (less electron would be captured) in the $K_2SO_4$ : Fe system than it is for $K_2SO_4$:Mg and $K_2SO_4$: Cu. The ionization potential for taking two electrons away from $Fe^{2+}$, $Mg^{2+}$ and $Cu^{2+}$ are as follows:

| | | | | | Total ionization potential (ev) |
|---|---|---|---|---|---|
| Fe | $\xrightarrow{7.87\ ev}$ | $Fe^+$ | $\xrightarrow{16.18\ ev}$ | $Fe^{2+}$ | 24.05 |
| Cu | $\xrightarrow{7.724ev}$ | $Cu^+$ | $\xrightarrow{20.29\ ev}$ | $Cu^{2+}$ | 28.01 |
| Mg | $\xrightarrow{7.644ev}$ | $Mg^+$ | $\xrightarrow{15.03\ ev}$ | $Mg^{2+}$ | 22.64 |

Since the energy required for taking two electrons away from Fe atom is not the lowest compared with Cu and Mg, the above assumption is not supported in terms of ionization potential. Another explanation is that $Fe^{2+}$ could easily be oxidised to $Fe^{3+}$, during the irradiation and/or during the preparation of the doped samples. Although care was taken to avoid oxidation of $Fe^{+2}$ during the preparation of the doped samples, due to sensitivity of the $FeSO_4$ towards oxidation, it is possible that some of the $Fe^{2+}$; has oxidized to $Fe^{3+}$. If this is the case, it is reasonable to see higher decrease in iodate in $K_2SO_4$:Fe system, because the number of cation vacancies introduced is higher than that of $Cu^{+2}$ and $Mg^{2+}$. Slight differences between $Cu^{2+}$ and $Mg^{2+}$ could not be explained. As can be seen from figs. 6.2, 6.3, $^{132}I$ behaved exactly the same as $^{133}I$ and $^{131}I$, although it always showed higher iodate fraction (~10%) compared with $^{131}I$ and $^{133}I$.

Table 6.1 Fractional activity of iodate in the $Li^+$-doped $K_2SO_4$

| NO | Atom % Li | $^{131}I$ | $^{133}I$ | $^{132}I$ |
|---|---|---|---|---|
| control | | | | |
| 1 | - | 0.524 | 0.523 | 0.62 |
| 2 | 1.04 | 0.55 | 0.544 | 0.68 |
| 3 | 1.82 | 0.54 | 0.544 | 0.63 |
| 4 | 3.42 | 0.53 | 0.533 | 0.63 |
| 5 | 5.73 | 0.525 | 0.523 | 0.61 |
| 6 | 8.78 | 0.57 | 0.548 | 0.64 |
| 7 | 12.11 | 0.565 | 0.55 | 0.615 |

Table 6.2 Fractional activity of iodate in the $Cs^{+}$-doped $K_2SO_4$

| NO | Atom % Cs | $^{131}I$ | $^{132}I$ |
|---|---|---|---|
| control | | | |
| 1 | - | 0.524 | 0.62 |
| 2 | 1.5 | 0.519 | 0.61 |
| 3 | 2.4 | 0.52 | 0.62 |
| 4 | 3.8 | 0.52 | 0.63 |
| 5 | 7.55 | 0.504 | 0.65 |
| 6 | 10.1 | 0.504 | 0.62 |

Table 6.3 Fractional activity of iodate in the $Mg^{2+}$-doped $K_2SO_4$

| NO | Atom % of Mg | $^{131}I$ | $^{133}I$ | $^{132}I$ |
|---|---|---|---|---|
| control | | | | |
| 1 | - | 0.524 | 0.523 | 0.62 |
| 2 | 0.47 | 0.51 | 0.502 | 0.60 |
| 3 | 0.91 | 0.48 | 0.475 | 0.59 |
| 4 | 3.8 | 0.47 | 0.47 | 0.57 |
| 5 | 5.62 | 0.456 | 0.45 | 0.55 |
| 6 | 8.86 | 0.452 | 0.44 | 0.55 |

Table 6.4 Fractional activity of iodate in the $Cu^{2+}$-doped $K_2SO_4$

| Sample No. | Cu Atom % | $^{131}I$ | $^{133}I$ | $^{132}I$ |
|---|---|---|---|---|
| control 1 | | 0.524 | 0.523 | 0.62 |
| 2 | 1.18 | 0.49 | 0.504 | 0.558 |
| 3 | 2.29 | 0.50 | 0.504 | 0.54 |
| 4 | 3.45 | 0.476 | 0.485 | 0.56 |
| 5 | 4.53 | 0.463 | 0.437 | 0.54 |
| 6 | 5.58 | 0.432 | 0.40 | 0.513 |
| 7 | 8.32 | 0.425 | 0.38 | 0.455 |

Table 6.5 Fractional activity of iodate in the $Fe^{2+}$-doped $K_2SO_4$

| Sample No. | Atom % Fe | $^{131}I$ | $^{133}I$ | $^{132}I$ |
|---|---|---|---|---|
| control 1 | - | 0.524 | 0.523 | 0.62 |
| 2 | 0.42 | 0.427 | 0.435 | 0.555 |
| 3 | 0.83 | 0.404 | 0.427 | 0.524 |
| 4 | 1.36 | 0.402 | 0.382 | 0.514 |
| 5 | 1.8 | 0.39 | 0.376 | 0.48 |

Table 6.6 Fractional activity of iodate in the $Al^{3+}$-doped $K_2SO_4$

| Sample No. | Atom % | $^{131}I$ | $^{133}I$ | $^{132}I$ |
|---|---|---|---|---|
| control 1 | - | 0.524 | 0.523 | 0.62 |
| 2 | 0.48 | 0.438 | 0.404 | 0.54 |
| 3 | 0.84 | 0.367 | 0.348 | 0.457 |
| 4 | 2.06 | 0.343 | 0.31 | 0.437 |
| 5 | 3.7 | 0.348 | 0.306 | 0.40 |
| 6 | 5.9 | 0.313 | 0.29 | 0.386 |
| 7 | 7.2 | 0.311 | 0.30 | 0.386 |

# CHAPTER 7

## Effects of pH and water of crystallization on the valency states of fission fragment iodine

### 7.1 Introduction

In this chapter the effects of pH and moisture in $K_2SO_4$ containing fission fragments is investigated. Acid samples of $K_2SO_4$ were prepared and the results were compared with neutral $K_2SO_4$ and pure $KHSO_4$. The effects of water of crystallization on the distribution of valency states of fission fragment iodine were also studied in different sulphates. The hydrous and anhydrous sulphates of Li, Cs, Na, Cu, Mg, Fe and Al were irradiated with fission fragments and the results were compared.

### 7.2 Experimental

All the samples studied were irradiated in the core tube two position 6 with a neutron flux of $0.7 \times 10^{12}$ n $sec^{-1}$ $cm^{-2}$. The active sample containing fission fragments was analysed three days after irradiation. The assembly used for the irradiation was the same as described in Chapter 3 section 2. The active samples were analysed as explained in Chapter 3 section 9, unless stated otherwise.

#### 7.2.1 Preparation of acid and alkaline $K_2SO_4$ for irradiation

$K_2SO_4$ was prepared from KOH and $H_2SO_4$ according to the following equation:

$$2KOH + H_2SO_4 \longrightarrow K_2SO_4 + 2H_2O \qquad (7.1)$$

A titration method (59) was used for preparing neutral, acid and alkaline samples of $K_2SO_4$. 20 mls of KOH solution (1.00 87M) were transferred to a 250 mls conical flask and 30 mls of water were added. The solution was titrated with $H_2SO_4$ (1.008 N) and methyl red (a few drops) was used as an indicator. 11.8 mls of $H_2SO_4$ were used to prepare a neutral solution of $K_2SO_4$. A neutral solution as described above was prepared and used as a

control. To prepare the acid solutions of $K_2SO_4$, to three 100mls beakers each containing neutral solutions of $K_2SO_4$, 0.2, 1.2 and 2.2 mls excess $H_2SO_4$ were added. Adding excess $H_2SO_4$ to the neutral solution of the $K_2SO_4$, caused production of the $KHSO_4$ according to the following equation:

$$H_2SO_4 + K_2SO_4 \longrightarrow 2KHSO_4 \qquad (7.2)$$

Three alkaline solutions were prepared by adding 0.5, 1, 1.5 mls excess KOH solution to three 100 mls beakers each containing neutral solution of $K_2SO_4$. The neutral acid and alkaline solutions were placed in the oven at 100°C and heated to complete dryness ( 16 hours). The samples were ground to a powder and kept in a desiccator before being sent to the reactor.

(A) Irradiation of $KHSO_4$ samples

The $KHSO_4$ powder was pressed in a mould under 15 atmospheres pressure. The diameter of the mould was slightly greater than that of the Pt discs (see Chapter 3, section 3). This meant that the area of the tablets would be greater than the area of uranium oxide film. This helped to minimise the edge effects. The weight of the pellets was 0.3 gms with a thickness of about 2mm. The samples were kept in a desiccator before being sent to the reactor. The active samples were halved and each part was analysed at room temperature.

7.2.2 Effect of dissolving the active samples in the acid before adding carrier solution

The standard procedure for analysing active samples was to dissolve samples in a mixed solution of the carriers (KI and $KIO_3$) and then add acid. In the following experiments, the active samples were dissolved in the acid solution first and then carrier solutions were added. The same procedure as described in Chapter 3, section 9 was used for analysing the samples.

(A) $K_2SO_4$ containing fission fragments was dissolved in 3 ml (0.2M) $H_2SO_4$ and diluted to 10 mls with distilled water and then a mixture of carrier solutions of KI and $KIO_3$ was added.

(B) $K_2SO_4$ containing fission fragments was dissolved in acid solution, $KIO_3$ carrier solution was added first, mixed and finally carrier solution of KI was added.

(C) After dissolving $K_2SO_4$ containing fission fragments in the acid, KI solution was added first, mixed and finally $KIO_3$ solution was added.

(D) Active samples of $K_2SO_4$ were dissolved and left in an acid solution for 24 hours. The carrier solutions of KI and $KIO_3$ was added and then the solution was analysed.

7.2.3 Test for the effect of moisture

These experiments were carried out in order to study the effect of moisture on the valency distribution of fission fragment iodine in $K_2SO_4$. To three samples of anhydrous $K_2SO_4$, amounts of 0.025, 0.05 and 0.075 ml of distilled water were added respectively, and then the samples sent to the reactor for irradiation.

7.2.4 Preparation of the sulphates of Li, Cs, Na, Cu Mg, Fe and Al for irradiation

The aim of these experiments was to investigate firstly the oxidation states of fission fragment iodine in different sulphates and secondly the effect of water of crystallization on each pair of sulphate (hydrous and anhydrous).

(A) Preparation of the hydrous sulphates

The sulphates (analar grade) of $LiSO_4 \cdot H_2O$, $Na_2SO_4.10\,H_2O$, $MgSO_4.7H_2O$, $FeSO_4.7H_2O$, $CuSO_4.5H_2O$ and $Al_2(SO_4)_3.16H_2O$, were ground to powder and the assembly described in Chapter 3 section 2 was used for irradiation. All samples (each in small polythene capsules) were placed in a large capsule and sent for irradiation.

(B) Preparation of the anhydrous sulphates

The anhydrous sulphates of Li, Mg, Cu and Al were prepared by the dehydration of the hydrous sulphates. Dehydration of the above salts was carried out at temperatures recommended by the literature. The salts

were ground to powder before heating. $Li_2SO_4.H_2O$ (69), $MgSO_4.7H_2O$ (70), and $Al_2(SO_4)_3.16\ H_2O$ (71) were placed in the oven at 210°C for 48 hours. Dehydration of $CuSO_4.5H_2O$ (72) needed a higher temperature, the powder was placed in the furnace at 360°C for 20 hours and heated to constant weight. All the dehydrated salts were kept in the desiccator before being sent to the reactor.

## 7.3 Results and discussion

### 7.3.1 Results of the pH effect

A significant decrease in the fractional activity of iodate has been observed in the acid samples of $K_2SO_4$. Alkaline samples of $K_2SO_4$ (excess KOH) did not show any change in the iodate fraction. The values of the fractional activity of iodate in acid and alkaline samples are shown in Table 7.1. As can be seen from this table, almost the same decrease in the iodate fraction has been observed for $^{131}I$, $^{133}I$ and $^{132}I$, although $^{132}I$ showed a higher iodate fraction.

Table 7.1

Fractional activity of iodate in acid and alkaline $K_2SO_4$ containing fission fragments

| No. | Excess Acid (ml) | $^{131}I$ | $^{133}I$ | $^{132}I$ |
|---|---|---|---|---|
| control 1 | - | 0.534 | 0.522 | 0.59 |
| 2 | 0.2 | 0.47 | 0.336 | 0.45 |
| 3 | 1.2 | 0.284 | 0.27 | 0.40 |
| 4 | 2.2 | 0.24 | 0.20 | 0.18 |
| | excess alkali ml | | | |
| 5 | 0.5 | 0.514 | 0.505 | 0.60 |
| 6 | 1 | 0.515 | 0.50 | 0.606 |
| 7 | 1.5 | 0.492 | 0.49 | 0.606 |

Irradiation of pure $KHSO_4$ showed a very small amount of iodate fraction. The average of four measurements is shown in Table 7.2. As can be seen from this table about 4% of the iodine fission fragments exist in the oxidising form, which compared with $K_2SO_4$ is very small. The samples were analysed 24 hours after irradiation, therefore it was possible to detect isotope $^{135}I$ as well as $^{131}I$ and $^{133}I$.

Table 7.2 Fractional activity of iodate in pure $KHSO_4$ containing fission fragments

| Sample | $^{131}I$ | $^{133}I$ | $^{135}I$ |
|---|---|---|---|
| $KHSO_4$ | 0.038±0.03 | 0.035±0.03 | 0.047±0.026 |

No significant differences have been observed between isotopes $^{131}I$, $^{133}I$ and $^{135}I$.

The results of dissolving $K_2SO_4$ containing fission fragments in acid solution prior to adding carrier solution are shown in Table 7.3. It can be seen that the sample that has been left in the acid solution for 24 hours showed the lowest fractional activity.

The results of the acid samples of $K_2SO_4$ and the samples which have been dissolved in acid prior to carrier solutions suggested that the iodate was reduced to iodine by the following reaction:

$$\overset{*}{I}O_3^- + 5\overset{*}{I}^- + 6H^+ \longrightarrow 3\overset{*}{I}_2 + 3H_2O \qquad (7.3)$$

Therefore when the carrier solution is added last there is only a small amount of $IO_3^-$ available to exchange with the $KIO_3$ carrier. The possibility of reduction of iodate did not exist for sample which was dissolved in carrier solution first followed by the addition of acid. As can be seen from Table 7.3, fractional activities of iodate are the same in experiments 2 and 3, but it is smaller in experiment 4. The reason for the lower iodate in experiment 4 is not clear. Results obtained for $^{131}I$ and $^{133}I$ are almost the same; $^{132}I$ showed higher iodate in all experiments (in Chapter 5 section 1A it is discussed why $^{132}I$ behaves differently).

Table 7.3 Effect of conditions of dissolution on the fractional activity of iodate

| Experiment No. | Conditions of dissolution of active sample in acid and carrier solution | $^{131}I$ | $^{133}I$ | $^{132}I$ |
|---|---|---|---|---|
| 1 | Sample first added to mixture of carrier solutions (KI and $KIO_3$) and then acid were added | 0.524 | 0.523 | 0.62 |
| 2 | Sample first dissolved in acid and then a mixture of carrier solution was added | 0.30 | 0.28 | 0.39 |
| 3 | Sample dissolved in acid, $KIO_3$ added first, mixed, and then KI added | 0.30 | - | 0.37 |
| 4 | Sample dissolved in acid, KI added first, mixed, and then $KIO_3$ added | 0.12 | 0.10 | 0.17 |
| 5 | Sample dissolved in acid left for 24 hours and then mixture of carriers added | 0.04 | 0.05 | 0.24 |

7.3.2 Results of the moisture effect

Adding different amounts of water to the powdered $K_2SO_4$ prior to irradiation, causes a decrease in the fractional activity of the iodate. The results are shown in Table 7.4. The results suggested that the water was acting as a reducing agent. The role of water is discussed in detail in the next section. A curve of fractional activity against the amounts of water added is shown in Fig. 7.1.

Table 7.4 Effect of moisture (water added to $K_2SO_4$ prior to irradiation) on the fractional activity of iodate

| Water added (mL) | $^{131}I$ | $^{133}I$ |
|---|---|---|
| control | 0.524 | 0.523 |
| 0.025 | 0.473 | 0.493 |
| 0.05 | 0.444 | 0.444 |
| 0.075 | 0.439 | 0.424 |

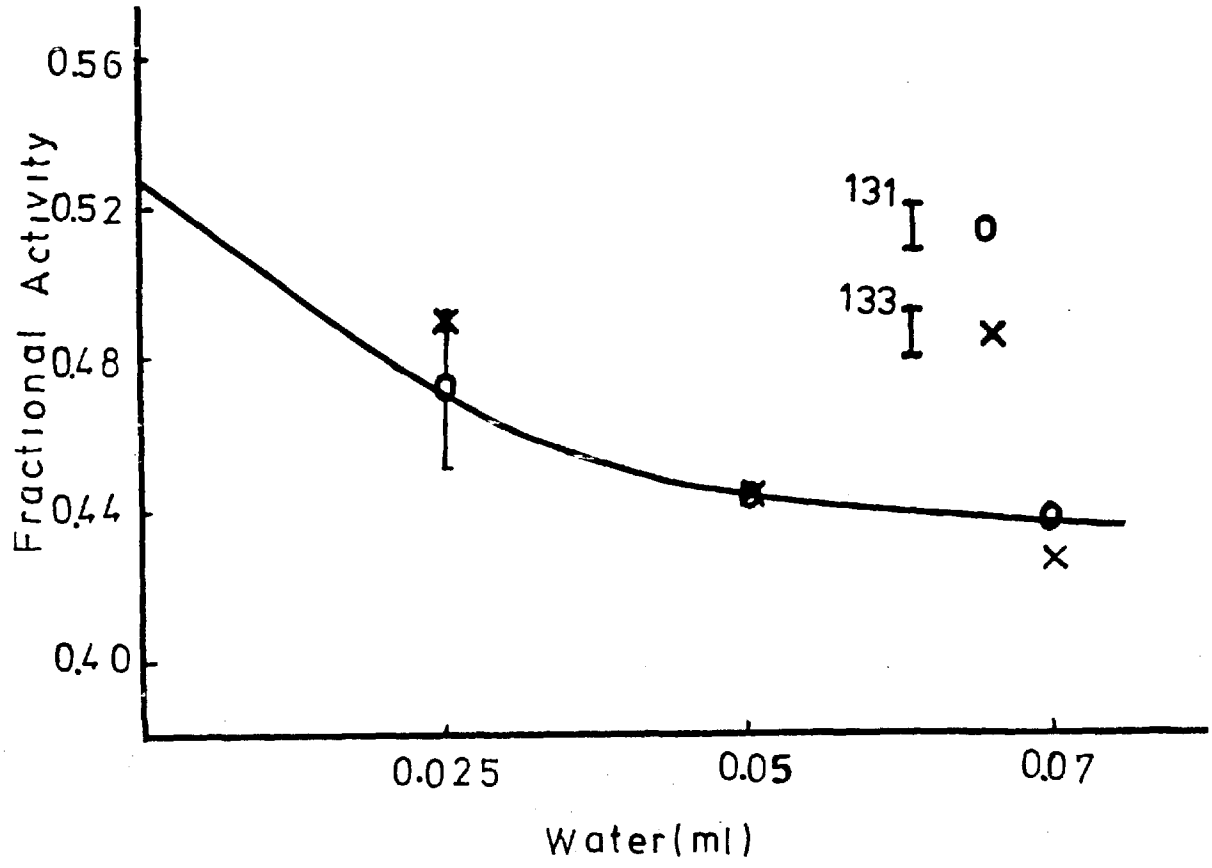


Fig. 7.1 Effect of moisture (water added to $K_2SO_4$ prior to irradiation) on the fractional activity of iodate

### 7.3.3 Results of the oxidation states of fission fragment iodine in hydrous and anhydrous sulphate of alkali metals, Mg, Cu, Fe and Al

The results obtained from irradiation of different sulphates by fission fragments are shown in Tables 7.5 (alkali metal sulphate) and 7.6 (Mg, Cu, Fe and Al , sulphate). These results reveal two major findings:

I • The hydrous sulphate in all cases showed a lower amount of iodate compared with its anhydrous sulphate.

II. Sulphates with different cations showed different amounts of iodate.

The following is a discussion on the above observation.

A. Effect of water of crystallization

The results obtained in this work suggested that the presence of water of crystallization in the lattice during the irradiation causes reduction of the recoil iodine atoms. It seems that the species with reducing properties such as hydrated electron or H atom produced from radiolysis of water (as described in Chapter 2) play a role in the reduction of the oxidized form of the iodine fission fragment. The hydrated electron possesses many features in common with electrons trapped in solids. The hydrated electron is a powerful reducing agent, and it can be captured by ions which have a positive electron affinity (32). Hydrogen atoms are less powerful reducing agents than hydrated electrons (32), but they are more likely to be formed in solids during irradiation. The role of the hydrated electron is more likely in the aqueous system. Anbar and Hart (74) have reported that the iodate ions were reduced by hydrated electrons produced as a result of radiolysis of water at pH7. The stopping power of liquid water for uranium fission fragments is ∿1800 KeV/μm, which is much higher than the other particle (see Chapter 2, Table 2.2). Fission fragments entering the lattice create thermal and displacement spikes (see Chapter 1, section 2.9). Thermal spikes create hot zones in the lattice whose temperature is very high, but because of the short duration, the spike region does not attain a true

Table 7.5 Fractional activity of iodate in hydrous and anhydrous sulphates of alkali metals.

| Sample | $^{131}I$ | $^{133}I$ | $^{132}I$ |
|---|---|---|---|
| $Li_2SO_4$ | 0.56 | 0.57 | 0.65 |
| $Li_2SO_4.H_2O$ | 0.25 | 0.20 | 0.49 |
| $Na_2SO_4$ | 0.50 | 0.47 | 0.624 |
| $Na_2SO_4,10H_2O$ | 0.44 | 0.426 | 0.54 |
| $K_2SO_4$ | 0.524 | 0.523 | 0.62 |
| $K_2SO_4$ + 0.075ml $H_2O$ | 0.439 | 0.424 | - |
| $Cs_2SO_4$ | 0.42 | 0.41 | 0.56 |

Table 7.6 Fractional activity of iodate in hydrous and unhydrous sulphates of Mg, Cu, Al and $FeSO_4.7H_2O$

| Sample | $^{131}I$ | $^{133}I$ | $^{132}I$ |
|---|---|---|---|
| $MgSO_4$ | 0.41 | 0.38 | 0.55 |
| $MgSO_4.7H_2O$ | 0.35 | 0.31 | 0.48 |
| $CuSO_4$ | 0.21 | 0.205 | 0.32 |
| $CuSO_4.5H_2O$ | 0.13 | 0.12 | 0.26 |
| $Al_2(SO_4)_3$ | 0.38 | 0.32 | 0.60 |
| $Al_2(SO_4)_3.16H_2O$ | 0.22 | 0.19 | 0.52 |
| $FeSO_4.7H_2O$ | 0.10 | 0.08 | 0.20 |

liquid state, and may be more accurately described as a superheated solid. Since the stopping power of the water is very high for fission fragments, the formation of the hydrated electron is not unlikely in these very hot regions. This possibility has also been suggested by Harbotte and Sutin (75). They proposed that the water molecules or ammonium ions are likely to reduce the recoiling fragments in the hot zones produced at the end of their tracks. Another model for the reduction of the recoil fragments by water of hydration has been suggested by Peixota and Maddock (39). In this extensive review on the role of water of hydration they have suggested that the differences observed in the initial retention can be explained not so much by the hot zone reactions and recoil event, but can arise because of the differences in the required energies to promote electrons from the different centres to the conduction band and therefore allow them to be captured by the other centres. Either of the two models explains the results obtained in this work but experiments carried out here do not allow us to distinguish between the two models. Table 7.7 shows the percentage decrease in the fractional activity of iodate in the hydrous form of different sulphates. As can be seen from this table a remarkable decrease has been observed for $LiSO_4.H_2O$. Sulphates of Na, Mg and Cu showed almost the same decrease in the iodate fraction. The decrease in the aluminium sulphate is higher than Na, Cu, and Mg but it is lower than that for Lithium Sulphate.

Table 7.7 Percentage decrease in the fractional activity of iodate in the hydrous form of different sulphates relative to anhydrous sulphates.

| Compound | $^{131}I$ | $^{133}I$ | $^{132}I$ |
|---|---|---|---|
| Lithium sulphate | 31 | 37 | 16 |
| Aluminium sulphate | 16 | 13 | 8 |
| Sodium sulphate | 6 | 5 | 8 |
| Magnesium sulphate | 6 | 7 | 7 |
| Copper sulphate | 8 | 8 | 6 |

The differences in the decrease of the fractional activity of iodate for different sulphates can be explained by their different crystal structure and the number of water molecules involved. The results obtained for isotopes, $^{131}I$ and $^{133}I$ were almost the same. In all experiments carried out so far $^{132}I$ always showed a higher fraction of iodate. It has been concluded (see Chapter 5, section 1A) that the different behaviour of isotope $^{132}I$ could well be due to its way of formation.

(B) Effects of cation and crystal structure on the valency states of the fission fragment iodine in different sulphates.

Significant differences observed in the fractional activity of iodate in different sulphates could not easily be explained. The following factors are considered to play a role in distribution of fission fragment iodine in its reduced and oxidised form.

I. Ionic radii

Graphs of fractional activity of iodate against ionic radii of the cations of the anhydrous alkali sulphates are shown in Fig. 7.2. As can be seen from this Figure, Li with the lowest ionic radius gives the highest iodate, while Cs with highest ionic radius gives the lowest iodate fraction. Sulphates of Na and K are behaving differently, although the amount of iodate in these sulphates is lower than Li and higher than Cs. The same relation exists between the cations of the anhydrous sulphates of Mg and Cu (see Fig. 7.3) and hydrous sulphate of Mg, Cu and Fe (see Fig. 7.4). The hydrous sulphates of Li and Na do not show the same behaviour.

The above observations suggested that the ionic radii is one of the major factors governing the distribution of the valency states of the fission fragment iodine in different sulphates. The ionic radius of the cations are shown in Table 7.8.

II. The crystal structure effect

Another factor which should be considered is the crystal structure of the materials studied. The crystal structures of all sulphates studied

Fig. 7.2 Variations of the fractional activity of iodate with the ionic radii of the alkali metals in the anhydrous sulphates of alkali metals

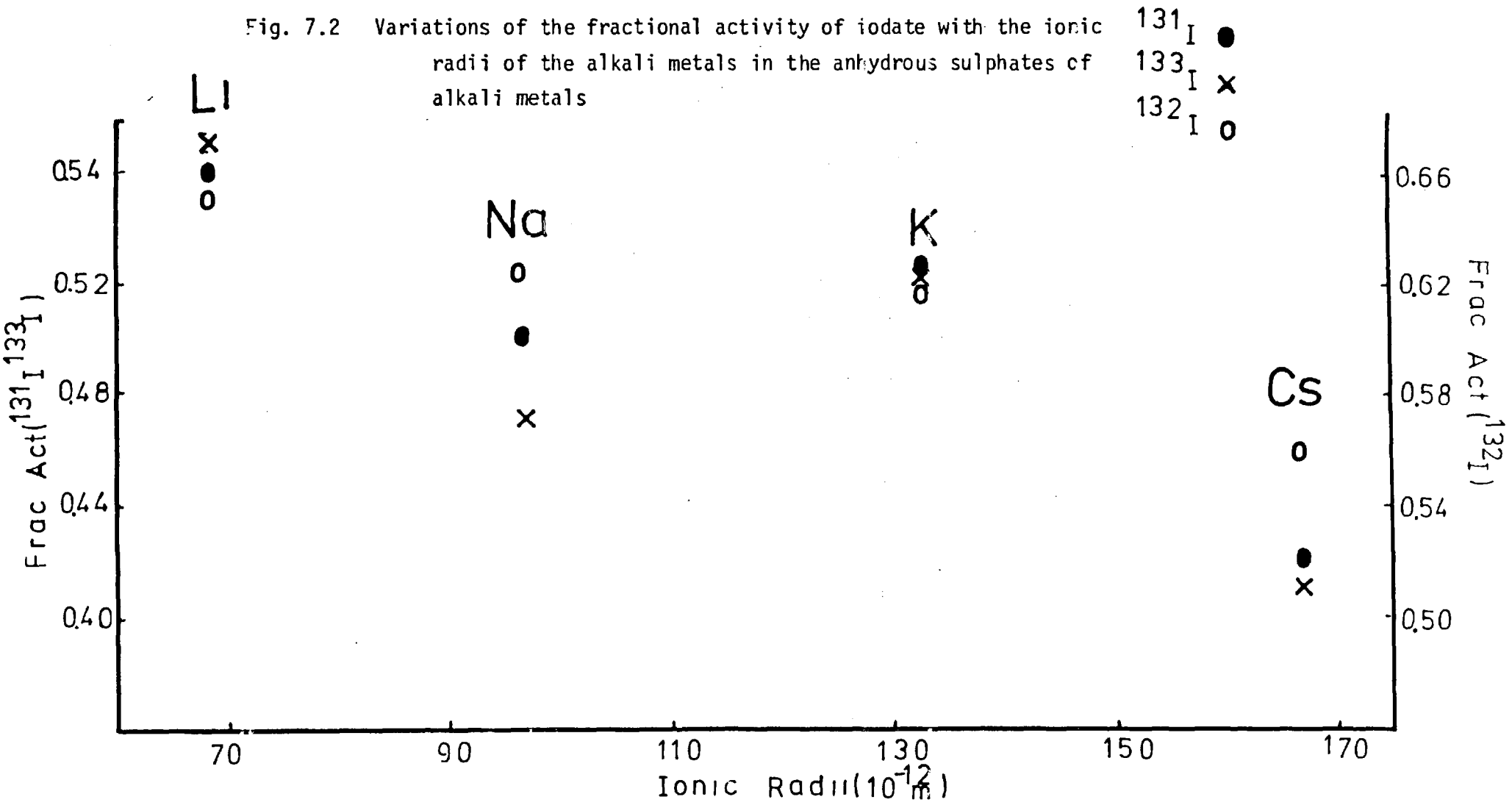

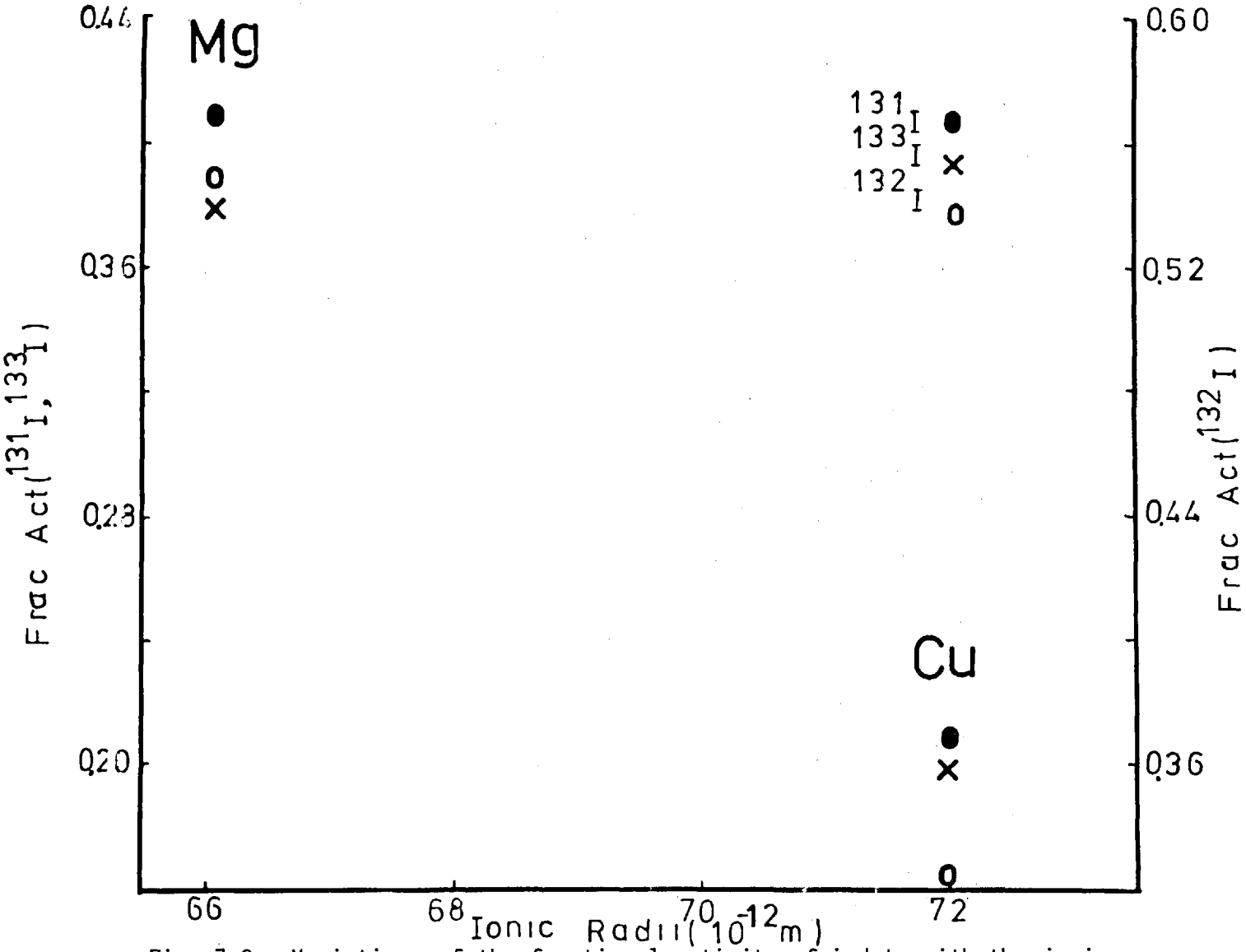


Fig. 7.3 Variations of the fractional activity of iodate with the ionic radii of the Mg and Cu in the anhydrous $MgSO_4$ and $CuSO_4$.

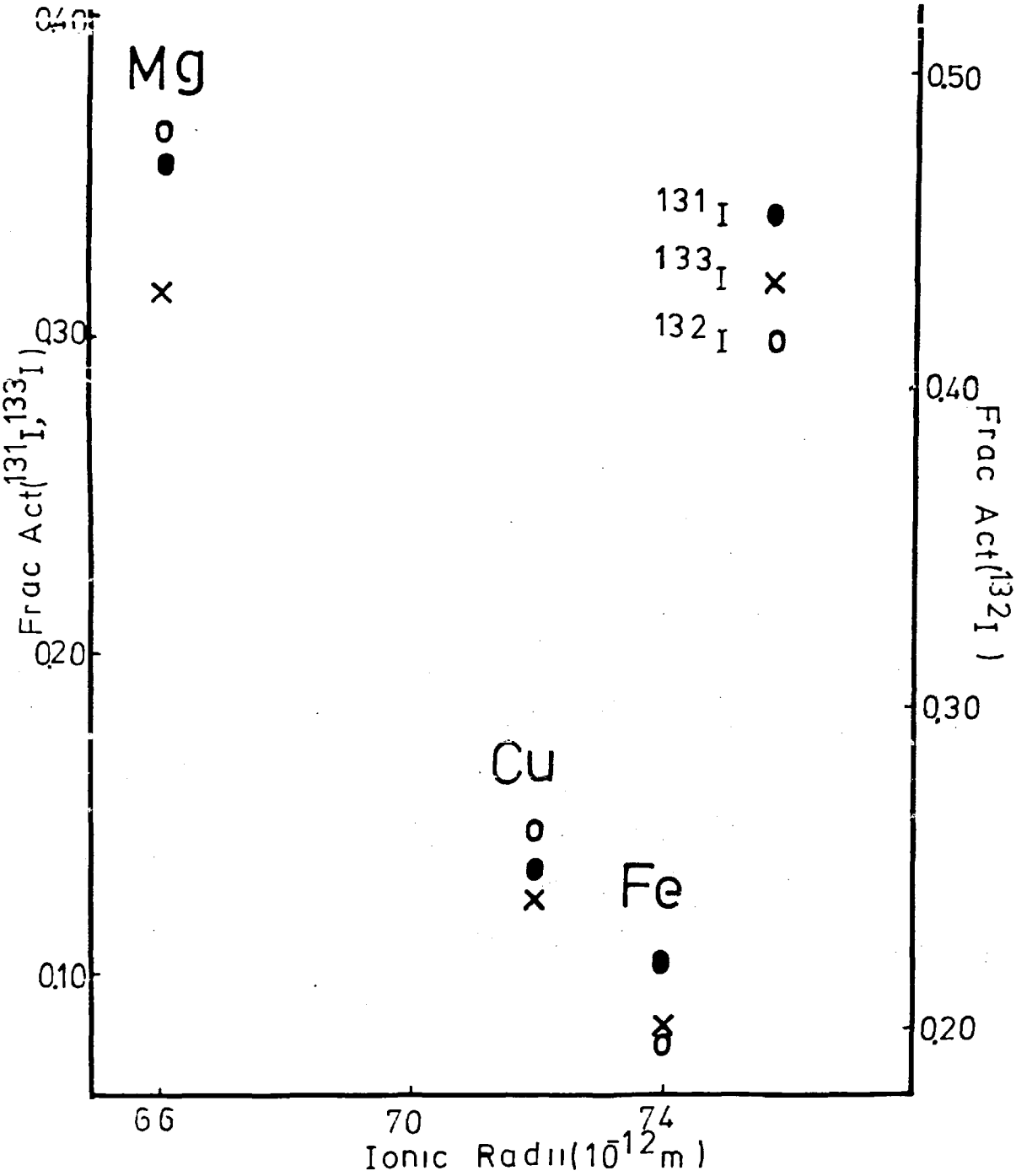


Fig. 7.4 Variations of the fractional activity of iodate with ionic radii of the Mg, Cu and Fe in the hydrous sulphates of Mg, Cu and Fe.

are shown in Table 7.9. As can be seen from this table the crystal structure of the sulphates used are not the same. In hydrous sulphate the bonding of the water molecule to the sulphate ion and metal atom is not in all samples the same, for instance in $CuSO_4.5H_2O$ four of the water molecules are closely associated with the copper atom, the fifth occupies a hole in the structure. The structure as a whole is an aggregate of sulphate and $Cu(H_2O)_4$ groups with the fifth water molecule adjacent to two sulphate oxygen atoms and to two of the water molecules (76). The structure of the hydrous and anhydrous sulphates of Li are completely different compared with the other sulphates. The volume of the unit cell and also the numbers of the molecules in the unit cell should also be taken into account. Hydrous sulphates of Li and Cu have two molecules in their unit cells while the others have four molecules (76).

(III) Sensitivity of the crystal towards radiation

The stabilities of the sulphates used towards irradiation are not the same. It has been reported that irradiation of the anhydrous alkali metals sulphates up to an absorbed dose of $4x10^{22}$ eV/g produces no detectable decomposition of the sulphate ion. For $MgSO_4.7H_2O$ and $CuSO_4.5H_2O$ only decomposition of the water of crystalization was observed (77). In this work using ESR (see Chapter 4) method, very small amounts of the radicals of $SO_3^-$ $SO_4^-$, $SO_2^-$ and $O_3^-$ were observed. Unlike the above sulphates, the $FeSO_4.7H_2O$ is much more sensitive towards irradiation (77). Therefore sensitivity towards irradiation is another major factor which should be considered.

(IV) Electron affinity of the cation

Another important factor which is also discussed in Chapter 6, is the electron affinity of cations for electrons. When cations are involved in the recoil reactions, the electron affinity of the cation may affect the oxidation state of the recoil atoms (78).

Table 7.8 Ionic radius for different cations (79)

| Cation | ionic radii ($10^{-12}$m) |
|---|---|
| Li | 68 |
| Na | 97 |
| K | 133 |
| Cs | 167 |
| Mg | 66 |
| Cu | 72 |
| Fe | 74 |

Table 7.9 Crystal structure of the sulphate studied (76)

| Compound | Type of cell | Numbers of molecules in unit cell |
|---|---|---|
| $Li_2SO_4$ | monoclinic | 4 |
| $Li_2SO_4.H_2O$ | monoclinic | 2 |
| $Na_2SO_4$ | orthorhombic | 4 or 8 |
| $Na_2SO_4.10H_2O$ | monoclinic | 4 |
| $K_2SO_4$ | orthorhombic | 4 |
| $Cs_2SO_4$ | orthorhombic | 4 |
| $MgSO_4$ | orthorhombic | 4 |
| $MgSO_4.7H_2O$ | orthorhombic | 4 |
| $CuSO_4$ | orthorhombic | 4 |
| $CuSO_4.5H_2O$ | triclinic | 2 |
| $FeSO_4.7H_2O$ | monoclinic | 4 |

# CHAPTER 8

## Conclusions

1. Atmospheric oxygen and air moisture had no effect on the fractional activity of iodate (see Chapter 5, section 1A).

2. Crushing had no effect on the distribution of the fission fragment iodine (see Chapter 5, section 1D).

3. The amounts of the radio iodine released during thermal annealing were negligible (see Chapter 5, section 2).

4. Decrease in the iodate fraction in thermal annealing was attributed to electron trapped species (defects) which acted as a reducing agent during thermal annealing. From the ESR work $SO_3^-$ was the most probable radical in reducing the fission fragment iodine ($I^F$) during the thermal annealing. The above hypothesis was consistent with a theoretical model written for the annealing processes in which electron exchange occurs between the $SO_3^-$ radicals and the fission fragment iodine. Activation energies for the annealing processes were derived (see Chapter 5, section 4).

5. A higher iodate fraction was observed in short irradiation times. This reveals that the fission fragment iodine when it initially enters the lattice is mostly in its oxidised form ($I^F$) and further irradiation up to a limiting dose reduces it (see Chapter 5, section 6).

6. Decrease in the fractional activity of iodate in the post irradiation of the $K_2SO_4$ containing the fission fragments suggests that $I^F$ is likely to be reduced to iodide by the defects in the lattice and by the radiation (see Chapter 5, section 7).

7. Thermal annealing of the $K_2SO_4$ (pre-irradiated with electrons before fission fragments injection) showed less decrease in the fractional activity of iodate compared with samples which had not been pre-irradiated. This was attributed to the faster reaction of $SO_3^-$ with itself during the thermal annealing (see Chapter 5, section 9).

8. The ESR of the irradiated $K_2SO_4$ revealed that in fission fragments irradiated $K_2SO_4$, the G-value observed for $SO_3^-$ radical formation was about eight times higher than that of the $\gamma$-irradiated $K_2SO_4$. This was attributed to the high LET of the fission fragments (see Chapter 4, sections 3.2 and 3.3).

9. $K_2SO_4$ doped with $Mg^{2+}$, $Cu^{2+}$, $Fe^{2+}$ and $Al^{3+}$ caused a decrease in the fractional activity of iodate. This was attributed to the cation vacancies and the transfer of holes in the lattice (see Chapter 6).

10. Significant decrease in the fractional activity of iodate in acid samples of $K_2SO_4$ and in the samples which were dissolved in the acid prior to carrier solution (relative to the neutral $K_2SO_4$) suggests that in the presence of $H^+$ ion, $I^*O_3^-$ reacts with $^*I^-$ and forms $I_2^*$ (see Chapter 7).

11. In all the sulphates studied, the hydrous sulphate gives lower iodate compared with its anhydrous sulphate. Results on wetted samples of $K_2SO_4$ showed the same effect. The observations suggested that water of crystallization and liquid water are acting as reducing agents. The hydrated electron or H atom or both could reduce $I^F$ (recoil atom) in the thermal spike region during the fission fragments irradiation. Alternatively the reduction of $I^F$ could result from the differences in the energies required to promote electrons from the different centres to the conduction bond and therefore allow them to be captured by the other centres (see Chapter 7, section 3.3A).

12. Irradiation of sulphates with different cations had a major effect on the distribution of the valency states of fission fragment iodine. The iodate fraction decreases with the increasing ionic radii of the cation, but no clear systematic effect could be established with crystal structures, or with sensitivity of the crystal towards irradiation damage and the electron affinity of the cations (see Chapter 7, section 3.3B).

13. In all cases $^{132}I$ gave higher fractional activity of iodate compared with the other isotopes, but $^{131}I$ and $^{133}I$ showed no differences (see Chapter 5, section 1A for discussion).

# APPENDIX 1

## Total number and energy of fission fragments entering $K_2SO_4$

### 1.1 Calculation of the range of fission fragments in $K_2SO_4$

The range of fission fragments in $K_2SO_4$ can be calculated using the following formula.

$$X_1\sqrt{Z1} = X_2\sqrt{Z2}$$

$X_1 = 3.73 \times 10^{-7}$ Average range of fission fragments in Al (3) in $gm/m^2$

$Z_1 = 13$ Atomic number of Al

$Z_2 = 12.28$ Average atomic number of $K_2SO_4$

The values of $Z_1$, $Z_2$ and $X_1$ were substituted in the above equation to give:

$X_2 = 4 \times 10^{-7} gm/m^2$ or $R_o$ (range) $= 15 \times 10^{-6} m$

where $X_2$ is the average range of fission fragments in $K_2SO_4$.

The range of $^{131}I$ (fission fragment) can also be calculated.

Range of $^{131}I$ in Al is $3.48 \times 10^{-7} gm/m^2$

therefore $X_2 = 3.58 \times 10^{-7}$ $gm/m^2$

or $R_o$ (range) $= 13.45 \times 10^{-6} m$

where $X_2$ is the range of $^{131}I$ in $K_2SO_4$.

### 1.2 Total number of fission fragments entering $K_2SO_4$ ($N_t$)

A source of $U_3O_8$ with film thickness H used as the source of the fission fragments. These fission fragments before entering $K_2SO_4$ pass through an aluminium foil of thickness d. Let the area of the source be A with thickness $\delta x$ (see fig. A.1). If the number of fission fragments generated per $cm^3$ in the source is $N_o$ then, total number of fragments generated is $N_o A \delta X$. The number of particles emitted through $\angle\theta$ with range $R_o$ is given by the number arriving on the surface of a band, generated by revolving PQ about X. The surface area of the band $= R_o \delta 92\pi R_o \sin\theta$. But $N_o A \delta X$ particles will fall on an area $4\pi R_o^2$

therefore:

number falling on surface area of band $= \frac{1}{2} N_o A \sin\theta \delta\theta \delta x$

Fig A.1 DIAGRAM FOR CALCULATING THE NUMBER OF FISSION FRAGMENTS ENTERING THE $K_2SO_4$

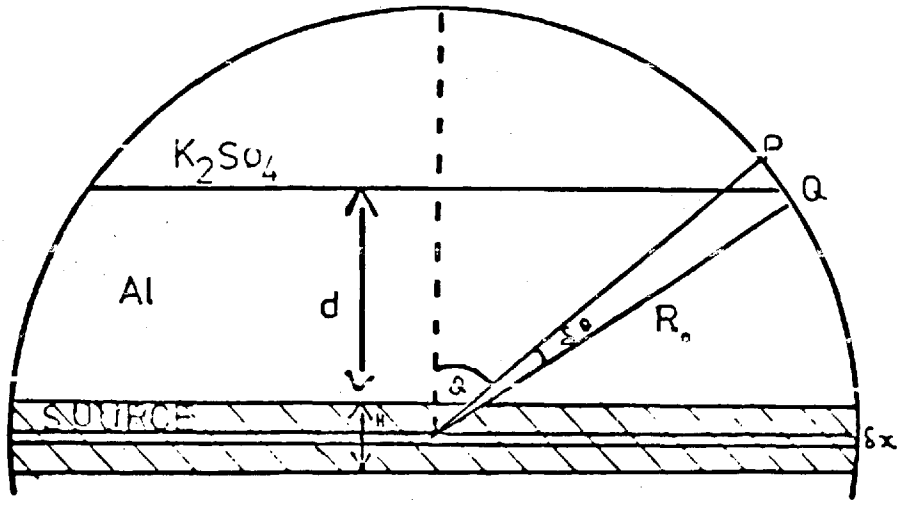

Now let d be the thickness of Al foil and H the thickness of the source. Fragments will not be emitted at angles larger than $\cos^{-1}\frac{x+d}{R_o}$ to the normal (81), where $R_o$ is the average range of fission fragments in $K_2SO_4$. therefore

$$N_t = \int_{x=0}^{x=H} \int_{\theta=0}^{\theta=\cos^{-1}(\frac{x+d}{R_o})} \tfrac{1}{2} A N_o \sin\theta \, d\theta \, dx$$

The first integration would give:

$$= \tfrac{1}{2} AN_o \int_{x=o}^{x=H} 1 - \frac{(x+d)}{R_o} \, dx$$

$$= \tfrac{1}{2}AN_o \left[ \frac{-x^2}{2R_o} - \frac{x(d-R_o)}{R_o} \right]_o^H$$

After the second integration

$$N_t = \tfrac{1}{2} AN_oH \left(1 - \frac{H+2d}{2R_o}\right) \qquad A.1$$

where $N_t$ is the total number of fission fragments entering $K_2SO_4$ from a source of thickness H through an absorber of thickness d. The values of A, $N_o$ and H are calculated in the next sections.

The thickness of Al (d) is known. The range of fission fragments and $^{131}I$ In $K_2SO_4$ are calculated in a previous section.

(a) Measurement of the thickness of $U_3O_8$ film (H)

The preparation of the $U_3O_8$ film is described in Chapter 3, section 3. Concentration of uranyl sulphate used for making $U_3O_8$ was 2.4176 µg/λ, 20λ(µml) of this solution (48.352µg) were used for each film.

From $3UO_2SO_4.3/2\ H_2O \xrightarrow{heat} U_3O_8$

the concentration of the $U_3O_8$ can be worked out.

$U_3O_8$ = 34.4463 µg for each film

Knowing the density of $U_3O_8$ (8.38 gm/cm$^3$) the volume of $U_3O_8$ film can be calculated.

$V = 4.1109 \times 10^{-6}$ cm$^3$

Diameter of the film = 10mm

The area of the film would be A = 78.5 mm$^2$. Therefore the thickness of the $U_3O_8$ would be

$$H = 5.34 \times 10^{-5} \text{mm}.$$

(b) Number of fission fragments generated in mm$^3$ (No)

Knowing the weight of $U_3O_8$ (34.4463 µg) the number of uranium atoms can be calculated.

Number of uranium atoms = $6 \times 10^{16}$ atoms

Neutron flux = $0.72 \times 10^{12}$ n sec$^{-1}$cm$^{-2}$

Uranium neutron cross section = 580 Barns

The fission rate would be

$$F_R = 2.5 \times 10^7 \text{ atom/sec}$$

The volume of the $U_3O_8$ is calculated in part (a) of this section ($4.1109 \times 10^{-3}$mm$^3$).

For 7.5 hours irradiation time the number of fission fragments generated per mm$^3$ can be calculated.

$$N_o = (2.5 \times 10^7 \times 7.5 \times 60 \times 60)/4.1109 \times 10^{-3}$$

$$N_o = 1.6419 \times 10^{14} \text{ fragments/mm}^3$$

The total number of fission fragments can be calculated as follows:

A = 78.5 mm$^2$ (the area of the source)

$N_o$ = $1.6419 \times 10^{14}$ (No of fission fragments/mm$^3$)

H = $5.2368 \times 10^{-5}$mm (the thickness of the source)

d = $7.62 \times 10^{-3}$mm (the thickness of Al foil)

$R_o$ = $15 \times 10^{-3}$mm (average range of fission fragments)

The above values are substituted into equation A.1 to give

$$N_t = 2.5117 \times 10^{11} \text{ fragments}$$

The total number of $^{131}I$ entering $K_2SO_4$ can also be calculated

$R_o$ = 13.45 x $10^{-3}$mm (range of $^{131}I$ in $K_2SO_4$)

The cumulative yield of $^{131}I$ is 2.9% of the fission fragment emitted. From the number of fission fragments generated per $mm^3$ (No = 1.6419 x $10^{14}$), $N_o$ for $^{131}I$ can be calculated

$N_o$ ($^{131}I$) = 4.7615 x $10^{12}$ (No of $^{131}I$ generated/$mm^3$)

Replacing the above values in the equation A.1, $N_t$ for $^{131}I$ would be

$N_t$ ($^{131}I$) = 4.2231 x $10^9$ $^{131}I$ atoms

## 1.3 Total energy of fission fragments entering $K_2SO_4$

The total energy $E_t$ of fragments emitted from a source ($U_3O_8$) of thickness H, and passing through an absorber (Al) of thickness d and finally entering $K_2SO_4$ can be calulated (81).

The energy emitted is related to the residual range R by

$$E = f(R)$$

where $$R = R_o - \frac{x+d}{\cos\theta}$$

$$E_t = \int_{x=0}^{x=H} \int_{\theta=0}^{\theta=\cos^{-1}(\frac{x+d}{R_o})} \tfrac{1}{2}AN_o\, f(R_o - \frac{x+d}{\cos\theta}) \sin\theta\, d\theta\, dx$$

Integration of the above equation gives

$$E_t = \frac{aAN_o}{2}\left[R_o^2 H - \frac{1}{3}\left\{(H+d)^3 - d^3\right\} + R_o H\,(H+2d)\left\{\mathrm{Ln}\,\frac{(H+d)}{R_o} - \tfrac{1}{2}\right\} + R_o d^2\,\mathrm{Ln}\left(\frac{H+d}{d}\right)\right] \qquad \text{A.2}$$

It is assumed that half the fission fragments energy is dissipated in the source. Therefore with E = 105 MeV

a can be calculated using $E = aR_o^2$

a = 1.9278 x $10^6$ MeV/$mm^2$

Substitution of the value of a and the values of A, $N_o$, H, $R_o$ and d (calculated in previous sections) in equation A.2 the total Energy ($E_t$) of the fission fragments entering $K_2SO_4$ would be $E_t$ = 1.9123 x $10^{12}$ MeV

APPENDIX 2 - CORRECTIONS FOR $^{132}I$ ACTIVITY

2.1 Calculation of the activity of $^{132}I$ at the end of irradiation

Most of the samples were analysed about three days after irradiation. At the time of analysis all the $^{132}I$ ($t_{\frac{1}{2}}$ 2.26 hours) activity due to fission were decayed away, therefore all the activity observed was from the decay of $^{132}Te$. The following corrections were done in order to calculate the activity of $^{132}I$ at the end of irradiation.

(A) Correction for decay during counting time

Activity observed after counting was corrected for decay during counting time, using the following formula:

Let $t_1$ be counting time.

$R_o$ be counting rate at the start of counting

N be total number of counts observed during counting time

$\delta N$ be total number of counts observed during time $\delta t$

$$\delta N = Re^{-\lambda t_1} \delta t_1$$

$$\frac{dN}{dt} = R_o e^{-\lambda t_1}$$

$$N = \int_{t=o}^{t=t_1} R_o e^{-\lambda t}$$

$$N = \frac{R_o}{\lambda} (1 - e^{-\lambda t_1})$$

$$R_o = \frac{N \lambda}{(1-e^{-\lambda t_1})} \qquad A.3$$

from equation (A.3) the activity of $^{132}I$ at the beginning of the counting can be calculated.

(B) Correction from dissolution to counting

This correction was not important in most cases, because the time from dissolution to counting for most of the samples was only a few minutes, but sometimes because of difficulties the analysed samples had to be counted a few hours after analysis. The following equation was used for this correction.

$$\lambda_B B_{dis} = R_o \exp(\lambda t) \qquad A.4$$

where $\lambda_B B_{dis}$ is activity of iodine atoms at the time of dissolution

$R_o$ = activity at start of counting

$t$ = time between dissolution to counting

(C) Correction from dissolution to end of irradiation

$^{132}I$ after irradiation starts to be produced from $^{132}Te$.

$$^{132}_{52}Te \xrightarrow{\beta^-} {}^{132}_{53}I$$

(A) (B)

Let the number of $^{132}Te$ atom at dissolution be $A_{dis}$, and the number of $^{132}I$ at dissolution be $B_{dis}$, the activity of $^{132}I$ at the end of irradiation can be calculated as follows:

$$\frac{dA}{dt} = -\lambda_A A_{dis} \qquad (A.5)$$

$$\frac{dB}{dt} = \lambda_A A_{dis} - \lambda_B B_{dis} \qquad (A.6)$$

$$e^{\lambda_B t_e}\frac{dB}{dt} + \lambda_B B e^{\lambda_B t_e} = \lambda_A A_{dis} e^{\lambda_B t_e}$$

$$e^{\lambda_B t_e}\left(\frac{dB}{dt} + \lambda_B B_{dis}\right) = \lambda_A A_{dis} e^{\lambda_B t_e} \qquad (A.7)$$

where $t_e$ is the time from end of irradiation to dissolution. From equation (A.6)

$$A_{dis} = A_e e^{-\lambda A t_e}$$

where $A_e$ is the number of Te atoms at the end of irradiation,

substitute the value of $A_{dis}$ in equation (A.7)

$$e^{\lambda_B t_e}\left(\frac{dB}{dt} + \lambda_B B_{dis}\right) = \lambda_A A_e e^{\lambda_B t_e} \cdot e^{-\lambda_A t_e}$$

$$= \lambda_A A_e \exp(\lambda_B t_e - \lambda_A t_e)$$

Integration of the above equations gives :

$$\lambda_B B_e\, e^{-\lambda_B t_e} = B_{dis}\lambda_B - \frac{\lambda_A A_e \lambda_B}{\lambda_B - \lambda_A}\,(e^{-\lambda_A t_e} - e^{-\lambda_B t_e}) \qquad (A.8)$$

where $B_e$ is the number of iodine atoms at the end of irradiation.

(D) Correction for decay during irradiation

The correction was also carried out for decay during irradiation.

$$\frac{dA}{dt} = \alpha F - \lambda_A A \qquad (A.9)$$

$$\frac{dB}{dt} = \lambda_A A - \lambda_B B_e \qquad (A.10)$$

From equation (A.9)

$$\alpha F = \frac{\lambda_A A}{(1-e^{-\lambda_A t_{irr}})} \qquad (A.11)$$

The value of $\lambda_A A$ from equation (A.11) was replaced in equation (A.10). The integration of this equation would give:

$$B_e = \frac{\alpha F}{\lambda_B}\,(1 - e^{-\lambda_B t_{irr}}) - \frac{\alpha F}{\lambda_B - \lambda_A}\,(e^{-\lambda_B t_{irr}} - e^{-\lambda_B t_{irr}}) \qquad (A.12)$$

The value of $\alpha F$, from equation (A.11) was replaced in equation (A.12) to give:

$$\lambda_A A_e = \frac{B_e(\lambda_B - \lambda_A)\lambda_B(1-e^{-\lambda_A t_{irr}})}{\lambda_B(1-e^{-\lambda_A t_{irr}}) - \lambda_A(1-e^{-\lambda_B t_{irr}})} \qquad (A.13)$$

The value of $\lambda_A A_e$ from equation (A.13) is substituted in equation (A.8) to give:

$$B_e \lambda_B = \frac{\lambda_B B_{dis}\, \exp(\lambda_B t_e)}{\left[1 + \frac{(1-\exp(-\lambda_A t_{irr}))(\exp(\lambda_B t_e - \lambda_A t_e) - 1)}{\lambda_B(1-\exp(-\lambda_A t_{irr})) - \lambda_A(1-\exp(\lambda_B t_{irr}))}\right]} \qquad (A.14)$$

From equation (A.14) the activity of the $^{132}I$ at the end of irradiation can be calculated. Where $\lambda_B B_{dis}$ is the activity of $^{132}I$ at dissolution, tirr is time of irradiation and $t_e$ is the time from the end of irradiation to dissolution. Equation (A.14) used in calculation as a correction factor for $^{132}I$ activity.

# APPENDIX 3 - COMPUTER PROGRAMME

## 3.1 Calculation of the iodine activity as iodide and iodate

The activity of the iodide and iodate was separated as follows:

Let carrier solution KI be X1 gm

$KIO_3$ be X2 gm

KI (excess) be X3 gm

Reaction of iodide and iodate in acidic condition is as follows:

$$IO_3^- + 5I^- + 6H^+ \longrightarrow 3I_2 + 3H_2O$$

According to the above equation, 1 gm of KI reacts with 0.258 gm $KIO_3$

therefore, $C = X1 \times 0.258$ gm

where C is the amount of iodate reacting with X1 gm of iodide

Therefore the remaining iodate in fraction B is (X2 - C) = C1 gm

In fact, $C_1$ gm $KIO_3$ requires $\frac{C1}{0.258}$ gm KI to be liberated as iodine. Thus activity in fraction B (see Chapter 3.9) is due to $C_1$ gm iodate. From the above explanation the activity of the iodate in fraction A (see Chapter 3.9) can be calculated.

The iodate activity in fraction A = $\frac{C}{C_1}$ x activity of fraction B subtracting the activity of iodate in A from the total activity of fraction A, the activity due to iodide ions can be calculated. Total activity of iodate can be obtained by adding the activity of iodate in A to the activity of fraction B. To find the specific activity of iodide and iodate, the activity of iodide and total activity of iodate are each divided by weight of iodine (in grams) in the iodide and iodate carrier solutions $X_1$ and $X_2$. In the calculation explained so far, no account was taken of the fact that in extracting the iodate in fraction B, the excess amount of ($X_3$ gram) KI carrier solution is added, the amount of KI required to react with the remaining iodate in fraction B is calculated above and is $\frac{C_1}{0.258}$ gm, since the amount of KI (X3) added is in excess, the remaining aqueous solution would have some iodide left.

The calculation is as follows:

$$\text{Iodine atoms in fraction before extraction} = X3 \times \frac{126.904}{166.006} + Cl \frac{126.904}{214.0042}$$

$$= 0.7645 \times X3 + 0.5930 \times Cl \text{ gm}$$

$$\text{Iodine atoms in } CCl_4 \text{ after extraction} = \frac{Cl}{0.258} \times \frac{126.904}{166.004} + Cl \frac{126.904}{214.0042}$$

$$= 3.556Cl \text{ gm}$$

$$\text{Iodine left in aqueous solution} = (x3 - \frac{Cl}{0.258}) \frac{126.904}{166.006}$$

$$= 0.7645X3 - 2.963Cl \text{ gm}$$

If the remaining iodine in the aqueous solution had undergone exchange with the active iodate atoms, then the count rate for fraction B should be increased by the following factor:

$$\text{Activity of extract B} \times \frac{0.7645X3 + 0.593Cl}{3.556Cl}$$

The above correction depends on the nature of the equilibrium between $I_2$ and $I^-$ under the condition present in the solution. Although no activity has been observed in the aqueous solution after extraction, but for more accuracy the above correction was carried out.

3.2 Computer program used for calculation

A computer program was written in FORTRAN to compute the distribution of active iodine atoms between iodide and iodate. The output of the program is the specific and fractional activity of iodide and iodate for each isotope. The following are the symbols and their meaning used in the program, program and a typical output for one of $K_2SO_4$ samples analysed at room temperature.

## Symbol listing for the programme

| Symbol | Meaning |
|---|---|
| RIN (M) | Percentage intensity for isotope (M) |
| HL (M) | Half life for isotope (M), in hours |
| A1 (M) | Observed activity for isotope (M), extract A, in count/sec |
| A2 (M) | Observed activity for isotope (M), extract B, in count/sec |
| X1 | Iodide carrier solution (gm) |
| X2 | Iodate carrier solution (gm) |
| X3 | Excess iodide carrier solution (gm) |
| W | Decay constant for $^{132}I$ |
| W1 | Decay constant for $^{132}Te$ |
| $z_3, z_5$ | Counting time for extract A and B respectively |
| $z_4, z_6$ | Counting time corrected for dead time for extract A and B respectively |
| $D_2$ | Dead time correction factor for extract A |
| $D_3$ | Dead time correction factor for extract B |
| T | Time of irradiation in hours |
| $T_2$ | Time from end of irradiation to counting for extract A, in hours |
| $T_3$ | Time from end of irradiation to counting for extract B, in hours |
| $T_4$ | Time from dissolution to counting for extract A, in hours |
| $T_5$ | Time from dissolution to counting for extract B, in hours |
| $T_6$ | Time from end of irradiation to dissolution in hours |
| $T_7$ | Time of counting for extract A, in mins. |
| $T_8$ | Time of counting for extract B, in mins. |
| $E_3(M)$ | DE% for isotope (M) |
| AMIOA | Amount of iodate in fraction A, in gm |
| AMIOL | Amount of iodate left in B, in gm |
| GITIO | Gramme iodine in all iodates |
| AA1 (M) | Activity of extract A, at the beginning of counting for isotope (M) in dis/sec. |
| AA2 (M) | Activity of extract A at the end of irradiation for isotope (M) in dis/sec. |
| V | The correction factor for $^{132}I$ activity (V represents equation A.14 in Appendix 2) |
| AB1 (M) | Activity of extract B at the beginning of counting for isotope (M) in dis/sec. |
| AB3 (M) | Activity of extract B at the end of irradiation for isotope (M) in dis/sec. |
| A1OA (M) | Activity of iodate in extract A for isotope (M) in dis/sec |
| TIOA (M) | Total iodate activity for isotope (M) in dis/sec |
| TIA (M) | Total iodide activity for isotope (M) in dis/sec. |
| SIA (M) | Specific iodide activity for isotope (M) |

| | |
|---|---|
| SIOA (M) | Specific iodate activity for isotope (M) |
| TIIO (M) | Total activity of iodide and iodate for isotope (M) in dis/sec. |
| FAAI (M) | Fractional activity of iodide for isotope (M) |
| FAIO (M) | Fractional activity of iodate for isotope (M) |

# COMPUTER PROGRAM

```
PROGRAM    JK
00100 PROGRAM NEW(INPUT,OUTPUT,TAPE5=INPUT,TAPE6=OUTPUT)
00110 DIMENSION RIN(3),HL(3),A1(3),A2(3),AA1(3),AA2(3),AB1(3),AB2(3),AB3(3),
00120+E3(3),AIOA(3),TIOA(3),TIA(3),SIA(3),SIOA(3),TIIO(3)   ,FAA1(3),FAIO(3)
00130 M=0
00140 WRITE(6,100)
00150 READ(5,*)Z3,Z4,Z5,Z6,T,T2,T3,T4,T5,T6,T7,T8,A1(1),A2(1),A1(2),A2(2),
00160+A1(3),A2(3),E3(1),E3(2),E3(3)
00170 100 FORMAT(X,*Z3,Z4,Z5,Z6,T,T2,T3,T4,T5,T6,T7,T8,A1(1)*,/,*A2(1),
00180+A1(2),A2(2),A1(3),A2(3),E3(1),E3(2),E3(3)=*)
00200 X1=7.11E-3
00210 X2=5.698E-3
00220 X3=14.43E-3

00230 RIN(1)=.82
00240 RIN(2)=.9
00250 RIN(3)=.89
00260 HL(1)=193.2
00270 HL(2)=20.3
00280 HL(3)=2.26
00290   W=.693/2.26
00300 W1=.693/77.7
00302 WRITE(6,100)
00304 WRITE(6,*)Z3,Z4,Z5,Z6,T,T2,T3,T4,T5,T6,T7,T8,A1(1),A2(1),A1(2),A2(2),
00306+A1(3),A2(3),E3(1),E3(2),E3(3)
00310 AMIOA=.258*X1
00320 WRITE(6,110)AMICA
00330 110 FORMAT(X,*AMOUNT OF IODATE IN A=*,E15.9)
00340 AMIOL=X2-AMIOA
```

```
00350 WRITE(6,120)AMIOL
00360 120 FORMAT(X,*AMOUNT OF IODATE LEFT=*,E15.9)
00370 GITIO=(AMIOA+AMIOL)*.592998
00380 WRITE(6,130)GITIO
00390 130 FORMAT(X,*GM IODINE IN ALL KIO3=*,E15.9)
00400 WRITE(6,140)
00410 140 FORMAT(X,*ISOTOPE 131*)
00420 5 CONTINUE
00430 M=M+1
00440 D2=Z3/Z4
00450 D3=Z5/Z6
00460 AA1(M)=((A1(M)*T7*.01155)/HL(M))/(1-EXP(-T7*.01155/HL(M)))
00470 IF(M.EQ.3)T2=T4
00480 IF(M.EQ.3)T3=T5
00490 AA2(M)=(((AA1(M)*EXP(.693*T2/HL(M)))/E3(M)/RIN(M)))*D2


00500 IF(M.LT.3)GO TO 166
00540 V= EXP(W*T6)*(W*(1-EXP(-W1*T))-W1*(1-EXP(-W*T))
00550+)/((1-EXP(-W1*T))*(W+(EXP(W*T6-W1*T6)-1))-W1*(1-EXP(-W*T)))
00560  AA2(M)=AA2(M)*V
00570 166 WRITE(6,170)AA2(M)
00580 170 FORMAT(X,*ACT OF EXTRACT A=*,E15.9)
00590 AB1(M)= ((A2(M)*T8*.01155)/HL(M))/(1-EXP(-T8*.01155/HL(M)))
00600 AB2(M)=((AB1(M)*EXP(.6930*T3/HL(M)))/E3(M)/RIN(M))*D3

00610 AB3(M)=AB2(M)*((.2148*X3+.1667*AMIOL)/AMIOL)
```

```
00620 IF(M.LT.3)GO TO 212
00660  AB3(M)=AB3(M)*V
00670 212 WRITE(6,220)AB3(M)
00680 220 FORMAT(X,*ACT OF EXTRACT B=*,E15.9)
00690 A1OA(M)=AB3(M)*AM1OA/AM1OL

00700 WRITE(6,240)A1OA(M)
00710 240 FORMAT(X,*ACT OF K1O3 IN A=*,E15.9)
00720 T1OA(M)=AB3(M)+A1OA(M)
00730 WRITE(6,250)T1OA(M)
00740 250 FORMAT(X,*TOTAL IODATE ACT=*,E15.9)
00750 T1A(M)=AA2(M)-A1OA(M)
00760 WRITE(6,260)T1A(M)
00770 260 FORMAT(X,*TOTAL IODIDE ACT=*,E15.9)
00780 S1A(M)=T1A(M)*1.3081/X1
00790 WRITE(6,270)S1A(M)
00800 270 FORMAT(X,*SPECI IODIDE ACT=*,E15.9)
00810 S1OA(M)=T1OA(M)/G1T1O
00820 WRITE(6,280)S1OA(M)
00830 280 FORMAT(X,*SPECI IODATE ACT=*,E15.9)
00840 T11O(M)=T1A(M)+T1OA(M)

00850 FAA1(M)=T1A(M)/T11O(M)
00860 WRITE(6,290)FAA1(M)
00870 290 FORMAT(X,*FR ACT AS IODIDE=*,E15.9)
00880 FA1O(M)=T1OA(M)/T11O(M)
00890 WRITE(6,300)FA1O(M)
00900 300 FORMAT(X,*FR AC AS IODATE=*,E15.9)
```

```
00910 IF(M.GT.1)GO TO 1000
00920 WRITE(6,310)
00930 310 FORMAT(X,*ISOTOPE 133*)
00940 GO TO 5
00950 1000 CONTINUE
00960 IF(M.GT.2)GO TO 2000
00970 WRITE(6,320)
00980 320 FORMAT(X,*ISOTOPE 132*)
00990 GO TO 5

01000 2000 CONTINUE
01010 STOPE
01020 END
```

# OUT PUT

```
 Z3,Z4,Z5,Z6,T,T2,T3,T4,T5,T6,T7,T8,A1(1)
A2(1),          A1(2),A2(2),A1(3),A2(3),E3(1),E3(2),E3(3)=
   1.00000       1.00000       1.00000       1.00000       7.23330
   66.7500       67.0000       8.33000E-02   .333300       66.6667
   10.0000       10.0000       38.1600       21.3100       68.2100
   37.1800       31.1100       22.3300       3.00000E-02   1.70000E-02
   1.30000E-02
 AMOUNT OF IODATE IN A= .183438000E-02
 AMOUNT OF IODATE LEFT= .386362000E-02
 GM IODINE IN ALL KIO3= .337890260E-02
 ISOTOPE 131
 ACT OF EXTRACT A= .197145066E+04
 ACT OF EXTRACT B= .106769915E+04
 ACT OF KIO3 IN A= .506925102E+03
 TOTAL IODATE ACT= .157462425E+04

 TOTAL IODIDE ACT= .146452556E+04
 SPECI IODIDE ACT= .269443866E+06
 SPECI IODATE ACT= .466016466E+06
 FR ACT AS IODIDE= .481886598E+00
 FR AC AS IODATE= .518113402E+00
 ISOTOPE 133
 ACT OF EXTRACT A= .436537299E+05
 ACT OF EXTRACT B= .232534621E+05
 ACT OF KIO3 IN A= .110403419E+05
 TOTAL IODATE ACT= .342938040E+05
 TOTAL IODIDE ACT= .326133880E+05
 SPECI IODIDE ACT= .600022121E+07
 SPECI IODATE ACT= .101493911E+08
 FR ACT AS IODIDE= .487442107E+00
 FR AC AS IODATE= .512557813E+00

 ISOTOPE 132
 ACT OF EXTRACT A= .920027129E+03
 ACT OF EXTRACT B= .690844816E+03
 ACT OF KIO3 IN A= .328001179E+03
 TOTAL IODATE ACT= .101884600E+04
 TOTAL IODIDE ACT= .592025951E+03
 SPECI IODIDE ACT= .108921118E+06
 SPECI IODATE ACT= .301531626E+06
 FR ACT AS IODIDE= .367518940E+00
 FR AC AS IODATE= .632481060E+00
```

REFERENCES

1. Chadderton, L.T. and McC. Torrens, I. "Fission damage in crystals", Methuen, London,(1969).

2. Walton, G.N. in "Atomic Energy Waste: its nature, use and disposal", (E. Glueokauf, ed.), Chapter 1, Butterworths, London, (1961).

3. Walton, G.N., in "Prog. Nuclear Physics, Vol.6" (O.R. Frisch, ed.), Chapter 7, Pergamon, London, (1957).

4. Glendenin, L.E., Coryell, C.D. and Edwards, R.R. N N E S. The fission products paper, 52, (1951).

5. Bohr, N., Dan. mat. Fys. Medd., 18, pp8, (1948)

6. Waller, C.M., Ph.D. thesis, Imperial College, Chem. Eng. Dept., University of London, 1976.

7. Chadderton, L.T. "Radiation damage in crystals", Methuen, London (1965).

8. Dienes, G.J., and Vineyard, G.H., Radiation effect in solids. interscience, New York, (1957).

9. Brinkman, J.A., J. Appl. Phys. 25. pp,96 (1954).

10. Brinkman, J.A., Nuclear Met. VI, 1,(1959)

11. Seeger, A., in Radiation damage in solids, IAEA (Viena) I, pp.101(1962)

12. Atkins, P.W. and Symons, M.C.R., "The structure of inorganic radicals", Elsevier Publishing Company, (1967).

13. Walton, G.N. and Croall, I.F., J. Inorg. Nucl. Chem., Vol.1, pp.149, (1955).

14. Walton, G.N., Bowles, B., and Croall, I.F., in First, Int. Conf. "The Peaceful Uses of Atomic Energy", 7, pp.155, (1955).

15. Hall, D. and Walton, G.N., J. Inorg. Nucl. Chem., Vol.19, pp.16, (1961).

16. Waller, C.M., and Walton, G.N., J. Inorg. Nucl. Chem. Vol.41, pp.135, (1979).

17. Spiridou, S. and Calusarua, A., J. Inorg. Nucl. Chem., vol.35, pp.713, (1973).

18. Spiridou, S., and Calusarua, A., J. Inorg. Nucl. Chem., Vol.38, pp.1429, (1976)

19. Chowdari, B.V. and Venkateswarlu, P., J. Chem. Phy vol.48, No.1, pp.318, (1968).

20. Abdulsabirov, R. Yu, Greznev, Yu.S., and Zaripov, M.M., Soviet physics, Solid State, vol.12, No.2, pp.509-(1970).

21. Krutikov, V.F., Silkin, N.T. and Stepanov, V.G., Soviet Physics, Solid State, vol.13, No.10, pp.2601 (1972).

22. Andersen, T. and Olesen, K., Trans. Faraday, Soc., 61, pp.781 (1965).

23. Andersen, T., and Maddock, A.G., Trans. Faraday Soc., 59, pp.2362 (1963).

24. Saito, N., Ambe, F. and Sano, H., Nature, 1, pp.505, (1965).

25. Saito, N., Ambe, F. and Sano, H., Radiochemica acta, vol.7, pp.131 (1967).

26. Dejesusf, M.F., Machad, R.M. and Duplater, G., Radiochemica Acta, 26, pp.41, (1979).

27. Kobayashi, T., Yakabe, M. and Hukuda, K., J. Phys. Soc. Japan 32, pp.578 (1972).

28. Kronrad, L., Radiochemica acta, vol.3, pp.191 (1964).

29. Ambe, F. and Saito, N., Radiochemica acta., vol.13, pp.105, (1970).

30. Weiss, J., Nature, 153, pp.748,(1944).

31. Allen, A.O., Discussion Faraday Soc., vol.12, pp.79, (1952).

32. Swallow, A.J. "Radiation chemistry". Longman, (1973).

33. Cerek, B., Nature, vol.223, pp.491, (1969).

34. McCalum, K.T. and Maddock, A.G., Trans. Faraday Soc. vol.49, pp.1150, (1953).

35. Maddock, A.G. and Muller, H., Trans. Faraday Soc., Vol.59, pp.509 (1960).

36. Ackerhalt, R., Ellerbe, P. and Harbottle, G., Radiochemica acta, vol.18, pp.73, (1972).

37. Arnkar, H.J., Sharma, D.K. and Patil, S.F., Radiochemica Acta, vol.13, pp.164, (1970).

38. Adams, A. and Campbell I.C., Trans. Faraday Soc., pp.2001, (1963).

39. Peixoto Cabral, J.M. and Maddock, A.G., J. Inorg. Nucl. Chim., vol.29 pp.1825 (1967).

40. Al-Siddique, F.R. and Maddock, A.G., J. Inorg. Nucl. Chem., vol.34, pp.3007, (1972).

41. Stamoul, I., Radiochemica Acta, vol.21, pp.90, (1974).

42. Khare, M., and Mohanty, S.R., J. Inorg. Nucl. Chem., Vol.29, pp.853, (1967)

43. Walton, G.N., Radiochemica Acta, vol.2, pp.108 (1964)

44. Ladrielle, T.G., Cogneau, M.A., and Apers, D.J., Radiochemica Acta, Vol.22, pp.173, (1975).

45. Gutlich, P., Frohlich, K. and Odar, S., J. Inorg. Nucl. Chem., Vol.33, pp.307 (1971).

46. Kasrai, M. and Maddock, A.G., J. Chem. Soc. (A), pp.1105, (1970).

47. Bracokova, V., and Cifka, J., J. Inorg. Nucl. Chem., vol.32, pp.365, (1970).

48. Gromov, V.V., and Morton, J.R., Canadian Journal of Chemistry, vol.44, pp.527, (1966).

49. Aiki, K. and Hukuda, K., J. Phys. Soc., Japan, vol.22 , pp.663, (1967).

50. Hariharan, N. and Sobhanadri, J., J. Magnetic resonance, vol.1, pp.639, (1969).

51. Sasaki, T., Phys. State-Sol. (a) 34, pp.339, (1976).

52. Erschler, B.V. and Lapteon, F.S., J. Nuclear Energy, 4, pp.471, (1957).

53. Hudswell, F., "The preparation of films and coatings", AERE C/R 392 (1949).

54. Galley, M.R., "The fission fragment irradiation of methane", Ph.D. thesis, Imperial College, London (1964).

55. Katz, J.J., and Rabinowitch, E., "Chemistry of uranium", nuclear energy series Division VIII, Vol.5, McGraw-Hill London (1951).

56. "Encyclopaedia of Chemical Technology" (Kirt-athmereed) 2nd edn., vol.21, (1970).

57. Currah , J.E. and Beamish, F.B., Industrial Chemistry, vol.19, No.8, pp.609 (1947).

58. Meller, J.W., "Inorganic and Theoretical Chemistry, vol.II, supplement 7 "Longmans, London (1922-37, 16v) .

59. Vogel, A.I. "A text book of quantitative inorganic analysis", Longmans, London (1961).

60. Lederer, C.M., Hollander, J.M. and Perlman, I., "Table of isotopes, 6th edn., Wiley, London (1967).

61. Covell, D.E., Analytical chemistry, vol. 31, no.11, (1959) ·

62. Mason, J.A., "Personal communication" University of London Reactor Centre

63. Cleary, R.E., Hamill, W.H. and Williams, R.R., J. of Amer. Chem. Soc. vol.74, pp.4675, (1952) ·

64. Breusov, O.N., Kashina, N.I. and Revzina, T.V., Russian Journal of Inorganic Chemistry, 15(3), pp.316, (1970) .

65. Simon, J., Gal, S., and Erdey, L., Acta chim. Acad. Sci. Hung, pp.175, 66(2) (1970).

66. Abel, E. and Cieben, R., Z. Phys. Chem., 139, 631, (1927) .

67. Bellido, A.V., Radiochim. Acta, 7, 122,(1967) .

68. Mellor, J.W., "Inorganic and Theoretical Chemistry, Vol.XIII, (1922-37, 16V) Longman, London.

69. Mellor, J.W. "Inorganic and theoretical chemistry", Vol.II, Longmans, London (1922-37, 16v)·

70. Mellor, J.W., "Inorganic and theoretical chemistry", vol.IV, (1922-37, 16v), Longmans, London ·

71. Mellor, J.W., "Inorganic and theoretical chemistry", Vol.V, (1922-37, 16v), Longmans, London.

72. Mellor, J.W., "Inorganic and theoretical chemistry", vol.III (1922-37, 16v), Longmans, London.

73. Cvoric, J., Journal of chromatography, pp.349, vol.44, (1969)·

74. Anbar, M. and Hart, E.J., J. Phys. Chem., vol.69, pp.973 (1965)·

75. Harbottle, G. and Sutin, N., Advances in Inorganic Chemistry and Radiochemistry, Academic Press, New York (1959).

76. Wyckoff, W.G., "Crystal Structure", vol.3, Inter Science, New York (1965)·

77. Huang, S., Johnson, E.R., Amer. Soc. Test. Mater., Special Publ. No. 400, pp.121 (1965)·

78. Fumitoshi, A. and Nobufusa, S., Radiochimica acta, vol.13, pp.105 (1970)·

79. Tennent, R.M., Science data book, Publiser: Oliver & Boyd, 1976 ·

80. Kneubuhl, F.K., J. Chem. Phys., vol.33, pp.1074 (1960) ·

81. Hall, D. and Walton, G.N., J. Inorg. Nucl., Chem., vol.10, pp.215 (1959).

82. Beardwood, P. Ph.D. Thesis, to be submitted, Imperial College, University of London